catalysts

MDPI

Article

Poisoning Effect of CO: How It Changes Hydrogen Electrode Reaction and How to Analyze It Using Differential Polarization Curve

Osami Seri [1,*] and Kazunao Furumata [2]

[1] Department of Mechanical System Engineering, Muroran Institute of Technology, 27-Mizumoto-cho, Muroran 050-8585, Japan
[2] Production System Engineering, National Institute of Technology, Hakodate College, Hakodate 042-8501, Japan; furumata@hakodate-ct.ac.jp
* Correspondence: seri@mmm.muroran-it.ac.jp; Tel.: +81-143-46-5365

Abstract: The hydrogen electrode reaction (*HER*) on Pt electrode in a H_2SO_4 solution when CO gas was injected/stopped was studied using polarization resistance curve. In order to elucidate and confirm the CO poisoning effect, a few curve techniques were proposed. Applying them, the kinetic parameters such as the number of electrons transferred (z) and the cathodic transfer coefficient (α_c) were determined. The *HER* in a 0.5 mol dm^{-3} H_2SO_4 solution saturated with H_2 was confirmed as a reversible reaction having $z = 2$. When the above solution was injected with CO, the reversible *HER* changed to an irreversible reaction having $z = 1$ and $\alpha_c \approx 0.6$. Once we stopped the CO injection, alteration from the irreversible to quasireversible reaction was gradually made after several cyclic polarizations. The proposed curve techniques can provide a reliable way to determine the kinetic parameters changing among reversible, irreversible, and quasireversible reactions.

Keywords: hydrogen evolution reaction; platinum electrode; CO poisoning; polarization resistance curve; Tafel slope

Citation: Seri, O.; Furumata, K. Poisoning Effect of CO: How It Changes Hydrogen Electrode Reaction and How to Analyze It Using Differential Polarization Curve. *Catalysts* **2021**, *11*, 1322. https://doi.org/10.3390/catal11111322

Academic Editor: Rahat Javaid

Received: 6 October 2021
Accepted: 28 October 2021
Published: 30 October 2021

1. Introduction

The hydrogen electrode reaction (*HER*) is one of the most fundamental electrolytic reactions in the field of electrochemistry [1–10]. This redox reaction consists of hydrogen oxidation reaction (*hor*) as an anodic branch reaction and hydrogen evolution reaction (*her*) as a cathodic branch reaction. The exchange current density of *HER*, which is the magnitude of the reciprocal reaction between *hor* and *her*, is widely used as a kinetic parameter to evaluate catalysts in technical fields such as fuel cells and water electrolysis. It is well known that power generation by fuel cells will be very important and become widespread in the very near future [2,3,7–10]. Since the hydrogen consumed in fuel cells is mainly produced by the steam reforming process of methane, it may contain byproducts such as CO and CO_2. Many papers reported that even a small amount of CO can poison the platinum catalyst and reduce its efficiency [11]. This poisoning phenomenon is said to be mainly caused by the firm adhesion of CO as CO_{ad} to the platinum electrode surface. A more detailed explanation of the CO poisoning effect from various aspects is needed to make the fuel cell fully functional. For an example, it is necessary to explain the degradation of the electrode not only from the surface inactivation caused by CO adsorption but also from the physical factors derived from it.

This paper explains the degradation of platinum catalysts from the viewpoint of polarization resistance. As far as the authors know, there are few papers that provide explanations with detailed polarization resistance curves. Exceptionally, A.C. Chialvo et al., devised their own theory of polarization resistance and applied it to *HER*. It was an experimental and theoretical study of CO poisoning *HER* [12–22]. However, their theory was limited to a single point at $j = 0$, and there was no mention or consideration from the

viewpoint of the whole curve. This paper, first of all, shows the continuous change of *HER* from reversible to irreversible reaction caused by CO injection. Using the polarization curve and its polarization resistance curve, which is derived from the differential polarization method (DPM) [23–26], the CO poisoning effect is discussed from two main points: (1) how to analyze the curve change caused by CO injection and (2) how to determine the kinetic parameters of *HER* in CO-free, CO-injected, and CO-stopped solution.

2. Results

2.1. Variation of the Open Circuit Potential with Time

To detect a variation of the open circuit potential, $E_{ocp}(t)$, the experiments were simulated in three environments:

Environment (I): 0.5 mol dm^{-3} H_2SO_4 solution saturated with H_2 only (abbreviation; H_2 + H_2SO_4 solution; as a reference);

Environment (II): the above H_2SO_4 solution injected with continuous CO bubbling (abbreviation; H_2 + H_2SO_4 + CO solution; as CO-contaminated solution);

Environment (III): the above H_2SO_4 solution when the CO-injection was stopped (abbreviation; H_2 + H_2SO_4 + CO-CO solution; as CO-restored solution).

An arrival time to the steady state by monitoring the $E_{ocp}(t)$ was investigated. The result is shown in Figure 1.

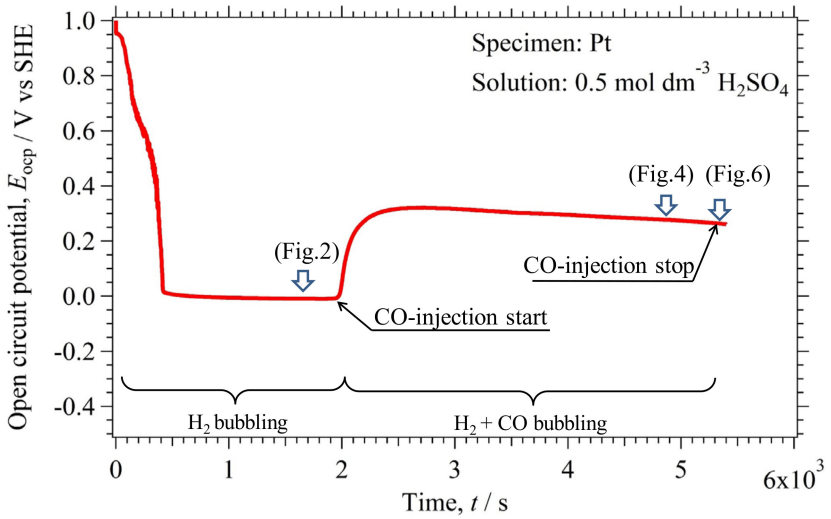

Figure 1. Time variation of the open circuit potential, $E_{ocp}(t)$ is measured in a 0.5 mol dm^{-3} H_2SO_4 solution continuously bubbled with H_2 and CO. At three arrow points, $E(j)$ was measured.

The E_{ocp} showing $\approx$ 1.0 V sharply descended to 0.0 V when the H_2 bubbling was started. The steady state showing $E_{ocp} = 0.0$ V was obtained in the period of 0.5 ks $\lesssim t \lesssim$ 2 ks. The $E_{ocp}(t \gtrsim 2$ ks$)$ increased to $\approx$0.34 V at start of CO injection and decreased to $\approx$0.25 V at the gradual stop of CO injection. In this experiment, it was found that the steady state condition is obtained at $t \gtrsim 4$ ks for the environment (I), 3 ks $\lesssim t \lesssim 5$ ks for the environment (II), and $t > 5.4$ ks for the environment (III).

2.2. $E_{exp}(j)$ and $h_{exp}(j)$

The polarization curves, $E_{exp}(j)$, in the above three solutions were measured at the immersion periods of 1.7 ks for environment (I), 4.9 ks for environment (II), and 5.4 ks for environment (III). Their polarization resistance curves, $h_{exp}(j)$ $(= \mathrm{d}\, E_{exp}(j)/\mathrm{d}\, j)$, were calculated using the finite difference method in a software.

2.2.1. $E_{exp}(j)$ and $h_{exp}(j)$ in the Environment (I)

Figure 2 shows the voltammogram (CV with seven cycles) curves in the H_2 + H_2SO_4 solution.

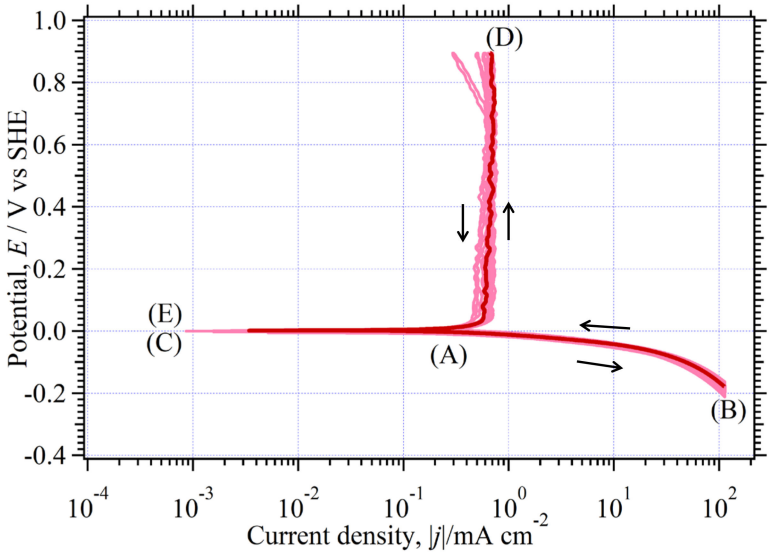

Figure 2. Seven-cycled CV curves (pink fine) of Pt electrode in a 0.5 mol dm^{-3} H_2SO_4 solution bubbled with H_2 are shown. The bold dark red curve as a representative is mathematically smoothed. It will be employed for analysis.

The starting point is (A), and the finishing point is (E). The potential-reverse operation is carried out at points of (B) and (D). We can see that $E_{exp}(j)$ follow same route and formed no hysteresis loop. The dark red curve of (B)–(C)–(D) was selected for analysis as a representative. Figure 3 shows that its $h_{exp}(j)$ is drawn in a deep blue bold line together with the experimental $h_{exp}(j)$ (sky blue fine).

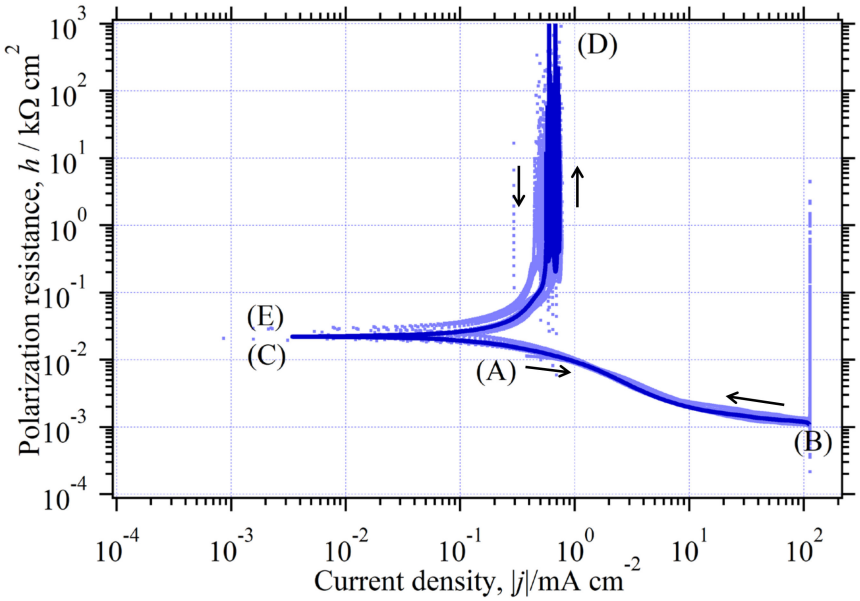

Figure 3. A representative $h_{exp}(j)$ (deep blue fine) and the experimental $h_{exp}(j)$ (sky blue fine), which were obtained by differentiating the $E_{exp}(j)$ in Figure 2.

The important readings in Figures 2 and 3 are summarized in Table 1. Symbols used in this paper are shown and explained in Appendix A.

Table 1. Experimental readings of $E(0)$ in Figure 2 and $h_{\mathrm{exp}}(0)$, $w_{\mathrm{c}}\, j_{\mathrm{H^+,L}}$, $w_{\mathrm{a}}\, j_{\mathrm{H_2,L}}$, and l/κ in Figure 3.

Item	Reading	Remarks
$E(0)$/ V vs. SHE	0	(C) and (E) in Figure 2
$h_{\mathrm{exp}}(0)/\mathrm{k\Omega\ cm^2}$	2.2×10^{-2}	(C) and (E) in Figure 3, $\approx \left[h_{\mathrm{exp}}\left(\lesssim 10^{-3}\right)\right]$
$\left\lvert w_{\mathrm{c}}\, j_{\mathrm{H^+,L}}\right\rvert/\mathrm{mA\ cm^{-2}}$	$10^2 <$	we cannot observe it in Figure 3
$w_{\mathrm{a}}\, j_{\mathrm{H_2,L}}/\mathrm{mA\ cm^{-2}}$	≈ 0.7	vertical line having (D) in Figures 2 and 3
$(l/\kappa)_{\mathrm{c}}/\mathrm{k\Omega\ cm^2}$	$\approx 10^{-3}$	asymptotic horizontal line; $\lesssim$(B) in Figure 3

A question will occur to readers that it is impossible to read the value of $h_{\mathrm{exp}}(0)$ in logarithm expression. The above answer is that the $h_{\mathrm{exp}}(0) \approx h_{\mathrm{exp}}\left(\lesssim 10^{-3}\right)$ is acceptable because the $h_{\mathrm{exp}}\left(\lesssim 10^{-3}\right)$ is almost horizontal line. We can see that the j at (D) is $\approx$0.7 mA cm^{-2}, which is related to the limiting anodic current density of H_2. We cannot observe the j relating to the limiting cathodic current density of H^+ due to the over-scaled value.

2.2.2. $E_{\mathrm{exp}}(j)$ and $h_{\mathrm{exp}}(j)$ in the Environment (II)

Similarly, the $E_{\mathrm{exp}}(j)$ and its $h_{\mathrm{exp}}(j)$ in the H_2 + H_2SO_4 + CO solution are shown in Figures 4 and 5, respectively.

Except for the first route of (F) $\rightarrow$ (G) (downward, red line), we can see that all curves (pink fine) repeat similar hysteresis loop of (G) $\rightarrow$ (H) $\rightarrow$ (I) $\rightarrow$ (J) $\rightarrow$ (K)(or (G)) $\rightarrow$ (L) (or (H)) $\rightarrow$ (I). The representative tracks of (G) $\rightarrow$ (H) $\rightarrow$ (I) (upward, green line) and (I) $\rightarrow$ (J) $\rightarrow$ (K) (downward, blue line) are shown with their bold colors. Characteristic readings appeared on Figures 4 and 5 are summarized in Table 2.

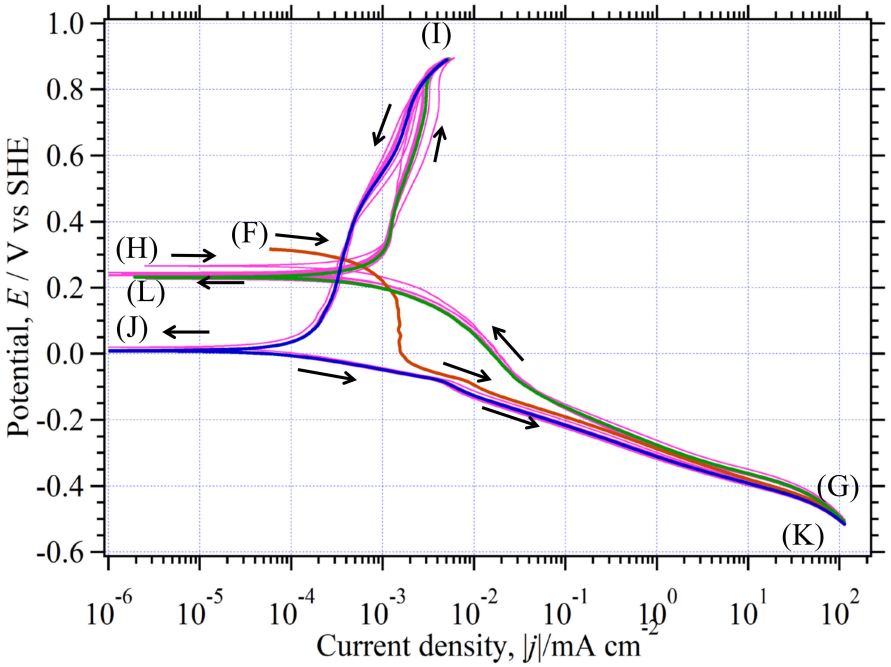

Figure 4. Seven-cycled $E_{\mathrm{exp}}(j)$ (pink and fine) in a 0.5 mol dm^{-3} H_2SO_4 solution bubbled with H_2 and CO. The red, green, and blue $E_{\mathrm{exp}}(j)$ are representative curves for analysis.

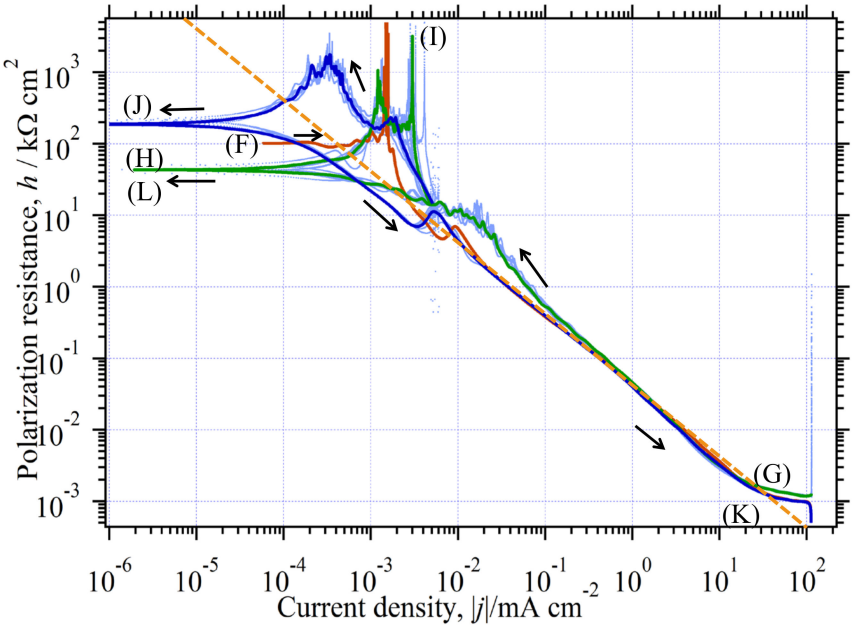

Figure 5. The $h_{\mathrm{exp}}(j)$ (sky blue; experimental curves) together with their representative curves (red, green, and blue bold curves corresponding to Figure 4). The orange dashed line with the Tafel slope is shown as a reference.

Table 2. Experimental readings in Figures 4 and 5 are shown. Explanations of items and symbols are shown in Section 3.9 and Appendix A.

Item	Reading	Remarks
$E(0)$/ V vs. SHE	0.24	(H) or (L) in Figure 4
	0.02	(J) in Figure 4
$h_{\mathrm{exp}}(0)$/kΩ cm^2	≈43	(H) or (L) in Figure 5
	≈190	(J) in Figure 5
$\left\|w_{\mathrm{c1}}\, j_{\mathrm{H^+,L}}\right\|$/mA cm^{-2}	$10^2 <$	we cannot observe it in Figure 5
$\|w_{\mathrm{c2}}\, j_{\mathrm{CO_2,L}}\|$/mA cm^{-2}	1.3×10^{-3}	red vertical line in Figure 5
$w_{\mathrm{a5}}\, j_{\mathrm{H_2,L}} + w_{\mathrm{a2}}\, j_{\mathrm{CO_{ad},L}}$/mA cm^{-2}	1.3×10^{-3}	green vertical line in Figure 5
$(w_{\mathrm{a2}} + w_{\mathrm{a5}})\, j_{\mathrm{H_2,L}} + w_{\mathrm{a4}}\, j_{\mathrm{CO_{ad},L}}$/mA cm^{-2}	3×10^{-3}	green vertical line in Figure 5
$(l/\kappa)_{\mathrm{c}}$/kΩ cm^2	≈10^{-3}	asymptotic line; (G) or (K) in Figure 5

2.2.3. $E_{\mathrm{exp}}(j)$ and $h_{\mathrm{exp}}(j)$ in the Environment (III)

The results in the H_2 + H_2SO_4 + CO-CO solution are shown in Figure 6 for $E_{\mathrm{exp}}(j)$ and Figure 7 for $h_{\mathrm{exp}}(j)$.

The complex shape of $E_{\mathrm{exp}}(j)$ in Figure 5 has disappeared, and the similar shape of Figure 1 appears. Close observation on $E_{\mathrm{exp}}(j)$ leads to an interesting fact that there is open loop in upward and close loop in downward. The $h_{\mathrm{exp}}(j)$ also shows complex shape, but there are two remarkable points: (1) the crowded route of $(\mathrm{P}) \rightarrow (\mathrm{Q}) \rightarrow (\mathrm{R})$ in Figure 7 is almost similar to the route of $(\mathrm{B}) \rightarrow (\mathrm{C}) \rightarrow (\mathrm{D})$ in Figure 3, and (2) the first line of $(\mathrm{M}) \rightarrow (\mathrm{N})$, on which the Tafel slope was satisfied, was disappeared and gathered into $(\mathrm{Q}) \rightarrow (\mathrm{R})$ after several CV. Characteristic readings appeared in Figures 4 and 5 are summarized in Table 3.

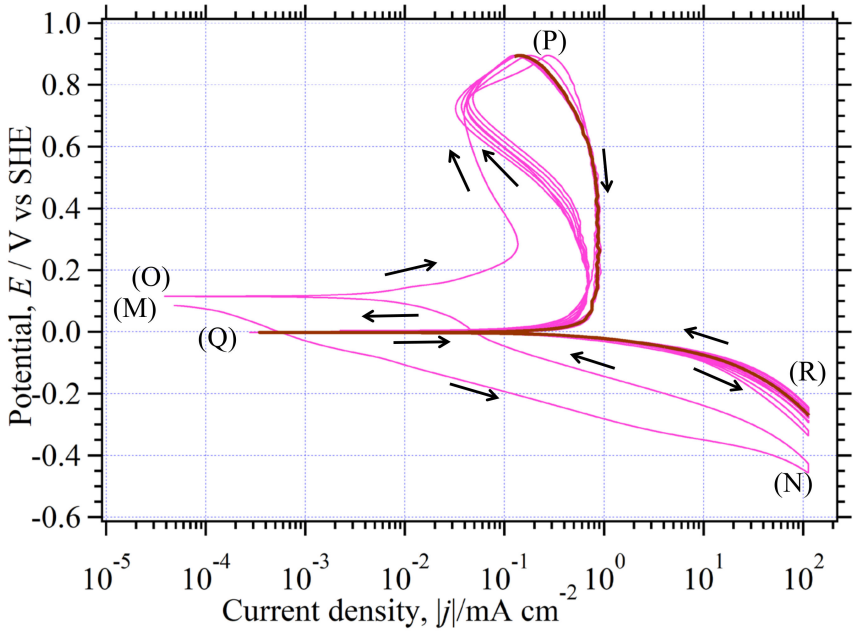

Figure 6. Changes of $E_{\mathrm{exp}}(j)$ (pink fine line) and the smoothed ones (bold red curve, a representative) when the CO injection was stopped.

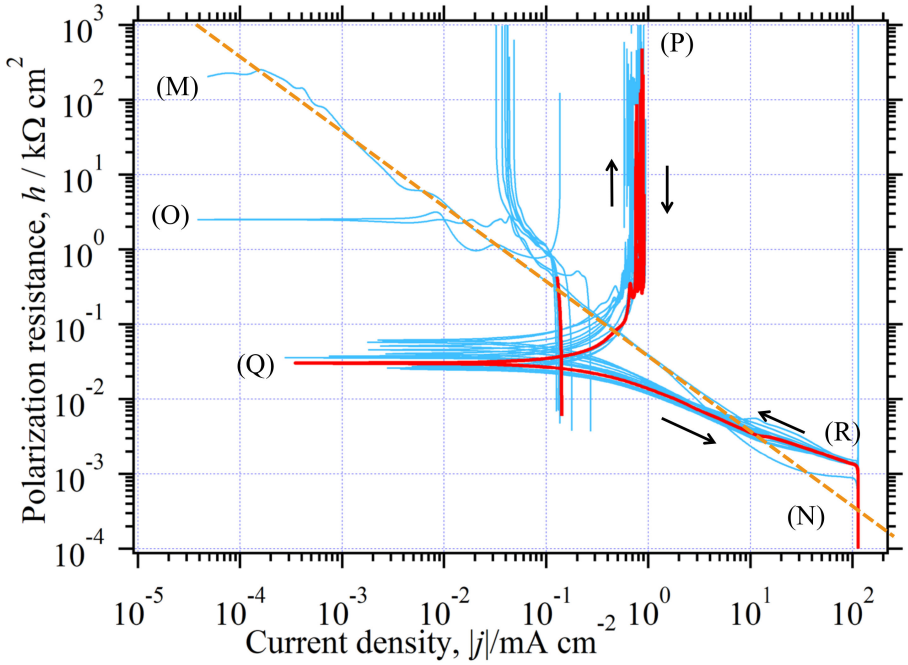

Figure 7. All $E_{\mathrm{exp}}(j)$ (blue fine line) are obtained by differentiating all $E_{\mathrm{exp}}(j)$ in Figure 6. The $h_{\mathrm{exp}}(j)$ as a representative is dawn with bold red. The orange dashed line with the Tafel slope is shown as a reference.

Table 3. Experimental readings in Figures 2 and 3.

Item	Reading	Remarks
$E(0)$/ V vs. SHE	≈ 0	(Q) in Figure 6
$h_{\mathrm{exp}}(0)$/kΩ cm^2	0.03 $\sim$ 0.06	(Q) in Figure 7
$\left\|w_{\mathrm{c}}\, j_{\mathrm{H^+,L}}\right\|$/mA cm^{-2}	$10^2 <$	we cannot observe it in Figure 3
$w_{\mathrm{a}}\, j_{\mathrm{H_2,L}}$/mA cm^{-2}	0.6 $\sim$ 0.9	vertical line having (P) in Figure 7
$(l/\kappa)_{\mathrm{c}}$/kΩ cm^2	$\approx 10^{-3}$	asymptotic horizontal line; (B) in Figure 7

3. Discussion

3.1. Single Electrode Reaction and Its Classification

The single electrode reaction is basic redox reaction in electrochemical field. In this paper, it is expressed as:

$$\mathrm{Red} \rightleftarrows \mathrm{Ox}^{z+} + \mathrm{ze}^{-}. \tag{1}$$

The Nernst equation for the above is expressed as:

$$E_{\mathrm{eq}} = E^{\varnothing} + \frac{R\,T}{z\,F} \ln \frac{\left[\mathrm{Ox}^{z+}\right]_{\mathrm{bulk}}}{[\mathrm{Red}]_{\mathrm{bulk}}} \tag{2}$$

When electrons are pumped up or into the system, the equilibrium state is lost. Consequently, the equilibrium potential, E_{eq} changes to a new E_{eq}. The difference between applied potential, E and the E_{eq} is the overpotential, η:

$$\eta = E - E_{\mathrm{eq}} \tag{3}$$

Applying η to the system, a net current, j is observed. The curve plotting between j and η is the polarization curve, $j(\eta)$. When charge transfer and diffusion transfer processes simultaneously occur, the $j(\eta)$ is expressed to [27]:

$$j(\eta) = \frac{\exp(f_{\mathrm{a}}\eta) - \exp(-f_{\mathrm{c}}\eta)}{1/j_0 + \exp(f_{\mathrm{a}}\eta)/j_{\mathrm{Red,L}} + \exp(-f_{\mathrm{c}}\eta)/-j_{\mathrm{Ox}^{z+},\mathrm{L}}} = j_{\mathrm{a}}(\eta) + j_{\mathrm{c}}(\eta), \tag{4}$$

where the $j_{\mathrm{a}}(\eta)$ and $j_{\mathrm{c}}(\eta)$ are the anodic and cathodic branch current density, respectively:

$$j_{\mathrm{a}}(\eta) = \frac{\exp(f_{\mathrm{a}}\eta)}{1/j_0 + \exp(f_{\mathrm{a}}\eta)/j_{\mathrm{Red,L}} + \exp(-f_{\mathrm{c}}\eta)/-j_{\mathrm{Ox}^{z+},\mathrm{L}}} \ (>0), \tag{5}$$

$$j_{\mathrm{c}}(\eta) = \frac{-\exp(-f_{\mathrm{c}}\eta)}{1/j_0 + \exp(f_{\mathrm{a}}\eta)/j_{\mathrm{Red,L}} + \exp(-f_{\mathrm{c}}\eta)/-j_{\mathrm{Ox}^{z+},\mathrm{L}}} \ (<0) \tag{6}$$

The $j_{\mathrm{a}}(0)$, total exchange current density is expressed as the reciprocal of the summation of the reciprocals of j_0, $j_{\mathrm{Red,L}}$, and $-j_{\mathrm{Ox}^{z+},\mathrm{L}}$:

$$j_{\mathrm{a}}(0) = -j_{\mathrm{c}}(0) = \frac{1}{1/j_0 + 1/j_{\mathrm{Red,L}} + 1/-j_{\mathrm{Ox}^{z+},\mathrm{L}}} \tag{7}$$

Therefore, the $j_{\mathrm{a}}(0)$ is a harmonic mean among j_0, $j_{\mathrm{Red,L}}$, and $-j_{\mathrm{Ox}^{z+},\mathrm{L}}$. Its value has a tendency to be close to the minimum value among them. The $j_{\mathrm{Red,L}}$ and $j_{\mathrm{Ox}^{z+},\mathrm{L}}$ are shortened into j_{d} in this paper:

$$j_{\mathrm{d}} = \frac{1}{1/j_{\mathrm{Red,L}} + 1/-j_{\mathrm{Ox}^{z+},\mathrm{L}}} \tag{8}$$

Then, Equation (7) is simplified as below:

$$j_{\mathrm{a}}(0) = \frac{1}{1/j_0 + 1/j_{\mathrm{d}}} \tag{9}$$

In order to simplify the complicated Equation (4), it is convenient to divide $j(\eta)$ into three approximations by considering relationship between j_0 and j_{d}.

(A) Reversible reaction; $j_0 \gg j_{\mathrm{d}}$ (or $j_{\mathrm{a}}(0) \approx j_{\mathrm{d}}$);
(B) Irreversible reaction; $j_0 \ll j_{\mathrm{d}}$ (or $j_{\mathrm{a}}(0) \approx j_0$);
(C) Quasireversible reaction; $j_0 \approx j_{\mathrm{d}}$ (or $j_{\mathrm{a}}(0) \approx j_{\mathrm{d}}/2 \approx j_0/2$).

The above classification may be archaic, but it plays an important role in the $h(j)$ expression.

Note that, at the equilibrium state ($j = 0$ or $\eta = 0$), the following relationship holds:

$$j_{\mathrm{a}}(\eta) + j_{\mathrm{c}}(\eta) = 0, \tag{10}$$

$$\eta = E - E_{\mathrm{eq}} = \left(E - E^{\varnothing}\right) + \left(E^{\varnothing} - E_{\mathrm{eq}}\right) = \eta^{\varnothing} - \frac{R\,T}{z\,F} \ln \frac{\left[\mathrm{Ox}^{z+}\right]_{\mathrm{bulk}}}{[\mathrm{Red}]_{\mathrm{bulk}}} \tag{11}$$

Substituting them into Equation (4), we can obtain same Equation (2). The same result shows that the Nernst equation is a special case of $j(\eta)$.

3.2. Single Electrode Reaction and Its Polarization Resistance

Polarization curve has been frequently employed as a simple and basic electrochemical method to elucidate reaction mechanism. Usually, the polarization curve has been expressed using two functions: $j(\eta)$ and $E(j)$. The former, $j(\eta)$, is possible for direct plotting using measuring data. It has a decided merit that current can be superposed. The latter, $E(j)$, is also commonly used, which is obtained by exchanging between the horizontal and vertical axes in $j(\eta)$. Having same vertical axis with potential scale, there is a superiority that $E(j)$ is easy to compare with the Tafel equation. Furthermore, its advantage will be clarified when predicting thermodynamically stable chemical species and their possible reaction by referring to the *E*-pH diagram. In addition to the above two expressions, we have another expression: polarization resistance curve, $h(j)$. The $h(j)$ is not so familiar, but it is possible to express the system. The great advantage of it lies in reduction of parameters, which must be experimentally determined. For example, overpotential, which is not so easy to determine in experimentally, is disappeared due to its constant value. As a result, the $h(j)$ tends to be a concise expression. These curves have very different forms, but mathematically, they are exactly the same and are interchangeable.

$$j(\eta) \rightleftarrows E(j) \rightleftarrows \begin{cases} \mathrm{d}E(j)/\mathrm{d}j = h(j) \\ E(0) = E_{\mathrm{eq}} \text{ (one initial condition)} \end{cases} \tag{12}$$

Detailed expressions of $h(j)$ are shown below. Differentiating Equation (4), we can obtain polarization conductance, $g(\eta)$:

$$g(\eta) = \frac{\mathrm{d}\,j(\eta)}{\mathrm{d}\,\eta} = \frac{\mathrm{d}\,\left(j_{\mathrm{a}}(\eta) + j_{\mathrm{c}}(\eta)\right)}{\mathrm{d}\,\eta} = g_{\mathrm{a}}(\eta) + g_{\mathrm{c}}(\eta) = f_{\mathrm{a}}\,j_{\mathrm{a}}(\eta) - f_{\mathrm{c}}\,j_{\mathrm{c}}(\eta) - j(\eta)\left\{\frac{f_{\mathrm{a}}\,j_{\mathrm{a}}(\eta)}{j_{\mathrm{Red,L}}} + \frac{f_{\mathrm{c}}\,j_{\mathrm{c}}(\eta)}{-j_{\mathrm{Ox}^{z+},\mathrm{L}}}\right\} \tag{13}$$

where,

$$g_{\mathrm{a}}(\eta) = \frac{\mathrm{d}j_{\mathrm{a}}(\eta)}{\mathrm{d}\eta} = f_{\mathrm{a}}\,j_{\mathrm{a}}(\eta) - j_{\mathrm{a}}(\eta)\left\{\frac{f_{\mathrm{a}}\,j_{\mathrm{a}}(\eta)}{j_{\mathrm{Red,L}}} + \frac{f_{\mathrm{c}}\,j_{\mathrm{c}}(\eta)}{-j_{\mathrm{Ox}^{z+},\mathrm{L}}}\right\}, \tag{14}$$

$$g_{\mathrm{c}}(\eta) = \frac{\mathrm{d}j_{\mathrm{c}}(\eta)}{\mathrm{d}\eta} = -f_{\mathrm{c}}\,j_{\mathrm{c}}(\eta) - j_{\mathrm{c}}(\eta)\left\{\frac{f_{\mathrm{a}}\,j_{\mathrm{a}}(\eta)}{j_{\mathrm{Red,L}}} + \frac{f_{\mathrm{c}}\,j_{\mathrm{c}}(\eta)}{-j_{\mathrm{Ox}^{z+},\mathrm{L}}}\right\} \tag{15}$$

Using the inverse function relation between $g(\eta)$ and $h(j)$, the below will be obtained:

$$\frac{\mathrm{d}\,j}{\mathrm{d}\,\eta}\frac{\mathrm{d}\,\eta}{\mathrm{d}\,j} = g(\eta)\frac{\mathrm{d}\,\left(E(j) - E_{\mathrm{eq}}\right)}{\mathrm{d}\,j} = g(\eta)\frac{\mathrm{d}\,E(j)}{\mathrm{d}\,j} = g(\eta)\,h(j) = 1. \tag{16}$$

The $g(\eta)$ is a function of η, but the $h(j)$ is a function of j. In order to express the $g(\eta)$ as a function of j, all of $j(\eta)$, $j_{\mathrm{a}}(\eta)$, and $j_{\mathrm{c}}(\eta)$ must be expressed as a function of j. Using the Maclaurin expand series, they are approximated to the linear relations:

$$j(\eta) = j(0) + \tfrac{j'(0)}{1!}\eta + \tfrac{j''(0)}{2!}\eta^2 + \cdots \approx g(0)\,\eta = g(0)\,h(0)\,j = j, \tag{17}$$

$$j_{\mathrm{a}}(\eta) = j_{\mathrm{a}}(0) + \tfrac{j_{\mathrm{a}}{}'(0)}{1!}\eta + \tfrac{j_{\mathrm{a}}''(0)}{2!}\eta^2 + \cdots \approx j_{\mathrm{a}}(0) + g_{\mathrm{a}}(0)\,\eta = j_{\mathrm{a}}(0) + \tfrac{g_{\mathrm{a}}(0)}{g_{\mathrm{a}}(0)+g_{\mathrm{c}}(0)}\,j, \tag{18}$$

$$j_c(\eta) = j_c(0) + \frac{j_c'(0)}{1!}\eta + \frac{j_c''(0)}{2!}\eta^2 + \cdots \approx j_c(0) + g_c(0)\,\eta = j_c(0) + \frac{g_c(0)}{g_a(0)+g_c(0)}\,j \tag{19}$$

By arranging the $\frac{g_a(0)}{g_a(0)+g_c(0)}$ and $\frac{g_c(0)}{g_a(0)+g_c(0)}$, $j_a(j)$, and $j_c(j)$ are expressed as:

$$j_a(j) = j_a(0) + \left\{\alpha_a - \left(\frac{\alpha_a\, j_a(0)}{j_{Red,L}} + \frac{\alpha_c\, j_c(0)}{-j_{Ox^{z+},L}}\right)\right\} j, \tag{20}$$

$$j_c(j) = j_c(0) + \left\{\alpha_c + \left(\frac{\alpha_a\, j_a(0)}{j_{Red,L}} + \frac{\alpha_c\, j_c(0)}{-j_{Ox^{z+},L}}\right)\right\} j. \tag{21}$$

Then, the $h(j)$ can be expressed as:

$$h(j) = \frac{1}{f_a\, j_a(j) - f_c\, j_c(j) - j\left\{f_a j_a(j)/j_{Red,L} + f_c\, j_c(j)/-j_{Ox^{z+},L}\right\}}. \tag{22}$$

At the equilibrium state ($j = 0$), common expression of $h(0)$ is obtained:

$$h(0) = \frac{1}{f_a\, j_a(0) - f_c\, j_c(0)} = \frac{1}{(f_a + f_c) j_a(0)} = \frac{RT}{z\,F}\frac{1}{j_a(0)} = \frac{0.026}{z}\frac{1}{j_a(0)} \tag{23}$$

We can see that the $h(0)$ is inversely proportional to $j_a(0)$ and has a constant of $0.026/z$. In other words, the above equation tells that the $j_a(0)$ will be easily calculated by reading the $h(0)$ when the z is already known. Around the equilibrium state ($j \approx 0$), $h(j)$ can be approximated to linear relation:

$$[h(j)]_{j\approx 0} = h(0)\left\{1 + \left(\frac{2\,\alpha_a}{j_{Red,L}} + \frac{2\,\alpha_c}{j_{Ox^{z+},L}} + \frac{1-2\,\alpha_a}{j_a(0)}\right) j\right\}. \tag{24}$$

We can see that the $[h(j)]_{j\approx 0}$ is a straight line having an intercept of $h(0)$ and a slope of $h(0)\left(\frac{2\,\alpha_a}{j_{Red,L}} + \frac{2\,\alpha_c}{j_{Ox^{z+},L}} + \frac{1-2\,\alpha_a}{j_a(0)}\right)$.

Being in a far polarized state ($|\eta| \gg 0$), information for each branch reaction can be obtained. The kinetic parameters for anodic branch will be obtained when the system is anodically far-polarized ($\eta \gg 0$):

$$j = j_a(j) + j_c(j) \approx j_a(j) \text{ (or } j_c(j) \approx 0). \tag{25}$$

Let j_{pa} be the minimum $j_a(j)$ in the above state. The polarization resistance curve for anodic branch, $h_{a-branch}(j_a)$, will be expressed by arranging Equation (22):

$$h_{a-branch}(j_a) = h_{a-branch}(j) = [h(j)]_{j_c(j)\approx 0} \approx \frac{1}{f_a\, j - j\,\{f_a j/j_{Red,L}\}} = \frac{RT}{\alpha_a\, z\, F}\left(\frac{1}{j} + \frac{1}{j_{Red,L} - j}\right). \tag{26}$$

The second term in the above will be close to zero if j is sufficiently large:

$$\left[\frac{RT}{\alpha_a\, z\, F}\frac{1}{j_{Red,L} - j}\right]_{j_{pa}\ll j} = \left[\frac{0.026}{\alpha_a\, z}\frac{1}{j_{Red,L} - j}\right]_{j_{pa}\ll j} \approx 0. \tag{27}$$

Then, Equation (26) is approximated to:

$$[h(j)]_{j_{pa}\ll j} \approx \frac{RT}{\alpha_a\, z\, F}\frac{1}{j} = \frac{0.026}{\alpha_a\, z}\frac{1}{j}. \tag{28}$$

Arranging the above, the $\alpha_a\, z$ can be calculated as:

$$\alpha_a\, z \approx \left[\frac{0.026}{h(j)\, j}\right]_{j_{pa}\ll j} (j > 0). \tag{29}$$

Similarly, information on the cathodic branch will be obtained when the system is cathodically far-polarized ($\eta \ll 0$):

$$j = j_a(j) + j_c(j) \approx j_c(j) \text{ (or } j_a(j) \approx 0). \tag{30}$$

Let j_{pc} be the maximum $j_c(j)$ in the above state. Then, the polarization resistance curve for cathodic branch, $h_{c-branch}(j_c)$ can be obtained:

$$h_{c-branch}(j_c) = h_{c-branch}(j) = [h(j)]_{j_a(j)\approx 0} \approx \frac{1}{-f_c\, j - j\left\{f_c j / -j_{Ox^{z+},L}\right\}} = \frac{RT}{\alpha_c\, z\, F}\left(\frac{1}{-j} + \frac{1}{j - j_{Ox^{z+},L}}\right). \tag{31}$$

For sufficiently large $-j$ ($j < 0$), the second term will be close to zero:

$$\left[\frac{RT}{\alpha_c\, z\, F}\frac{1}{j - j_{Ox^{z+},L}}\right]_{j \ll j_{pc}} = \left[\frac{0.026}{\alpha_c\, z}\frac{1}{j - j_{Ox^{z+},L}}\right]_{j \ll j_{pc}} \approx 0. \tag{32}$$

Then, Equation (31) is approximated to:

$$[h(j)]_{j \ll j_{pc}} \approx \frac{RT}{\alpha_c\, z\, F}\left(\frac{1}{-j}\right) = \frac{0.026}{\alpha_c\, z\, F}\left(\frac{1}{-j}\right). \tag{33}$$

The $\alpha_c\, z$ can be calculated as:

$$\alpha_c\, z \approx \left[\frac{0.026}{h(j)\ |j|}\right]_{|j_{pc}| \ll |j|} (j < 0) \tag{34}$$

Each of j_{pa} and j_{pc} will be expressed by arranging Equations (20), (21), (25) and (30):

$$j_{pa} = \left(\frac{\alpha_c}{j_a(0)} + \frac{\alpha_a}{j_{Red,L}} - \frac{\alpha_c}{-j_{Ox^{z+},L}}\right)^{-1}, \tag{35}$$

$$j_{pc} = -\left(\frac{\alpha_a}{j_a(0)} - \frac{\alpha_a}{j_{Red,L}} + \frac{\alpha_c}{-j_{Ox^{z+},L}}\right)^{-1}. \tag{36}$$

When we can find two inflection points on the curve, a very interesting relationship between Equations (35) and (36) is shown as:

$$\frac{1}{j_a(0)} = \frac{1}{j_{pa}} + \frac{1}{-j_{pc}}. \tag{37}$$

The same equation had been already established by J.M. Pearson in 1942 in the corrosion field [28].

3.3. The Relationship between the Tafel Extrapolation Method (tem) and H(j)

The Tafel equation is an empirical equation showing the relationship between η (usually, $|\eta| \gg 0$) and j. It is expressed as:

$$\eta = a + b \log|j| = a + \frac{b}{2.3} \ln|j|. \tag{38}$$

Naturally, it is possible to express the Tafel equation in differential form:

$$\frac{\mathrm{d}\,\eta}{\mathrm{d}\,j} = \frac{\mathrm{d}\left(E(j) - E_{eq}\right)}{\mathrm{d}\,j} = \frac{\mathrm{d}\,E(j)}{\mathrm{d}\,j} = h(j) = \frac{b}{2.3}\frac{1}{|j|}. \tag{39}$$

We can see that the above is inverse-proportional to $|j|$ and has a constant of $b/2.3$. Taking the logarithm, the following is obtained:

$$\log h(j) = \log \frac{b}{2.3} - \log|j|. \tag{40}$$

The above expression can give us a clear guide when finding the Tafel region: (1) the differentiated Tafel equation has a linear relationship between the $\log h(j)$ and $\log|j|$, and (2) its straight line always has slope of -1. Namely, the linear slope region observed on $\log h(j)$ vs. $\log|j|$ curve exactly corresponds to the Tafel slope region, and vice versa.

$$\frac{\mathrm{d}\log h(j)}{\mathrm{d}\log|j|} = -1 \;\leftrightarrows\; \text{Tafel slope.} \tag{41}$$

The existence of this straight line is extremely helpful in finding the Tafel slope region and in determining its accurate value.

The graphical representation of $h(j)$ brings direct benefits to our understanding. Example data shown in Table 4 were employed to draw the $h(j)$ curves.

Table 4. Example data for graphical representation for three classified reactions are shown: (A) reversible, (B) irreversible, and (C) quasireversible reactions.

Item	$j(\eta) = \frac{\exp(f_a\eta)-\exp(-f_c\eta)}{1/j_0+\exp(f_a\eta)/j_{\mathrm{Red,L}}+\exp(-f_c\eta)/-j_{\mathrm{Ox^{z+},L}}}$			Remarks
	(A): Reversible	**(B): Irreversible**	**(C): Quasi-Reversible**	
	$(j_0 \gg j_d)$	$(j_0 \ll j_d)$	$(j_0 \approx j_d)$	
$j_{\mathrm{Red,L}}/\mathrm{mAcm^{-2}}$	1	1	1	
$j_{\mathrm{Ox^{z+},L}}/\mathrm{mAcm^{-2}}$	−100	−100	−100	
$j_d/\mathrm{mAcm^{-2}}$	0.99	0.99	0.99	$j_d = \frac{1}{1/j_{\mathrm{Red,L}}+1/-j_{\mathrm{Ox^{z+},L}}}$
$j_0/\mathrm{mAcm^{-2}}$	1000	0.001	1	
$\alpha_a\ (-)$	0.3	0.3	0.3	
$\alpha_c\ (-)$	0.7	0.7	0.7	
$z\ (-)$	2	2	2	
$j_a(0)/\mathrm{mAcm^{-2}}$	0.989	0.000989	0.497	$j_a(0) = \frac{1}{1/j_0+1/j_d}$
$h(0)/\mathrm{mAcm^{-2}}$	0.013	13	0.026	

The $j(\eta)$ of the above three reactions are shown in Figure 8 for reference.

We can see a general tendency that (1) the $j_{\mathrm{Red,L}}$ and $j_{\mathrm{Ox^{z+},L}}$ indicate the upper and lower limit, respectively; (2) the $j_a(0)$ relates to the awayness between $j_a(\eta)$ and $j_c(\eta)$ (not depicted); and (3) the α_a and α_c affect the symmetry of the curve. The quasireversible $j(\eta)$ is located between reversible and irreversible and slightly closer to the reversible. This close position is thought to be the reason why "quasi" was given. To illustrate the benefits of the $h(j)$ expression, each curve is shown in Figure 9 using the same data in Table 3.

The straight lines concerning Equation (41) are drawn with three orange dashed lines. We can see that the Tafel slope are visually held in the wider anodic branch (5×10^{-3} mA cm^{-2} $\lesssim j \lesssim$ 10^{-1} mA cm^{-2}) and the widest cathodic branch (3×10^{-2} mA cm^{-2} $\lesssim |j| \lesssim$ 10 mA cm^{-2}) for irreversible reaction (blue). The Tafel slope for the quasireversible reaction (green) is satisfied in the narrow cathodic region ($\approx$ 12 mA cm^{-2}). In the case of reversible $h(j)$ (red), we can see that the Tafel slope is valid for only one point ($\approx$ 6 mA cm^{-2}). The curve of $\log h(j)$ vs. $\log|j|$ clarified that the TEM is eminently valid for irreversible reaction.

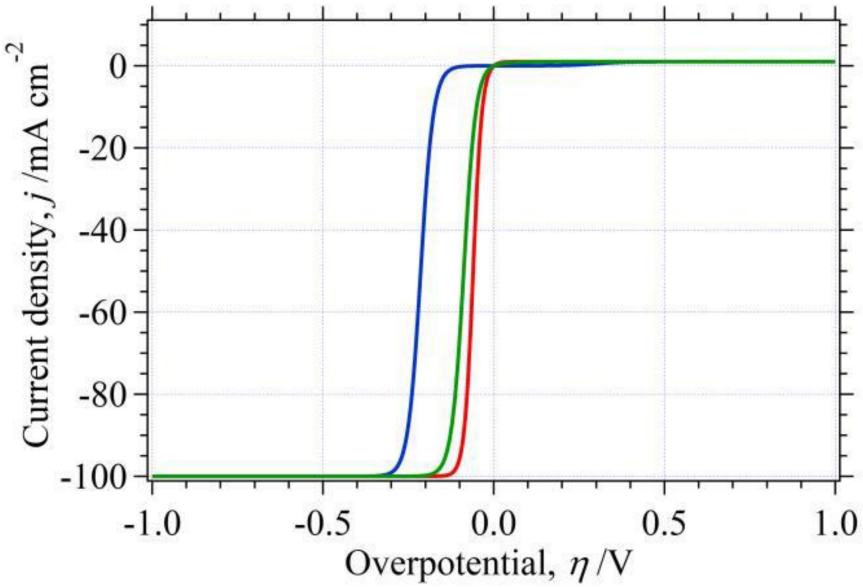

Figure 8. Three $j(\eta)$ curves corresponding to the three-classified reaction: (A) reversible, (B) irreversible, and (C) quasireversible reactions are drawn using data in Table 4.

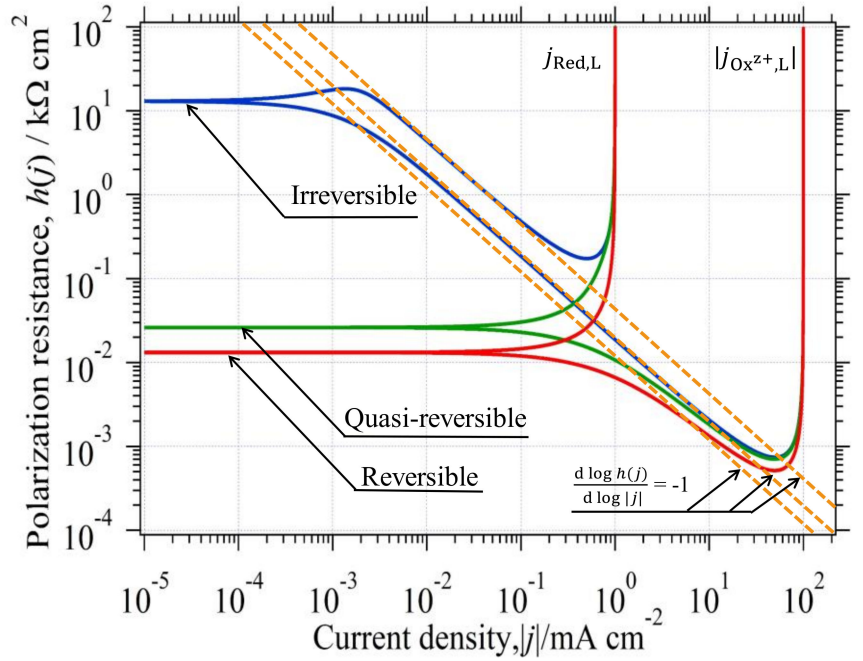

Figure 9. Curves of $\log h(j)$ vs. $\log|j|$ for three classified reactions are drawn for the graphical explanation. The same data listed in Table 3 are employed. For reference, three orange dashed lines with Tafel slope of -1 are shown.

3.4. Kinetic Parameter Determination Using $h(j)$

Since graphical $j(\eta)$ can be classified into the above three reactions, $h(j)$ can also be classified into the three.

3.4.1. Reversible Reaction

The $j_a(j)$ and $j_c(j)$ of the reversible reaction are simplified to the below by arranging Equations (20) and (21), respectively:

$$j_a(j) = j_d + \frac{j_{Red,L}}{j_{Red,L} - j_{Ox^{z+},L}} j = j_d \left(1 + \frac{j}{-j_{Ox^{z+},L}}\right), \tag{42}$$

$$j_c(j) = -j_d + \frac{-j_{Ox^{z+},L}}{j_{Red,L} - j_{Ox^{z+},L}} j = -j_d \left(1 + \frac{j}{j_{Red,L}}\right). \tag{43}$$

Substituting them into Equation (22), we can obtain the reversible $h(j)$.

$$h(j) = \frac{RT}{z\,F}\left(\frac{1}{j_{Red,L} - j} + \frac{1}{j - j_{Ox^{z+},L}}\right). \tag{44}$$

At the equilibrium state ($j = 0$),

$$h(0) = \frac{RT}{z\,F}\left(\frac{1}{j_{Red,L}} + \frac{1}{-j_{Ox^{z+},L}}\right) = \frac{0.026}{z}\frac{1}{j_d}\left(= \frac{0.026}{z}\frac{1}{j_a(0)}\right). \tag{45}$$

If we can read the three values ($h(0)$, $j_{Red,L}$, and $j_{Ox^{z+},L}$) from experiments, we can easily determine z. If that is impossible or ambiguous, there is another way to know it: a curve technique, which is known as the parallel displacement in geometry. The following simultaneous equation discloses the technique:

$$h(j + j_{Red,L}) = \frac{RT}{z\,F}\left(\frac{1}{-j} + \frac{1}{j + j_{Red,L} - j_{Ox^{z+},L}}\right), \tag{46}$$

$$\frac{RT}{z\,F}\frac{1}{j + j_{Red,L} - j_{Ox^{z+},L}} \approx 0. \tag{47}$$

Substituting the precondition (Equation (47)) into Equation (46), the below equation is obtained:

$$h(j + j_{Red,L}) \approx \frac{RT}{z\,F}\frac{1}{-j} = \frac{0.026}{z\,|j|}(j < 0). \tag{48}$$

We can see that the above has an inverse proportional relation between $h(j)$ and $|j|$, which has the same relation as Equation (39). From the above, we can determine the z:

$$z = \frac{0.026}{|j|h(j + j_{Red,L})}\ (j < 0). \tag{49}$$

Similarly, the same displacement for another side will lead to the same z:

$$z = \frac{0.026}{j\,h\left(j + j_{Ox^{z+},L}\right)} = \frac{0.026}{|j|h\left(j + j_{Ox^{z+},L}\right)}(j > 0). \tag{50}$$

Around the equilibrium state ($j \approx 0$), the reversible $h(j)$ is linearly expressed to:

$$[h(j)]_{j\approx 0} = h(0)\left\{1 + \left(\frac{1}{j_{Red,L}} + \frac{1}{j_{Ox^{z+},L}}\right)j\right\}. \tag{51}$$

Arranging Equations (42) and (43), j_{pa} and j_{pc} will be expressed as:

$$j_{pa} = j_{Red,L} \tag{52}$$

$$j_{pc} = j_{Ox^{z+},L} \tag{53}$$

We can see that Equation (37) holds true in the reversible system.

3.4.2. Irreversible Reaction

Considering $j_0 \ll j_d$, the $j_a(j)$ and $j_c(j)$ are simplified below:

$$j_a(j) = j_0 + \left\{ \alpha_a - j_0 \left(\frac{\alpha_a}{j_{Red,L}} + \frac{-\alpha_c}{-j_{Ox^{z+},L}} \right) \right\} j \approx j_0 + \alpha_a\, j, \tag{54}$$

$$j_c(j) = j_0 + \left\{ \alpha_c + j_0 \left(\frac{\alpha_a}{j_{Red,L}} + \frac{-\alpha_c}{-j_{Ox^{z+},L}} \right) \right\} j \approx -j_0 + \alpha_c\, j. \tag{55}$$

Substituting them into Equation (22), we can obtain the irreversible $h(j)$.

$$\begin{aligned} h(j) &= \frac{j_{Red,L}\, j_{Ox^{z+},L}}{f_c(j - j_0)\left(j - j_{Ox^{z+},L}\right) j_{Red,L} + f_a\, j_0\, j_{Ox^{z+},L}(\, j_{Red,L} - j) + \alpha_a\, j \left\{ f_c\, (\, j_{Ox^{z+},L} - j)\, j_{Red,L} + f_a\, j_{Ox^{z+},L}(\, j_{Red,L} - j) \right\}} \\ &\approx \frac{RT}{z\,F} \frac{1}{j_0 + (\alpha_a - \alpha_c)\, j} = \frac{0.026}{z} \frac{1}{j_0 + (\alpha_a - \alpha_c)\, j}. \end{aligned} \tag{56}$$

At the equilibrium state ($j = 0$),

$$h(0) = \frac{1}{f}\frac{1}{j_0} = \frac{RT}{z\,F}\frac{1}{j_0} = \frac{0.026}{z}\frac{1}{j_0}\left(= \frac{0.026}{z}\frac{1}{j_a(0)} \right). \tag{57}$$

Around the equilibrium state ($j \approx 0$), $h(j)$ is linearly expressed as:

$$[h(j)]_{j \approx 0} = h(0)\left\{ 1 + \left(\frac{\alpha_a}{j_{Red,L}} + \frac{\alpha_c}{j_{Ox^{z+},L}} + \frac{1 - 2\,\alpha_a}{j_0} \right) j \right\}. \tag{58}$$

At anodically far polarized state ($\eta \gg 0$, or $j \approx j_a$, or $j_c \approx 0$, or $j_{pa} < j$), anodic $h(j)$ of the irreversible reaction is expressed:

$$[h(j)]_{\eta \gg 0} = \frac{RT}{\alpha_a\, z\, F}\left(\frac{1}{j} + \frac{1}{j_{Red,L} - j} \right). \tag{59}$$

The second term above will be close to zero when $(j_{Red,L} - j) \gg 0$:

$$\frac{RT}{\alpha_a\, z\, F}\left(\frac{1}{j_{Red,L} - j} \right) \approx 0, \tag{60}$$

Then, Equation (59) is simplified to:

$$[h(j)]_{\eta \gg 0} \approx \frac{RT}{\alpha_a\, z\, F}\left(\frac{1}{j} \right) = \frac{0.026}{\alpha_a\, z}\left(\frac{1}{j} \right). \tag{61}$$

Similarly, when being cathodically far polarized ($\eta \ll 0$, or $j \approx j_c$, or $j_a \approx 0$, or $j < j_{pc}$), $[h(j)]_{\eta \ll 0}$ is:

$$[h(j)]_{\eta \ll 0} = \frac{RT}{\alpha_c\, z\, F}\left(\frac{1}{-j} + \frac{1}{j - j_{Ox^{z+},L}} \right). \tag{62}$$

When the second term is close to zero:

$$\frac{RT}{\alpha_c\, z\, F}\left(\frac{1}{j - j_{Ox^{z+},L}} \right) \approx 0. \tag{63}$$

Then, the far cathodic $h(j)$ is expressed below, which is the same as Equation (33):

$$[h(j)]_{\eta \gg 0} = \frac{RT}{\alpha_c\, z\, F}\left(\frac{1}{-j}\right). \tag{64}$$

It is important to notice that irreversible z is the number of electrons transferred in the rate determine step (rds), not z of the whole reaction of Equation (1). Arranging Equations (54) and (55), j_{pa} and j_{pc} will be expressed as:

$$j_{pa} = j_0/\alpha_c \tag{65}$$

$$j_{pc} = -j_0/\alpha_a \tag{66}$$

We can see that the relation of Equation (37) holds true in the irreversible system.

3.4.3. Quasireversible Reaction

The $j_a(j)$ and $j_c(j)$ are expressed as:

$$j_a(j) = \frac{j_d}{2} + \left\{\alpha_a - \frac{j_d}{2}\left(\frac{\alpha_a}{j_{Red,L}} + \frac{\alpha_c}{j_{Ox^{z+},L}}\right)\right\} j, \tag{67}$$

$$j_c(j) = \frac{-j_d}{2} + \left\{\alpha_c + \frac{j_d}{2}\left(\frac{\alpha_a}{j_{Red,L}} + \frac{\alpha_c}{j_{Ox^{z+},L}}\right)\right\} j. \tag{68}$$

Substituting them into Equation (22), we can obtain the quasireversible:

$$h(j) = \frac{2\, j_{Red,L}\, j_{Ox^{z+},L}\left(j_{Ox^{z+},L} - j_{Red,L}\right)}{\alpha_a\, j\, \left(j_{Ox^{z+},L} - j_{Red,L}\right)\left\{ f_c\, j_{Red,L}\left(j_{Ox^{z+},L} - j\right) + f_a\, j_{Ox^{z+},L}\left(\, j_{Red,L} - j\right)\right\} + \left(j - j_{Ox^{z+},L}\right) j_{Red,L}\left\{f_a\, j_{Ox^{z+},L}(j - j_{Red,L}) + f_c\left(2\, j\, j_{Ox^{z+},L} - j\, j_{Red,L} - j_{Red,L}\, j_{Ox^{z+},L}\right)\right\}} \tag{69}$$

The above equation has little practical use due to its overcomplicated expression. Another expression is needed for quasireversible $h(j)$, which will be discussed in detail in Section 3.6.3. At the equilibrium state ($j = 0$):

$$h(0) = \frac{RT}{z\, F}\frac{2}{j_d}\left(= \frac{RT}{z\, F}\frac{2}{j_0}\right) = \frac{0.052}{z}\frac{}{j_d}\left(= \frac{0.052}{z\, j_0}\right) = \left(\frac{0.026}{z}\frac{1}{j_a(0)}\right). \tag{70}$$

Each of j_{pa} and j_{pc} will be expressed as:

$$j_{pa} = \left(\frac{\alpha_c}{j_d} + \frac{1}{j_{Red,L}}\right)^{-1} = \left(\frac{1+\alpha_c}{j_{Red,L}} + \frac{\alpha_c}{-j_{Ox^{z+},L}}\right)^{-1} \tag{71}$$

$$j_{pc} = -\left(\frac{\alpha_a}{j_d} + \frac{1}{-j_{Ox^{z+},L}}\right)^{-1} = -\left(\frac{\alpha_a}{j_{Red,L}} + \frac{1+\alpha_a}{-j_{Ox^{z+},L}}\right)^{-1} \tag{72}$$

It can be seen that the relationship in Equation (37) is satisfied in the quasireversible reaction. Since Equations (23) and (37) are valid for all reactions, the follow is a common relation:

$$j_a(0) = \frac{R\, T}{z\, F}\frac{1}{h(0)} = \frac{0.026}{z\, h(0)} = \frac{1}{1/j_{pa} + 1/ - j_{pc}}. \tag{73}$$

3.5. Graphical Determination of $j_a(0)$

In addition to the above algebraic way, it is worth glancing at the geometric way. This section shows that the reason why the graphical estimation of $j_a(0)$ is possible and how to use it. The common $h(0)$ at the equilibrium state is expressed as:

$$h(0) = \frac{R\,T}{z\,F}\frac{1}{j_a(0)} = \frac{0.026}{z}\left(\frac{1}{j_0} + \frac{1}{j_{\mathrm{Red,L}}} + \frac{1}{-\,j_{\mathrm{Ox}^{z+},\mathrm{L}}}\right). \tag{74}$$

We can regard the $h(0)$ as a function of j_0 because three value of z, $j_{\mathrm{Red,L}}$, and $j_{\mathrm{Ox}^{z+},\mathrm{L}}$ are usually constant. Here, let us consider the new function, $h_{a0}(j_0)$, which can be expressed below:

$$h_{a0}(j_0) = \frac{0.026}{z}\left(\frac{1}{j_0} + \frac{1}{j_{\mathrm{Red,L}}} + \frac{1}{-\,j_{\mathrm{Ox}^{z+},\mathrm{L}}}\right) = \frac{0.026}{z}\left(\frac{1}{j_0} + \frac{1}{j_d}\right). \tag{75}$$

Using the above relation, each $h_{a0}(j_0)$ in the (A), (B), and (C) is shown as:

$$[h_{a0}(j_0)\,]_{j_0 \gg j_d} \simeq \frac{0.026}{z}\left(\frac{1}{j_{\mathrm{Red,L}}} + \frac{1}{-\,j_{\mathrm{Ox}^{z+},\mathrm{L}}}\right) = \frac{0.026}{z}\left(\frac{1}{j_d}\right) : \text{ constant for reversible;} \tag{76}$$

$$[h_{a0}(j_0)\,]_{j_0 \ll j_d} \approx \frac{0.026}{z}\left(\frac{1}{j_0}\right) : \text{ variable for irreversible;} \tag{77}$$

$$[h_{a0}(j_0)\,]_{j_0 \approx j_d} \approx \left[\frac{0.026}{z}\left(\frac{1}{j_0} + \frac{1}{j_{0d}}\right)\right]_{j_0 \approx j_d} = \frac{0.052}{z\,j_0}\left(= \frac{0.052}{z\,j_d}\right) : \text{ variable for quasireversible} \tag{78}$$

The curves of Equations (76)–(78) are shown with pink chain line in Figure 10 together with the $h(j)$ in Figure 9.

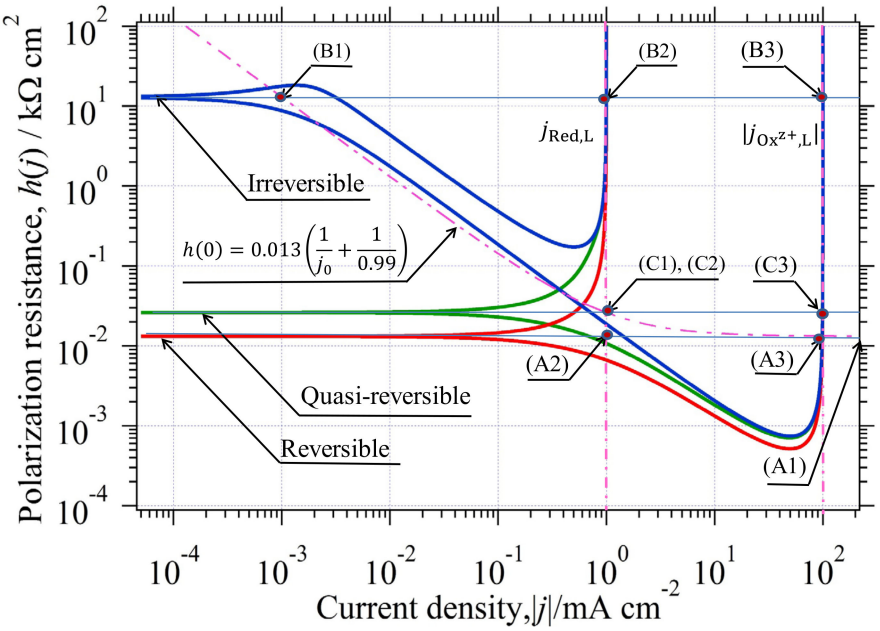

Figure 10. The $\log h(j)$ vs. $\log|\,j|$ of the (A), (B), and (C) are shown for the graphical estimation.

The $h_{a0}(j_0)$, which is a function of j_0, is drawn in pink with a chain curve. The employed data for drawings are the same data shown in Table 3. Three pink chain lines of $j_{\mathrm{Red,L}}$ and $\left|j_{\mathrm{Ox}^{z+},\mathrm{L}}\right|$ are added for easy readings.

The $h_{a0}(j_0)$ curve and vertical lines of $j_{\mathrm{Red,L}}$ and $\left|j_{\mathrm{Ox}^{z+},\mathrm{L}}\right|$ are shown in Figure 10 with a pink chain curve. In the irreversible reaction, the horizontal straight line of

$h(0)(=13\ \mathrm{k\Omega\ cm^2})$ meets the $h_{a0}(j_0)$ at a point (B1) and two vertical lines of $j_{\mathrm{Red,L}}$ and $\left|j_{\mathrm{Ox}^{z+},\mathrm{L}}\right|$ at (B2) and (B3), respectively. Three crossed points can be graphically read as:

$$j_0 \approx 10^{-3}\ \mathrm{mA\ cm^{-2}}:\ \text{cross point (B1)} \tag{79}$$

$$j_{\mathrm{Red,L}} = 1\ \mathrm{mA\ cm^{-2}}:\ \text{cross point (B2)} \tag{80}$$

$$-\,j_{\mathrm{Ox}^{z+},\mathrm{L}} = 100\ \mathrm{mA\ cm^{-2}}:\ \text{cross point (B3)} \tag{81}$$

Substituting the above readings into Equation (7), we can calculate the $j_a(0)$:

$$j_a(0) = \frac{1}{1/j_0 + 1/\ j_{\mathrm{Red,L}} + 1/-\ j_{\mathrm{Ox}^{z+},\mathrm{L}}} = \frac{1}{1/(\approx 10^{-3}) + 1/1 + 1/100} \approx 10^{-3}\ \mathrm{mA\ cm^{-2}}\ (= j_0). \tag{82}$$

Employing the $j_a(0)$ and the $h(0)$, the z can be confirmed:

$$z = \frac{RT}{F}\frac{1}{j_a(0)\ h(0)} = \frac{0.026}{(10^{-3})(13)} = 2. \tag{83}$$

Similarly, we can obtain the reversible $j_a(0)$ by reading three crossed points of (A1), (A2), and (A3):

$$j_0 \to \infty : \cong \text{(A1)},\ \text{the } h(0) \text{ never crosses the Equation (75) curve, but is asymptotic to it.} \tag{84}$$

$$j_{\mathrm{Red,L}} = 1\ \mathrm{mA\ cm^{-2}}:\ \text{cross point (A2)}. \tag{85}$$

$$-\,j_{\mathrm{Ox}^{z+},\mathrm{L}} = 100\ \mathrm{mA\ cm^{-2}}:\ \text{cross point (A3)}. \tag{86}$$

Then,

$$j_a(0) = \frac{1}{1/(\infty) + 1/(1) + 1/(+100)} \approx 0.99\ \mathrm{mA\ cm^{-2}}\ (= j_d). \tag{87}$$

Using the above, the z is calculated:

$$z = \frac{RT}{F}\frac{1}{j_a(0)\ h(0)} = \frac{0.026}{(0.99)(0.013)} \approx 2. \tag{88}$$

For the quasireversible reaction, the crossed points are (C1), (C2), and (C3):

$$j_0 \approx 1\ \mathrm{mA\ cm^{-2}}:\ \text{cross point (C1)} \tag{89}$$

$$j_{\mathrm{Red,L}} = 1\ \mathrm{mA\ cm^{-2}}:\ \text{cross point (C2)} \tag{90}$$

$$-\,j_{\mathrm{Ox}^{z+},\mathrm{L}} = 100\ \mathrm{mA\ cm^{-2}}:\ \text{cross point (C3)} \tag{91}$$

Then,

$$j_a(0) = \frac{1}{1/(\approx 1) + 1/(1) + 1/(+100)} \approx 0.498\ \mathrm{mA\ cm^{-2}}\left(\approx \frac{j_d}{2}\right). \tag{92}$$

Therefore,

$$z = \frac{RT}{F}\frac{1}{j_a(0)\ h(0)} = \frac{0.026}{(0.498)(0.026)} \approx 2. \tag{93}$$

As was so often the case after experiments had finished, one of $j_{\mathrm{Red,L}}$ or $j_{\mathrm{Ox}^{z+},\mathrm{L}}$ may be lost or cannot be read with clarity. In this case, graphical estimation is particularly helpful. No appearance of $j_{\mathrm{Red,L}}$ or $\left|j_{\mathrm{Ox}^{z+},\mathrm{L}}\right|$ usually means that their contribution to Equation (7) can be neglected due to the characteristic of harmonic mean. In short, the larger value is smaller or neglectable contribution.

3.6. Physical Factors Influenced on $h(j)$

The physical factors such as effective area and solution resistance sometimes distort $E(j)$ and always prevent us from quantitative approach. The following two factors are important and discussed in this paper.

3.6.1. Effective Area of Electrode

As a matter of fact, what was actually obtained in the experiments was always the total net current, $J(\eta)$. It consists of the anodic branch current, $J_a(\eta)$, and cathodic branch current, $J_c(\eta)$, expressed as:

$$J(\eta) = J_a(\eta) + J_c(\eta). \tag{94}$$

Using the geometric surface of the electrode, S, the $J(\eta)$ is normalized to the net current density, $j(\eta)$:

$$j(\eta) = J(\eta)/S. \tag{95}$$

When, for instance, gas adsorption layers or reaction deposits are present on the electrode surface, the effective area for the reaction will shrink. The $j(\eta)$ having $J_a(\eta)$ with the effective anode area, S_a, and $J_c(\eta)$ with the effective cathode area, S_c, it is arranged and expressed as:

$$j(\eta) = \frac{J_a(\eta) + J_c(\eta)}{S} = \frac{S_a\, j_a(\eta)}{S} + \frac{S_c\, j_c(\eta)}{S} = w_a\, j_a(\eta) + w_c\, j_c(\eta) = j_A(\eta) + j_C(\eta), \tag{96}$$

$$j_A(\eta) = \frac{w_a \exp(f_a\eta)}{1/j_0 + \exp(f_a\eta)/j_{Red,L} + \exp(-f_c\eta)/-j_{Ox^{z+},L}} \ (>0), \tag{97}$$

$$j_C(\eta) = \frac{-w_c \exp(-f_c\eta)}{1/j_0 + \exp(f_a\eta)/j_{Red,L} + \exp(-f_c\eta)/-j_{Ox^{z+},L}} \ (<0). \tag{98}$$

where, the $w_a(=S_a/S)$ and $w_c(=S_c/S)$ are weighting factors that have suitably weighted values in proportion to the surface of anode and cathode, respectively ($0 < w_a,\ w_c \leq 1$) [29]. The $j_A(\eta)$ and $j_C(\eta)$ are effective anodic and cathodic branch current density, respectively. It is important to note that $E(0)$ when $w_a \neq w_c$ is different from $E(0)$ when $w_a = w_c(=1)$. When the overpotential having $w_a \neq w_c$ is termed as η_w, the equilibrium state is expressed as:

$$j(\eta_w) = j_A(\eta_w) + j_C(\eta_w) = 0. \tag{99}$$

Arranging the above,

$$\frac{w_a}{w_c} = \frac{-j_c(\eta_w)}{j_a(\eta_w)} = \frac{\exp(-f_c\,\eta_w)}{\exp(f_a\,\eta_w)} = \exp(-f\,\eta_w). \tag{100}$$

The above shows that the relation between w_a/w_c and η_w is mutually dependent and restricted by the above equation. Taking into account w_a/w_c, Equation (22) is arranged and expressed as:

$$h(j) = \frac{1}{g_A(\eta) + g_C(\eta)} = \frac{1}{f_a\, j_A(j) - f_c\, j_C(j) - j\left\{\frac{f_a\, j_A(j)}{w_a\, j_{Red,L}} + \frac{f_c\, j_C(j)}{-w_c\, j_{Ox^{z+},L}}\right\}}, \tag{101}$$

where

$$g_A(\eta) = \frac{\mathrm{d}\, j_A(\eta)}{\mathrm{d}\,\eta} = f_a\, j_A(j) - j_A(j)\left\{\frac{f_a\, j_A(j)}{w_a\, j_{Red,L}} + \frac{f_c\, j_C(j)}{-w_c\, j_{Ox^{z+},L}}\right\}, \tag{102}$$

$$g_C(\eta) = \frac{\mathrm{d}\, j_C(\eta)}{\mathrm{d}\,\eta} = -f_c\, j_C(j) - j_C(j)\left\{\frac{f_a\, j_A(j)}{w_a\, j_{Red,L}} + \frac{f_c\, j_C(j)}{-w_c\, j_{Ox^{z+},L}}\right\}, \tag{103}$$

$$j(\eta) = j(\eta_w) + \frac{j'(\eta_w)}{1\,!}(\eta - \eta_w) + \frac{j''(\eta_w)}{2\,!}(\eta - \eta_w)^2 + \cdots \approx g(\eta_w)\,(\eta - \eta_w) = j, \tag{104}$$

$$j_A(j) \approx j_A(\eta_w) + \frac{g_A(\eta_w)}{g_A(\eta_w)+g_C(\eta_w)}\, j = j_A(\eta_w) + \left\{\alpha_a - \left(\frac{\alpha_a\, j_A(\eta_w)}{w_a\, j_{Red,L}} + \frac{\alpha_c\, j_C(\eta_w)}{-w_c\, j_{Ox^{z+},L}}\right)\right\} j\,, \quad (105)$$

$$j_C(j) \approx j_C(\eta_w) + \frac{g_C(\eta_w)}{g\, g_A(\eta_w)+g_C(\eta_w)}\, j = j_C(\eta_w) + \left\{\alpha_c + \left(\frac{\alpha_a\, j_A(\eta_w)}{w_a\, j_{Red,L}} + \frac{\alpha_c\, j_C(\eta_w)}{-w_c\, j_{Ox^{z+},L}}\right)\right\} j \quad (106)$$

The $h(0)$ is expressed as:

$$h(0) = \frac{1}{f_a\, j_A(\eta_w) - f_c\, j_C(\eta_w)} = \frac{1}{f\, j_A(\eta_w)} = \frac{RT}{z\,F}\frac{1}{j_A(\eta_w)}\left(= \frac{RT}{z\,F}\frac{1}{-j_C(\eta_w)}\right). \quad (107)$$

The $[h(j)]_{j\approx 0}$ is approximated to the linear relation:

$$[h(j)]_{j\approx 0} = h(0)\left\{1 + \left(\frac{2\,\alpha_a}{w_a\, j_{Red,L}} + \frac{2\,\alpha_c}{w_c\, j_{Ox^{z+},L}} + \frac{1-2\,\alpha_a}{j_A(\eta_w)}\right) j\right\}. \quad (108)$$

where,

$$j_A(\eta_w) = -j_C(\eta_w) = w_a\, j_a(\eta_w) = -w_c\, j_c(\eta_w) = \frac{{w_a}^{\alpha_c}\, {w_c}^{\alpha_a}}{1/j_0 + \left(\frac{w_c}{w_a}\right)^{\alpha_a}/\, j_{Red,L} + \left(\frac{w_a}{w_c}\right)^{\alpha_c}/\left(-j_{Ox^{z+},L}\right)}. \quad (109)$$

We can see that the $[h(j)]_{j\approx 0}$ is approximated to a straight line having an intercept of $h(0)$ and a slope of $h(0)\left(\frac{2\,\alpha_a}{w_a\, j_{Red,L}} + \frac{2\,\alpha_c}{w_c\, j_{Ox^{z+},L}} + \frac{1-2\,\alpha_a}{j_A(\eta_w)}\right)$.

Graphical representation is helpful to see the influence of w_a/w_c on the $h(j)$ shape. Employing reversible reaction data in Table 3, three reversible $j(\eta)$ curves were drawn as an example. Reversible $j(\eta)$, having ratios of $w_a/w_c = 1$ (as a reference), $w_a/w_c = 0.1/0.9$, and $w_a/w_c = 0.6/0.8$, are shown in Figure 11. Their $h(j)$ are shown in Figure 12.

We can see that not only the $j(\eta)$ but also $h(j)$ is strongly influenced by the w_a/w_c ratio. Equation (100) will be useful when estimating the w_a/w_c ratio. It is necessary to pay careful attention when determining the kinetic parameters using the reversible $[h(j)]_{j\approx 0}$. Namely, graphical determination of α_a and α_c of reversible reaction is very difficult. The reason is that the line slope when $w_a/w_c = 1$ and 0.75 (= 0.6/0.8) is too small to determine. Even if it were possible, a 4–5 decimal place reading is needed for accurate determination.

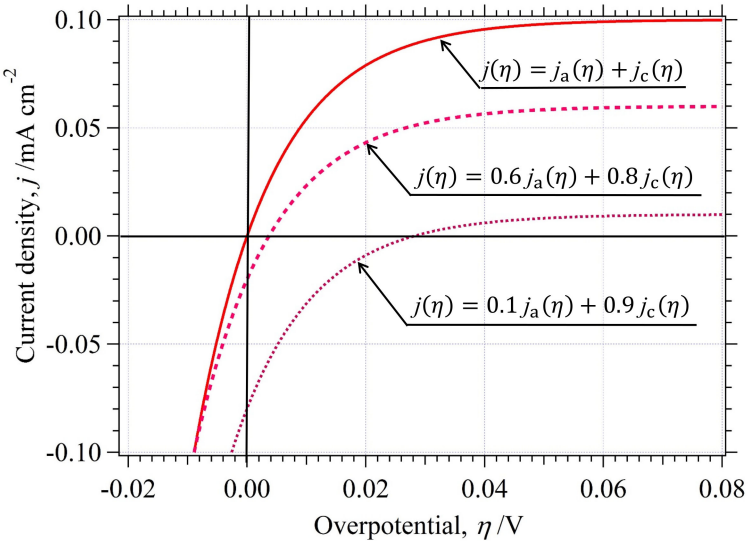

Figure 11. Influence of $\eta(w)$ on the shape of reversible $j(\eta)$ curve having various ratios of w_a/w_c; $w_a/w_c = 1$ (as a reference), 0.1/0.9, and 0.6/0.8 are shown.

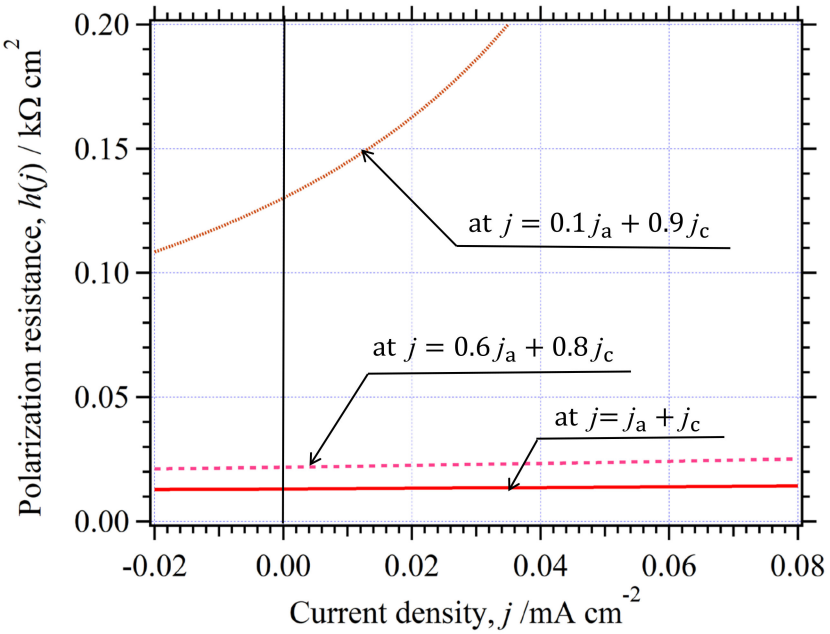

Figure 12. Influence of $h(j)$ on the shape of reversible $j(\eta)$ curve having various ratios of w_a/w_c.

In the case of the irreversible system having $w_a/w_c \neq 1$, the information on the anodic branch will be possible when being in a far polarized state ($|\eta| \gg 0$):

$$j = j_A(j) + j_C(j) \approx j_A(j) \text{ (or } j_C(j) \approx 0). \tag{110}$$

Let j_{pA} be the minimum $j_A(j)$ in the above state. The $h_{A-branch}(j_A)$ can be obtained:

$$h_{A-branch}(j_A) = h_{A-branch}(j) = [h(j)]_{j_{pA}<j} \approx \frac{1}{f_A\, j - j\,\{f_A\, j\,/(w_a\, j_{Red,L})\}} = \frac{RT}{\alpha_a\, z\, F}\left(\frac{1}{j} + \frac{1}{w_a\, j_{Red,L} - j}\right). \tag{111}$$

The second term will be close to zero when $(w_a\, j_{Red,L} - j) \gg 0$:

$$\left[\frac{RT}{\alpha_a\, z\, F}\frac{1}{w_a\, j_{Red,L} - j}\right]_{j_{pA}<j\ll w_a\ j_{Red,L}} = \left[\frac{0.026}{\alpha_a\, z}\frac{1}{w_a\, j_{Red,L} - j}\right]_{j_{pA}<j\ll w_a\ j_{Red,L}} \approx 0. \tag{112}$$

Then, Equation (111) is approximated as:

$$[h(j)]_{j_{pA}<j\ll w_a\ j_{Red,L}} \approx \frac{RT}{\alpha_a\, z\, F}\frac{1}{j} = \frac{0.026}{\alpha_a\, z}\frac{1}{j}. \tag{113}$$

The value of $\alpha_a\, z$ can be calculated by readings of $h(j)$ and j:

$$\alpha_a\, z \approx \left[\frac{0.026}{h(j)\, j}\right]_{j_{pA}<j\ll w_a\ j_{Red,L}} (j > 0). \tag{114}$$

Similarly, $\alpha_c\, z$ of the irreversible cathodic branch will be obtained when the system is cathodically far-polarized ($\eta \ll 0$):

$$j = j_A(j) + j_C(j) \approx j_C(j) \text{ (or } j_A(j) \approx 0). \tag{115}$$

Let j_{pC} be the maximum $j_C(j)$ in the above state. Then, the $h_{C-branch}(j_C)$ can be obtained:

$$h_{C-branch}(j_C) = h_{C-branch}(j) = [h(j)]_{j<j_{pC}} \approx \frac{1}{-f_c\, j - j\left\{f_c\, j/\left(-w_c\, j_{Ox^{z+},L}\right)\right\}} = \frac{RT}{\alpha_c\, z\, F}\left(\frac{1}{-j} + \frac{1}{j - w_c\, j_{Ox^{z+},L}}\right). \tag{116}$$

When $\left(j - w_c\, j_{Ox^{z+},L}\right) \gg 0$, the second term will be close to zero:

$$\left[\frac{RT}{\alpha_c\, z\, F}\frac{1}{j - w_c\, j_{Ox^{z+},L}}\right]_{w_c\, j_{Ox^{z+},L} \ll j < j_{pC}} = \left[\frac{0.026}{\alpha_c\, z}\frac{1}{j - w_c\, j_{Ox^{z+},L}}\right]_{w_c\, j_{Ox^{z+},L} \ll j < j_{pC}} \approx 0. \quad (117)$$

Then, Equation (116) is approximated as:

$$[h(j)]_{w_c\, j_{Ox^{z+},L} \ll j < j_{pC}} \approx \frac{RT}{\alpha_c\, z\, F}\left(\frac{1}{-j}\right) = \frac{0.026}{\alpha_c\, z}\left(\frac{1}{-j}\right). \quad (118)$$

The value of $\alpha_c\, z$ can be calculated as:

$$\alpha_c\, z \approx \left[\frac{0.026}{h(j)\ |j|}\right]_{|j_{pC}| \langle |j| \ll |w_c\, j_{Ox^{z+},L}|} (j < 0). \quad (119)$$

It is important to notice that the w_a and w_c can influence diffusion currents ($j_{Red,L}$ and $j_{Ox^{z+},L}$) but not charge current (j_0). Arranging Equations (105), (106), (110), and (115), j_{pA} and j_{pC} will be expressed as:

$$j_{pA} = \left(\frac{\alpha_c}{j_A(\eta_w)} + \frac{\alpha_a}{w_a\, j_{Red,L}} - \frac{\alpha_c}{-w_c\, j_{Ox^{z+},L}}\right)^{-1}, \quad (120)$$

$$j_{pC} = \left(\frac{\alpha_a}{j_C(\eta_w)} - \frac{\alpha_a}{w_a\, j_{Red,L}} + \frac{\alpha_c}{-w_c\, j_{Ox^{z+},L}}\right)^{-1}. \quad (121)$$

Each of j_{pA} and j_{pC} is graphically characterized as inflection points on $h(j)$. We can obtain the relationship between j_{pA} and j_{pC} from Equations (120) and (121):

$$\frac{1}{j_A(\eta_w)} = \frac{1}{j_{pA}} + \frac{1}{-j_{pC}} \quad (122)$$

We can see that the above relation is essentially same as Equation (37).

3.6.2. Solution Resistance

In the practical analyses, all $h(j)$ must be compensated with physical factors such as oxide film resistance and solution resistance. For instance, the cathodic branch $h(j)$ of the irreversible reaction must be compensated by oxide film resistance. It is expressed as:

$$[h(j)]_{j<j_{pC}} = \frac{0.026}{\alpha_c\, z}\left(\frac{1}{-j} + \frac{1}{j - w_c\, j_{Ox^{z+},L}}\right) + \left(\frac{l}{\kappa}\right)_f \quad (123)$$

The experimentally obtained curve always contains the solution resistance $(l/\kappa)_s$.

$$[h_{exp}(j)]_{j<j_{pC}} = [h(j)]_{j<j_{pC}} + \left(\frac{l}{\kappa}\right)_s = \frac{0.026}{\alpha_c\, z}\left(\frac{1}{-j} + \frac{1}{j - w_c\, j_{Ox^{z+},L}}\right) + \left(\frac{l}{\kappa}\right)_f + \left(\frac{l}{\kappa}\right)_s = \frac{0.026}{\alpha_c\, z}\left(\frac{1}{-j} + \frac{1}{j - w_c\, j_{Ox^{z+},L}}\right) + \left(\frac{l}{\kappa}\right)_c. \quad (124)$$

where, $(l/\kappa)_c$ is the total cathodic polarization resistance $(= (l/\kappa)_f + (l/\kappa)_s)$. The above consists of three terms: $\frac{0.026}{\alpha_c\, z}\left(\frac{1}{-j}\right)$, $\frac{0.026}{\alpha_c\, z}\left(\frac{1}{j - w_c\, j_{Ox^{z+},L}}\right)$, and $\left(\frac{l}{\kappa}\right)_c$. The first term is related to the charge transfer process; the second term, to the diffusion transfer process; and the third term, to the physical factor. Since the $(l/\kappa)_c$ is a constant value, it will graphically emerge as a horizontal line when $|j|$ becomes large:

$$[h_{exp}(j)]_{|j_{pC}| < (|j| \to \text{large})} = \left[\frac{0.026}{\alpha_c\, z}\left(\frac{1}{-j} + \frac{1}{j - w_c\, j_{Ox^{z+},L}}\right) + \left(\frac{l}{\kappa}\right)_c\right]_{|j| \to \text{large}} \gtrsim (l/\kappa)_c \quad (125)$$

Employing the above inequality, we can graphically estimate the value of $(l/\kappa)_c$ as a horizontal line (an asymptote line). In order to visualize the relation between $(l/\kappa)_c$ and the curve shape, the cathodic branch of the $h_{exp}(j)$ ($w_c = 1$) was drawn using example data of $(l/\kappa)_c = 10^{-3}, 10^{-2}$, and 10^{-1} kΩ cm^2. Their concrete expressions are shown below. Their curves are shown in Figure 13.

$$h_1(j) = [h_{C-branch}(j) + 0]_{|j|\to large} = \left[0.019\left(\frac{1}{-j} + \frac{1}{j+100}\right) + 0\right]_{|j|\to large} > 0 \text{ kΩ cm}^2 \quad (126)$$

$$h_2(j) = \left[h_{C-branch}(j) + 10^{-3}\right]_{|j|\to large} = \left[0.019\left(\frac{1}{-j} + \frac{1}{j+100}\right) + 10^{-3}\right]_{|j|\to large} > 10^{-3} \text{ kΩ cm}^2 \quad (127)$$

$$h_3(j) = \left[h_{C-branch}(j) + 10^{-2}\right]_{|j|\to large} = \left[0.019\left(\frac{1}{-j} + \frac{1}{j+100}\right) + 10^{-2}\right]_{|j|\to large} \gtrsim 10^{-2} \text{ kΩ cm}^2 \quad (128)$$

$$h_4(j) = \left[h_{C-branch}(j) + 10^{-1}\right]_{|j|\to large} = \left[0.019\left(\frac{1}{-j} + \frac{1}{j+100}\right) + 10^{-1}\right]_{|j|\to large} \cong 10^{-1} \text{ kΩ cm}^2 \quad (129)$$

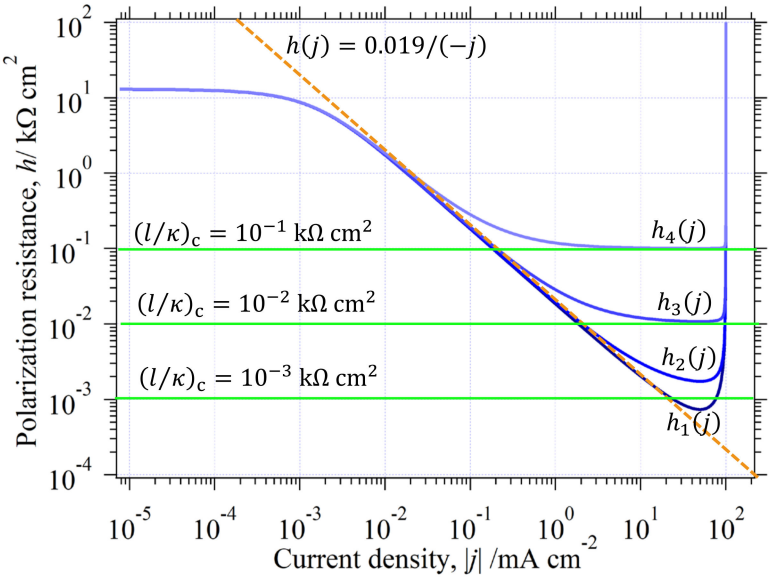

Figure 13. Influence of $(l/\kappa)_c$ on the shape of cathodic $h(j)$. There are four example curves with $(l/\kappa)_c = 0$ (as a blank), $10^{-3}, 10^{-2}$, and 10^{-1}kΩ cm^2. Orange dashed line of $h(j) = \frac{RT}{\alpha_c z F}\left(\frac{1}{-j}\right) = \frac{0.026}{(0.7)(2)}\left(\frac{1}{-j}\right) = 0.019\left(\frac{1}{-j}\right)$, on which the Tafel slope is satisfied, is added as a reference. All data for drawing are the same values listed in Table 1.

Examining the relation between the curve shape and the horizontal lines, we can see a clear tendency that the $h(j)$ curve with the larger $(l/\kappa)_c$ has the wider horizontal region. In addition to that, we can also see a tendency between $(l/\kappa)_c$ and the Tafel slope region; the larger $(l/\kappa)_c$, the narrower the Tafel slope region. The latter tendency gives us empirical advice that, to obtain the errorless Tafel parameters, we should employ an environment having scanty oxide film resistance and small electrolyte resistance. The above discussion is also valid for reversible and quasireversible reactions.

3.6.3. The $h_{exp}(j)$ in the Whole Current Range

When the curve shape of $h(j)$ largely depends on the degree of polarization, division of $h(j)$ is needed for accurate analysis. Using j_{pA} and j_{pC}, we can divide $h_{exp}(j)$ into three parts:

$$[h_{exp}(j)]_{j_{pA}<j<w_a\, j_{Red,L}} = h_{A-branch}(j) + (l/\kappa)_a = \frac{RT}{\alpha_a z F}\left(\frac{1}{j} + \frac{1}{w_a j_{Red,L} - j}\right) + (l/\kappa)_a \quad (130)$$

$$\left[h_{\exp}(j)\right]_{j_{\mathrm{pC}}\le j\le j_{\mathrm{pA}}} = [h(j)]_{j_{\mathrm{pC}}\le j\le j_{\mathrm{pA}}} + (l/\kappa) \tag{131}$$

$$\left[h_{\exp}(j)\right]_{w_{\mathrm{a}}\ j_{\mathrm{Red,L}}<j<j_{\mathrm{pC}}} = h_{\mathrm{C-branch}}(j) + (l/\kappa)_{\mathrm{c}} = \frac{RT}{\alpha_{\mathrm{c}}\ z\ F}\left(\frac{1}{-j} + \frac{1}{j-w_{\mathrm{c}}\ j_{\mathrm{Ox}^{z+},\mathrm{L}}}\right) + (l/\kappa)_{\mathrm{c}} \tag{132}$$

$[h(j)]_{j_{\mathrm{pC}}\le j\le j_{\mathrm{pA}}}$ in Equation (131) is almost identical to the $[h(j)]_{j\approx 0}$ in Equation (108), but we often encounter that the linear (the first order) approximation is graphically impossible. In this case, the second or third order approximation is necessary. Since the high-order approximation generally becomes complicated, the use of $[h(j)]_{j_{\mathrm{pC}}\le j\le j_{\mathrm{pA}}}$ will be helpful and effective. Its content is detailed as:

$$[h(j)]_{j_{\mathrm{pC}}\le j\le j_{\mathrm{pA}}} = \frac{1}{\left(1/[h_{\mathrm{A}}(j)]_{j_{\mathrm{pC}}\le j\le j_{\mathrm{pA}}} + 1/[h_{\mathrm{C}}(j)]_{j_{\mathrm{pC}}\le j\le j_{\mathrm{pA}}}\right)}. \tag{133}$$

where the $[h_{\mathrm{A}}(j)]_{j_{\mathrm{pC}}\le j\le j_{\mathrm{pA}}}$ and $[h_{\mathrm{C}}(j)]_{j_{\mathrm{pC}}\le j\le j_{\mathrm{pA}}}$ is anodic and cathodic branch polarization resistance, respectively. They can be expressed by considering the following graphical relation:

$$[h_{\mathrm{A}}(j)]_{j_{\mathrm{pC}}\le j\le j_{\mathrm{pA}}} = \begin{cases} h_{\mathrm{A}}(j_{\mathrm{pA}}) = h(j_{\mathrm{pA}}) \\ h_{\mathrm{A}}(j_{\mathrm{pC}}) \to \infty \end{cases} \tag{134}$$

$$[h_{\mathrm{C}}(j)]_{j_{\mathrm{pC}}\le j\le j_{\mathrm{pA}}} = \begin{cases} h_{\mathrm{C}}(j_{\mathrm{pC}}) = h(j_{\mathrm{pC}}) \\ h_{\mathrm{C}}(j_{\mathrm{pA}}) \to \infty \end{cases} \tag{135}$$

Since $[h_{\mathrm{A}}(j)]_{j_{\mathrm{pC}}\le j\le j_{\mathrm{pA}}}$ is the deformed curve of $h_{\mathrm{A-branch}}(j_{\mathrm{A}})$ and $[h_{\mathrm{C}}(j)]_{j_{\mathrm{pC}}\le j\le j_{\mathrm{pA}}}$ is that of $h_{\mathrm{C-branch}}(j_{\mathrm{C}})$, the following expressions are available in the experimental reality:

$$[h_{\mathrm{A}}(j)]_{j_{\mathrm{pC}}\le j\le j_{\mathrm{pA}}} = \frac{RT}{\alpha_{\mathrm{a}}\ z\ F}\frac{w_{\mathrm{a}}\ j_{\mathrm{Red,L}}(j_{\mathrm{pA}}-j_{\mathrm{pC}})}{j_{\mathrm{pA}}(w_{\mathrm{a}}j_{\mathrm{Red,L}}-j_{\mathrm{pC}})}\left(\frac{1}{j-j_{\mathrm{pC}}} + \frac{1}{w_{\mathrm{a}}j_{\mathrm{Red,L}}-j}\right) \tag{136}$$

$$[h_{\mathrm{C}}(j)]_{j_{\mathrm{pC}}\le j\le j_{\mathrm{pA}}} = \frac{RT}{\alpha_{\mathrm{c}}\ z\ F}\frac{w_{\mathrm{c}}\ j_{\mathrm{Ox}^{z+},\mathrm{L}}(j_{\mathrm{pA}}-j_{\mathrm{pC}})}{j_{\mathrm{pC}}\left(j_{\mathrm{pA}}-w_{\mathrm{c}}\ j_{\mathrm{Ox}^{z+},\mathrm{L}}\right)}\left(\frac{1}{j_{\mathrm{pA}}-j} + \frac{1}{j-w_{\mathrm{c}}\ j_{\mathrm{Ox}^{z+},\mathrm{L}}}\right) \tag{137}$$

The advantage of the above expressions is easy embodiment because the j_{pA} and j_{pC} can be directly read as inflection points appeared on $h_{\exp}(j)$. Fortunately, the $h_{\exp}(j)$ of reversible reaction can be expressed as a single equation shown below:

$$\left[h_{\exp}(j)\right]_{w_{\mathrm{c}}\ j_{\mathrm{Ox}^{z+},\mathrm{L}}\le j\le w_{\mathrm{a}}\ j_{\mathrm{Red,L}}} = \frac{RT}{z\ F}\left(\frac{1}{w_{\mathrm{a}}\ j_{\mathrm{Red,L}}-j} + \frac{1}{j-w_{\mathrm{c}}\ j_{\mathrm{Ox}^{z+},\mathrm{L}}}\right) + (l/\kappa) \tag{138}$$

Of course, the reversible $h_{\exp}(j)$ can also be obtained using Equation (133). The reason is that Equation (138) can be obtained by only substituting $j_{\mathrm{pA}} = w_{\mathrm{a}}\ j_{\mathrm{Red,L}}$ and $j_{\mathrm{pC}} = w_{\mathrm{c}}\ j_{\mathrm{Ox}^{z+},\mathrm{L}}$. After all, the $h_{\exp}(j)$ for all reactions can be summarized as follows;

$$\left[h_{\exp}(j)\right]_{j_{\mathrm{pA}}\le j\le w_{\mathrm{a}}\ j_{\mathrm{Red,L}}} = \frac{RT}{\alpha_{\mathrm{a}}\ z\ F}\left(\frac{1}{j} + \frac{1}{w_{\mathrm{a}}\ j_{\mathrm{Red,L}}-j}\right) + (l/\kappa)_{\mathrm{a}} \tag{139}$$

$$\left[h_{\exp}(j)\right]_{j_{\mathrm{pC}}\le j\le j_{\mathrm{pA}}} = \frac{1}{1/[h_{\mathrm{A}}(j)]_{j_{\mathrm{pC}}\le j\le j_{\mathrm{pA}}} + 1/[h_{\mathrm{C}}(j)]_{j_{\mathrm{pC}}\le j\le j_{\mathrm{pA}}}} + (l/\kappa) \tag{140}$$

where, $[h_{\mathrm{A}}(j)]_{j_{\mathrm{pC}}\le j\le j_{\mathrm{pA}}}$ is Equation (136), and $[h_{\mathrm{C}}(j)]_{j_{\mathrm{pC}}\le j\le j_{\mathrm{pA}}}$ is Equation (137).

$$\left[h_{\exp}(j)\right]_{w_{\mathrm{c}}\ j_{\mathrm{Ox}^{z+},\mathrm{L}}\le j\le j_{\mathrm{pC}}} = \frac{RT}{\alpha_{\mathrm{c}}\ z\ F}\left(\frac{1}{-j} + \frac{1}{j-w_{\mathrm{c}}\ j_{\mathrm{Ox}^{z+},\mathrm{L}}}\right) + (l/\kappa)_{\mathrm{c}} \tag{141}$$

Here, at practical curve analysis, we can use a few distinctive characteristics on the $h_{\exp}(j)$: (1) If we can observe a straight line having a slope of -1, it is an appearance of

irreversible process corresponding to rds. (2) When a vertical line is found, its current corresponds to a limiting diffusion current; the anodic vertical line corresponds to the limiting diffusion of reductant, Red, and the cathodic vertical line to that of oxidant, Ox^{z+}. (3) When we can find a horizontal line at large $|j|$, its value corresponds to physical resistance.

3.7. Determination of Stable Chemical Species on $E_{exp}(j)$ Using E-pH Diagram

The stable species appearing on $E_{exp}(j)$ was examined using the *E*-pH diagram [30]. Since H_2 and CO have been directly injected into the test solution, two *E*-pH diagrams must be considered. The *E*-pH diagram of CO/CO_2 system superimposed by the H_2/H^+ system is shown in Figure 14.

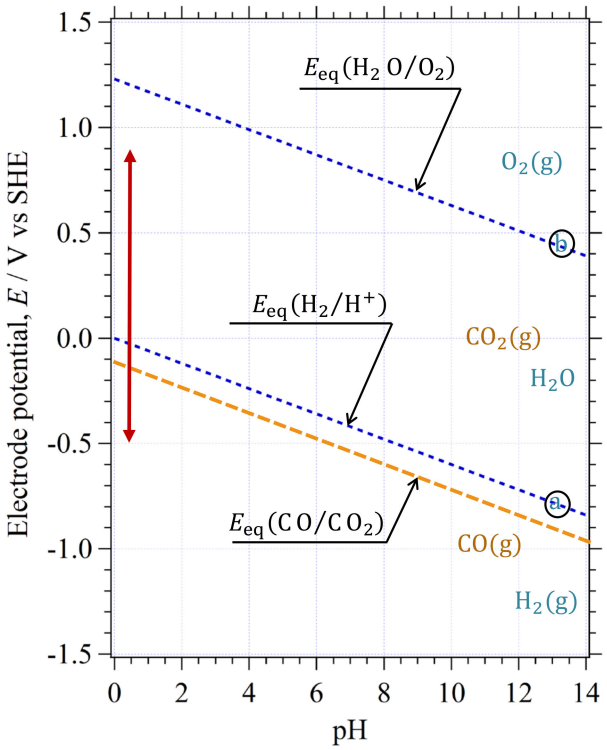

Figure 14. Potential pH equilibrium diagram for the carbon–water system superimposed by the hydrogen system is shown. The orange dashed line indicates the E_{eq} of CO/CO_2 redox reaction. The region between blue dashed line of ⓐ and ⓑ shows the thermodynamically stable region of water.

Three equilibrium lines, an upper blue dashed line (ⓑ) of $E_{eq}(H_2O/O_2) = 1.23 - 0.059$ pH, a lower blue dashed line (ⓐ) of $E_{eq}(H_2/H^+) = -0.059$ pH, and a lowest orange dashed line of $E_{eq}(CO/CO_2) = -0.10 - 0.059$ pH are depicted in Figure 14. A red vertical line shows experimental tracks of $E_{exp}(j)$. The reason why all curves of $E_{exp}(j)$ follow along the red vertical line is that a 0.5 mol dm^{-3} H_2SO_4 has remained at constant ($\approx$ pH 0.3) due to the very strong acid. Therefore, the thermodynamically stable chemical species can only appear on the red vertical line. Their chemical species are H_2, H_2O (rich H^+), CO, and CO_2. The reactions discussed in this paper were restricted to the redox reactions related to the four species. There is an opinion that the derivatives must be also discussed due to the unstable CO in the water [30]. For instance, they said that the following chemical reaction is necessary to be discussed:

$$CO + H_2O = HCOOH. \quad (142)$$

Furthermore, they said that, since the HCOOH is also unstable [30], the below oxidation reactions are possible when being anodically polarized:

$$\mathrm{HCOOH} + \mathrm{H_2O} \rightarrow \mathrm{H_2CO_3} + 2\mathrm{H^+} + 2\mathrm{e}, \tag{143}$$

or

$$\mathrm{HCOOH} \rightarrow \mathrm{CO_2} + 2\mathrm{H^+} + 2\mathrm{e}. \tag{144}$$

Although carbon derivatives such as HCOOH and H_2CO_3 are considered as chemical attendants in actual operating environments, this paper limits to the redox reactions among four species (H_2, H^+, CO, and CO_2) for the sake of simple and essential discussion.

3.8. Curve Analysis for Reversible HER in Environment (I)

Stable chemical species and their redox reactions appearing on $E_{\mathrm{exp}}(j)$ in H_2 + H_2SO_4 solution were examined. Since the *E*-pH diagram showed that the stable species at the state $\left(\mathrm{pH} \approx 0.3,\ E_{\mathrm{ocp}} \approx 0\ \mathrm{V}\right)$ are H_2 and H^+, the redox reaction is the reversible *HER*:

$$\mathrm{H_2} \rightleftarrows 2\mathrm{H^+} + 2\mathrm{e} \tag{145}$$

The reciprocal redox reaction occurs at E_{eq}; the injected H_2 is oxidized to H^+, and at the same time, the H^+ is reduced to H_2. The $h(j)$ belongs properly to the reaction of the category (A). The analysis will be carried out employing curve techniques in this category.

3.8.1. Estimation of w_{a} and w_{c}

First, the estimation of w_{a} and w_{c} is examined. The representative tracks of $(\mathrm{A}) \rightarrow (\mathrm{B}) \rightarrow (\mathrm{C}) \rightarrow (\mathrm{D}) \rightarrow (\mathrm{E}) \rightarrow (\mathrm{B})$ in Figure 2 was employed. The polarizing start point (A) stays on the line ⓐ, on which the reversible *HER* occurs. When $\eta < 0$, the cathodic branch as *her* will be increased. Since H^+ abundantly exists in the solution, the *her* exponentially increases with increase of $|\eta|$. When $\eta \ll 0$, the system will be overwhelmed by *her* (point (B)). When $\eta > 0$, on the contrary, the anodic branch as *hor* can be observed at $(\mathrm{C}) \rightarrow (\mathrm{D})$. Due to the poor solubility of H_2, the anodic current of *hor* will reach a certain limit. This vertical line has its root in the limiting diffusion current of H_2, $j_{\mathrm{H_2,L}}$. We can calculate the theoretical $j_{\mathrm{H_2,L}}$ based on two suppositions: (1) a moderate agitation using magnetic stirrer ($\delta_{\mathrm{H_2}}$ dependincg on agitation. It was estimated to ≈ 0.01 cm in this experiment [2,6,7,31]), and (2) the test solution in the H_2-saturated state ($\approx 10^{-3}$ mol dm^{-3}) [5,32]. Their calculations are shown as:

$$j_{\mathrm{H_2,L}} = z\,F\,\frac{D_{\mathrm{H_2}}}{\delta_{\mathrm{H_2}}}[\mathrm{H_2}]_{\mathrm{sat.}} \approx (2)\left(96.5\times10^{3}\ \mathrm{A\ s\ mol^{-1}}\right)\left(\frac{3.8\times10^{-5}\ \mathrm{cm^2\ s^{-1}}}{0.01\ \mathrm{cm}}\right)\left(10^{-3}\ \mathrm{mol\ dm^{-3}}\right) \approx 0.73\ \mathrm{mA\ cm^{-2}}. \tag{146}$$

Table 1 tells that the $w_{\mathrm{a}}\ j_{\mathrm{H_2,L}}$ as an anodic vertical line was:

$$w_{\mathrm{a}}\ j_{\mathrm{H_2,L}} \approx 0.7\ \mathrm{mA\ cm^{-2}}. \tag{147}$$

Then, w_{a} can be calculated as:

$$w_{\mathrm{a}} = \frac{w_{\mathrm{a}}\ j_{\mathrm{H_2,L}}}{j_{\mathrm{H_2,L}}} = \frac{0.7\ \mathrm{mA\ cm^{-2}}}{0.74\ \mathrm{mA\ cm^{-2}}} = 0.96. \tag{148}$$

On the other hand, we can estimate the $w_{\mathrm{a}}/w_{\mathrm{c}}$ ratio by employing Equation (100). Substituting $\eta_{\mathrm{w}} = 0$ V into Equation (100) returns the following:

$$\frac{w_{\mathrm{a}}}{w_{\mathrm{c}}} = \exp\left(\frac{-z\,F}{RT}\,\eta_{\mathrm{w}}\right) = \exp\left(\frac{-2}{0.026}\times 0\right) = 1. \tag{149}$$

The above two results can lead to the conclusion of $w_{\mathrm{a}} = w_{\mathrm{c}} = 0.96$. Using $w_{\mathrm{c}} = 0.96$, we can estimate the $w_{\mathrm{c}}\ j_{\mathrm{H^+,L}}$:

$$w_c\, j_{H^+,L} = -w_c\, z\, F\, \frac{D_{H^+}}{\delta_{H^+}} [H^+]_{bulk} \approx -(0.96)(1)\left(96.5 \times 10^3 \text{ A s mol}^{-1}\right)\left(\frac{7\times10^{-5} \text{ cm}^2 \text{ s}^{-1}}{0.01 \text{ cm}}\right)\left(10^{-0.3} \text{ mol dm}^{-3}\right) = -325 \text{ mA cm}^{-2}. \quad (150)$$

Unfortunately, we cannot find the actual $w_c\, j_{H^+,L}$ experimentally because it is over-scaled in Figure 2.

3.8.2. Determination of z for Reversible HER

Using the readings in Table 1, rough estimation of z is possible. The z is calculated by Equation (45), which is modified by w_a, w_c, and l/κ:

$$z = \frac{R\,T}{F}\frac{1}{h_{exp}(0) - l/\kappa}\left(\frac{1}{w_a\, j_{H_2,L}} + \frac{2}{-w_c\, j_{H^+,L}}\right) \approx \frac{0.026}{2.2\times10^{-2} - 10^{-3}}\left(\frac{1}{0.7} + \frac{2}{325}\right) = 1.8. \quad (151)$$

If the 1.8 can be rounded to an integer, the z becomes 2. In order to obtain the more accurate z, the parallel displacement technique will be helpful. Employing Equation (48), we can plot the relation between $\log\{h(j + w_a\, j_{H_2,L}) - l/\kappa\}$ and $\log|j|$. The results of all curves are shown in Figure 15.

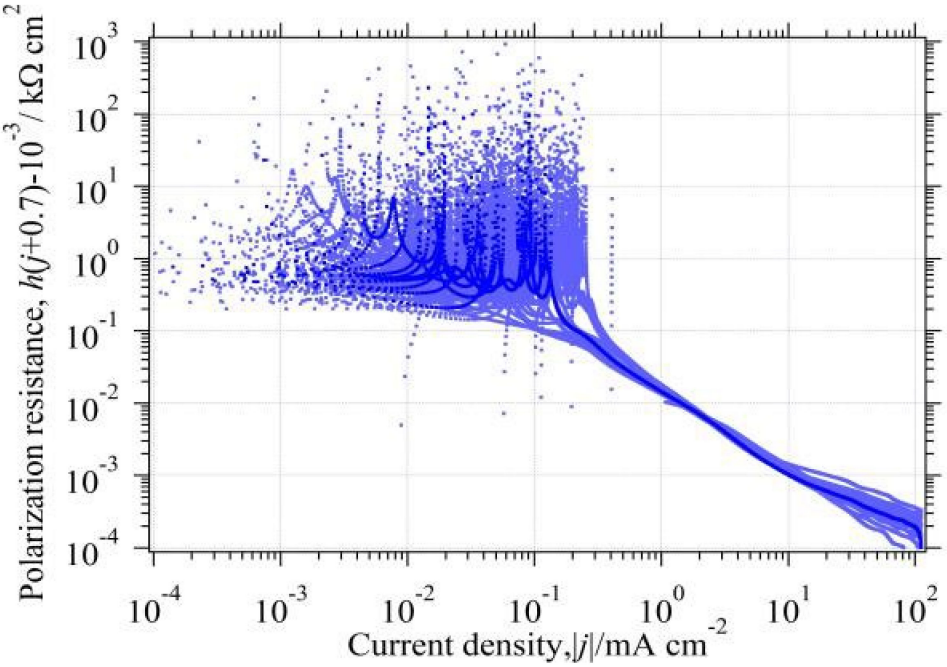

Figure 15. Relation between $\{h_{exp}(j + 0.7) - 10^{-3}\}$ vs. $|j|$ is plotted. The z was estimated using the green region data because their data satisfied the Tafel slope. The Tafel slope of -1 is shown with the orange dashed line as a reference.

We can find that there is a current region satisfying the Tafel slope, which is depicted as the green-toned region (4 mA cm^{-2} $\lesssim |j| \lesssim$ 8 mA cm^{-2}). The relation between the calculated z and the green-toned $|j|$ were plotted. The results are shown in Figure 16.

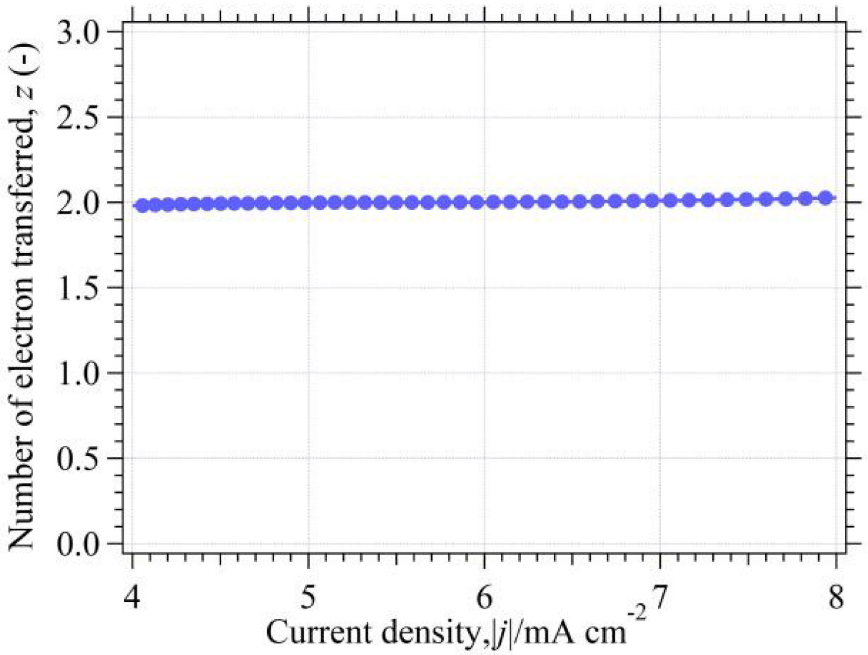

Figure 16. Relation between the calculated z and the current region of 4 mA cm^{-2} $\lesssim |j| \lesssim$ 8 mA cm^{-2}.

We can see that the *HER* occurred on Pt electrode has exactly z = 2. In this calculation, the precondition of Equation (47) has been confirmed in advance:

$$\left[\frac{RT}{z\,F}\frac{2}{j + w_a\,j_{H_2,L} - w_c\,j_{H^+,L}}\right]_{4\lesssim|j|\lesssim 8} = \frac{0.026}{2}\frac{2}{(4\sim 8)+0.7+325} \lesssim 10^{-4.1}. \quad (152)$$

It is acceptable in the margin of error that the approximation of $\lesssim 10^{-4.1}$ is ≈ 0.

3.8.3. Confirmation of $j_A(0) \approx j_d$ for Reversible HER

When $w_a = w_c = 0.96$, the j_d is calculated to:

$$j_d = \frac{1}{1/(w_a\,j_{H_2,L}) + 1/\left(-w_c\,j_{H^+,L}\right)} = \frac{1}{1/0.7 + 1/325} \approx 0.70 \text{ mA cm}^{-2}. \quad (153)$$

Another way is possible by employing Equation (122):

$$[j_A(\eta_w)]_{\eta_w=0} = [j_A(j)]_{j=0} = \frac{1}{\frac{1}{j_{pA}} + \frac{1}{-j_{pC}}} = \frac{1}{\frac{1}{(w_a\,j_{H_2,L})} + \frac{1}{(-w_c\,j_{H^+,L})}} = \frac{1}{\frac{1}{0.7} + \frac{1}{325}} \approx 0.70 \text{ mA cm}^{-2}. \quad (154)$$

We can see that $j_A(0)$ for reversible *HER* is confirmed to 0.70 mA cm^{-2}, and it is exactly the same as the j_d ($= w_a\,j_{H_2,L}$). In addition to the above, there is another way to obtain the $j_A(0)$. Its value can be calculated by substituting the experimental readings in Table 1 into Equation (109):

$$j_A(0) = \frac{0.96^{\alpha_c}\,0.96^{\alpha_a}}{1/j_0 + (0.96/0.96)^{\alpha_a}/\,0.74 + (0.96/0.96)^{\alpha_c}/\,339} \approx \frac{(0.96)^1}{1/\infty + (1)^{\alpha_a}/\,0.74 + (1)^{\alpha_c}/\,339} = 0.71 \text{ mA cm}^{-2}. \quad (155)$$

We can see that the above $j_A(0)$ well agrees with the above two results.

3.8.4. Determination of Kinetic Parameters for Reversible HER

It is reported that the Tafel slope of reversible *HER* is $\approx$ 30 mV decade^{-1}, although the reported values have a scattered tendency [2,3,33]. It has been also pointed out that

reliable value will be obtained in a low overpotential region [33,34]. Ambiguous problems have been remained when employing the TEM. The employment of $h(j)$ can bring the clear conclusion to $b = 30$ mV decade^{-1}. Since the slope of the differentiated Tafel equation (Equation (39)) is identical with the slope as a result of the parallel displacement (Equation (48)), $\mathrm{d}\,\eta/\mathrm{d}\,j \approx h\left(j + w_\mathrm{a}\, j_{\mathrm{H_2,L}}\right)$. Namely,

$$\frac{\mathrm{d}\,\eta}{\mathrm{d}\,j} = \frac{b}{2.3}\frac{1}{|j|} = \left[\frac{0.026}{z\,|j|}\right]_{z=2} \tag{156}$$

From the above, the b is as below:

$$b = 2.3 \times 0.013 = 0.0299 \text{ V decade}^{-1} \approx 30 \text{ mV decade}^{-1}. \tag{157}$$

Using $h(j)$, it is conclusively proved that the Tafel slope of reversible *HER* is proved to be 30 mV decade^{-1}.

3.8.5. Agreement between $E_\mathrm{exp}(j)$ and $E_\mathrm{th}(j)$

Employing three data ($l/\kappa = 10^{-3}$ kΩ cm^2, $w_\mathrm{a}\, j_{\mathrm{H_2,L}} = 0.7$ mA cm^{-2}, and $w_\mathrm{c}\, j_{\mathrm{H^+,L}} = -325$ mA cm^{-2}), the $h_\mathrm{th}(j)$ is shown as:

$$h_\mathrm{th}(j) = h_\mathrm{rev}(j) + \frac{l}{\kappa} = \frac{R\,T}{z\,F}\left(\frac{1}{w_\mathrm{a}\, j_{\mathrm{H_2,L}} - j} + \frac{2}{j - w_\mathrm{c}\, j_{\mathrm{H^+,L}}}\right) + \frac{l}{\kappa} = \frac{0.026}{2}\left(\frac{1}{0.7 - j} + \frac{2}{j + 325}\right) + 10^{-3}. \tag{158}$$

The above $h_\mathrm{th}(j)$ was plotted on the $h_\mathrm{exp}(j)$ in Figure 3. The result is shown in Figure 17.

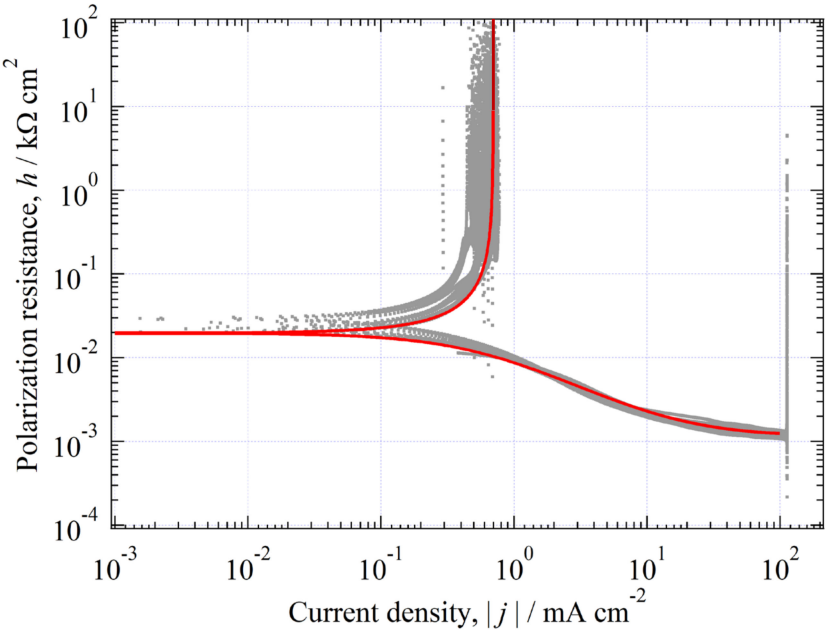

Figure 17. The $h_\mathrm{th}(j)$ was plotted on the $h_\mathrm{exp}(j)$. We can see that the red $h_\mathrm{th}(j)$ is overlaid on the gray $h_\mathrm{exp}(j)$.

We can see that the red $h_\mathrm{th}(j)$ is on the gray $h_\mathrm{exp}(j)$. In addition to the case of $h(j)$, it is also necessary to confirm the agreement between $E_\mathrm{exp}(j)$ and $E_\mathrm{th}(j)$. The $E_\mathrm{th}(j)$ can be obtained by solving the following differentiated equation under an initial condition:

$$\frac{\mathrm{d}\,E_\mathrm{th}(j)}{\mathrm{d}\,j} = h_\mathrm{th}(j) = \frac{0.026}{2}\left(\frac{1}{0.7 - j} + \frac{2}{j + 325}\right) + 10^{-3} \tag{159}$$

$$E_{\mathrm{th}}(0) = 0 \text{ V (initial condition)} \tag{160}$$

The above solution is as below:

$$E_{\mathrm{th}}(j) = 0.013 \ \ln \frac{(j+325)^2}{0.7 - j} \frac{0.7}{325^2} + 10^{-3} j \tag{161}$$

The concrete $E_{\mathrm{th}}(j)$ is drawn with red on the gray $E_{\mathrm{exp}}(j)$. The result is shown in Figure 18.

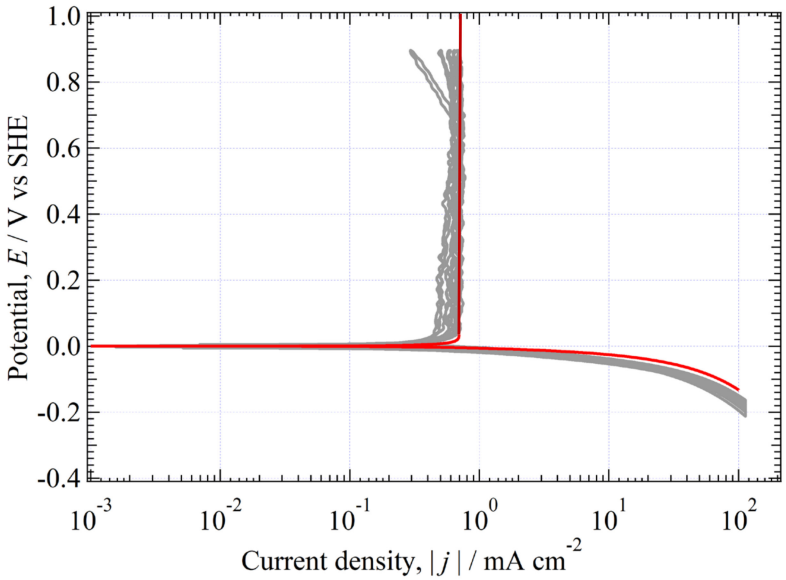

Figure 18. The curve of $E_{\mathrm{th}}(j)$, which was obtained by solving the differentiated equations, is drawn with red on the gray $E_{\mathrm{exp}}(j)$.

The result that $E_{\mathrm{th}}(j)$ considerably overlapped with $E_{\mathrm{exp}}(j)$ is conclusive evidence for the valid approximation.

When the $E(j)$ was embodied, η can be expressed as a function of j:

$$\eta = E - E_{\mathrm{eq}} = E(j) - E(0) = 0.013 \ln \frac{0.7}{325^2} \frac{(j+325)^2}{(0.7-j)} + 10^{-3} \ (= \eta(j)). \tag{162}$$

The relation between $|\eta|$ and $|j|$ is shown in Figure 19.

Figure 19 shows that small overpotential of $|\eta| \approx 1$ mV can flow $|j| \approx 0.1$ mA cm^{-2} to both of branches. In a case of $|\eta| \approx 10$ mV, a current deference between the branches takes place; ≈ 0.6 mA cm^{-2} flowing to the anodic branch and ≈ -2 mA cm^{-2} to the cathodic branch. We can see that the current flowing to the cathodic branch is easier than that of the anodic branch in the case of *HER*.

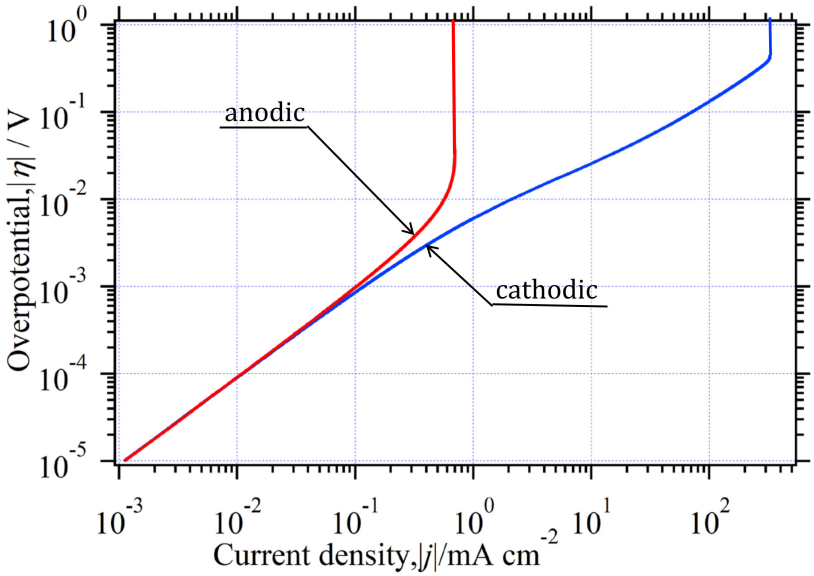

Figure 19. The relation between $|\eta|$ and $|j|$ is drawn.

3.9. Curve Analysis of $h_{\exp}(j)$ in Environment (II)

Figure 1 shows that the E_{ocp} was shifted to noble potential ($0.26 \sim 0.34$ V) when CO was added into the H_2 + H_2SO_4 solution. The stable species at this potential are H^+ and CO_2. The injected H_2 and CO will be oxidized to H^+ and CO_2 when they come to contact with Pt:

$$H_2 \rightarrow 2H^+ + 2e. \tag{163}$$

$$CO + H_2O \rightarrow CO_2 + 2H^+ + 2e, \tag{164}$$

Although the CO/CO_2 redox reaction is usually slow, it will be stimulated by the Pt catalysis and raise to a reasonable rate [30]. Being cathodically far polarized, Figure 4 shows that $|j|$ exponentially increases and reaches (G). Since (G) is located at -0.5 V, the E-pH diagram shows that the stable species are changed to H_2 and CO from the previous H^+ and CO_2. At (G), the following cathodic reactions will take place:

$$H_2 \leftarrow 2H^+ + 2e, \tag{165}$$

$$CO + H_2O \leftarrow CO_2 + 2H^+ + 2e. \tag{166}$$

The former reaction can vigorously occur due to sufficient supply of H^+ and the latter poorly occur due to insufficient supply of CO_2. Reversing potential, the anodic current was observed around (H). Since this point is in the stable region of CO_2 and H^+, the H_2 and CO (actually H_{ad} and CO_{ad}, discussed later) will be oxidized to H^+ and CO_2 again.

$$H_{ad} \rightarrow H^+ + e, \tag{167}$$

$$CO_{ad} + H_2O \rightarrow CO_2 + 2H^+ + 2e. \tag{168}$$

Since the repeated reactions shown above influence on the curve shape, their $h(j)$ will become complicated. In order to be simple $h(j)$, the route of (F) $\rightarrow$ (G) $\rightarrow$ (H) $\rightarrow$ (I) $\rightarrow$ (J) $\rightarrow$ (K) in Figure 5 was broadly divided into three parts: (1) (F) $\rightarrow$ (G) (downward); (2) (G) $\rightarrow$ (H) $\rightarrow$ (I) (upward); and (3) (I) $\rightarrow$ (J) $\rightarrow$ (K) (downward). If necessary, some of them were further separated into smaller parts.

3.9.1. Analysis of (F) $\rightarrow$ (G)

The $h_{\exp}(j)$ of downward (F) $\rightarrow$ (G) is picked up and shown again in Figure 20 together with the $E_{\exp}(j)$.

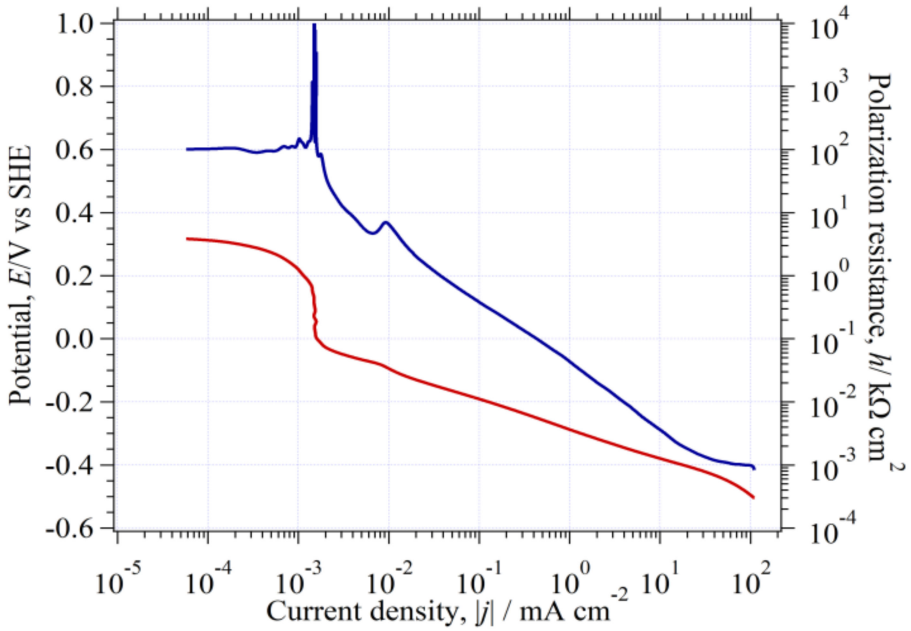

Figure 20. The (F) → (G) of $E_{exp}(j)$ in Figure 4 and $h_{exp}(j)$ in Figure 5 are picked up as representatives. The orange dashed line with the Tafel slope is shown as a reference.

(a) Point Analysis of (F)

Since the stable chemical species at (F) are CO_2 and H^+, the injected H_2 and CO are changed to H^+ and CO_2. The redox reactions related to them are shown as:

$$H_2 \rightleftarrows 2H^+ + 2e \ (j_1, E_{eq1}), \tag{169}$$

$$CO \ + \ H_2O \rightleftarrows CO_2 + 2H^+ + 2e \ (j_2, E_{eq2}). \tag{170}$$

Since $E_{eq1}(= 0\ V) > E_{eq2}(= -0.1\ V)$, the mixed system will be built up. The following reactions having mixed potential (E_m, $E_{eq2} < E_m < E_{eq1}$) will proceed:

$$H_2 \leftarrow 2H^+ + 2e \ (j_{c1}, E_{eq1}), \tag{171}$$

$$CO \ + \ H_2O \rightarrow CO_2 + 2H^+ + 2e \ (j_{a2}, E_{eq2}). \tag{172}$$

The net current at E_m is expressed as:

$$j = \ j_A + \ j_C = w_{a_1} \ j_{a_1} + w_{c_1} \ j_{c_1} + w_{a_2} \ j_{a_2} + w_{c_2} \ j_{c_2} \approx w_{c_1} \ j_{c_1} + w_{a_2} \ j_{a_2} = 0. \tag{173}$$

In the actual state, the j_{c_1} is prevented from attending because the solution is saturated with continuous H_2 bubbling and there is no space of the H_2 solubility. As a result, the *her* hardly occurs.

$$w_{c_1} \ j_{c_1} \approx 0. \tag{174}$$

In the other hand, Equation (172) can occur because the continuous injections of H_2 and CO will purge the CO_2 from the solution. There is a space for the CO_2 solubility. Its solubility can be estimated using the Nernst equation:

$$E_{eq2} = -0.10 - 0.059 \ pH + 0.03 \log \frac{p_{CO_2}}{p_{CO}} \tag{175}$$

The relation between CO and CO_2 is calculated at $E_{eq2} = 0.32\ V \ (\approx E_{ocp})$:

$$\frac{p_{CO_2}}{p_{CO}} = 10^{\frac{0.32+0.10+0.059(0.3)}{0.03}} \approx 10^{14} \tag{176}$$

The thermodynamic answer tells us that the solution at (F) contains huge amounts of CO_2. However, the huge amount does not mean infinite CO_2 solubility. We know that here is a solubility restriction; the actual CO_2 solubility is up to its saturation [32]:

$$[CO_2]_{bulk} \leq [CO_2]_{sat} \approx 10^{-1.5} \text{ mol dm}^{-3}. \quad (177)$$

The CO_2 in the solution is probably over-saturated. As a result, the Pt electrode at (F) will be entirely surrounded with a plenty of CO and CO_2.

(b) Part analysis of (F) → (F1)

The reaction occurring on (F) → (F1) → (F1′) is Equation (172). It is the cathodic branch of the reversible reaction of Equation (170). A clear vertical line observed on the way of (F1) → (F1′) is a sign of the CO_2 reduction reaction having a diffusion process. We can analyze Equation (172) using $h(j)$. In order to compare the theoretical $h_{th}(j)$ with the experimental $h_{exp}(j)$, the $h_{th}(j)$ of the stationary state can be expressed as below:

$$h_{th}(j) = \frac{RT}{z\,F}\left(\frac{1}{w_{a2}\,j_{CO,L} - j} + \frac{1}{j - w_{c2}\,j_{CO_2,L}}\right) + \frac{l}{\kappa}. \quad (178)$$

Employing $w_{c2}\,j_{CO_2,L} = -1.5 \times 10^{-3}$ mA cm^{-2} (cathodic vertical line, (F1) in Figure 5) and $w_{a2}\,j_{CO,L} = 1.2 \times 10^{-3}$ mA cm^{-2} (anodic vertical line, (I1) in Figure 21 shown later), $l/\kappa \approx 80$ kΩ cm^2 (estimated using actual value of $h_{exp}(0)$). It is expressed concretely as:

$$h_{th}(j) = \frac{0.026}{2}\left(\frac{1}{1.2 \times 10^{-3} - j} + \frac{1}{j + 1.5 \times 10^{-3}}\right) + 80. \quad (179)$$

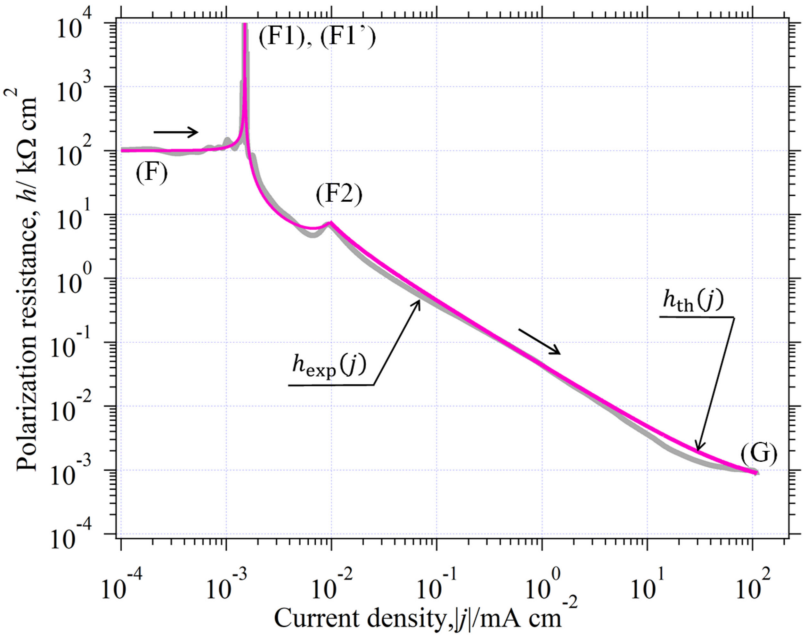

Figure 21. Comparisons between $h_{th}(j)$ (pink) and the $h_{exp}(j)$ (gray): a part of (F) → (F1), together with all parts of (F1) → (F2) and (F2) → (G), is also shown, which will be discussed later.

The cathodic part shown above is drawn on the gray (F) → (F1) with pink in Figure 21, in which the gray $h_{exp}(j)$ is shown for comparison.

The large value of l/κ $\left(= 80\ \text{k}\Omega\ \text{cm}^2\right)$ suggests that the Pt electrode surface was heavily covered with adsorption CO_2 and CO. In addition to the large l/κ, there is other evidence relating to the heavy coverage. Considering the actually observed values of CO and CO_2, the w_a and w_c can be roughly estimated using the following $j_{CO,L}$ and $j_{CO_2,L}$:

$$j_{\mathrm{CO,L}} = zF\,\frac{D_{\mathrm{CO}}}{\delta_{\mathrm{CO}}}[\mathrm{CO}]_{\mathrm{sat.}} \approx (2)\left(96.5\times10^{3}\ \mathrm{A\ s\ mol^{-1}}\right)\left(\frac{10^{-5}\ \mathrm{cm^2\ s^{-1}}}{0.01\ \mathrm{cm}}\right)\left(10^{-3}\ \mathrm{mol\ dm^{-3}}\right) = 0.19\ \mathrm{mA\ cm^{-2}}, \quad (180)$$

$$j_{\mathrm{CO_2,L}} = -zF\,\frac{D_{\mathrm{CO_2}}}{\delta_{\mathrm{CO_2}}}[\mathrm{CO_2}]_{\mathrm{sat.}} \approx -(2)\left(96.5\times10^{3}\ \mathrm{A\ s\ mol^{-1}}\right)\left(\frac{10^{-5}\ \mathrm{cm^2\ s^{-1}}}{0.01\ \mathrm{cm}}\right)\left(10^{-1.5}\ \mathrm{mol\ dm^{-3}}\right) = -6.1\ \mathrm{mA\ cm^{-2}}. \quad (181)$$

Each of w_{a2} and w_{c2} can be calculated using the above results:

$$w_{\mathrm{a2}} = \frac{w_{\mathrm{a2}}\,j_{\mathrm{CO,L}}}{j_{\mathrm{CO,L}}} = \frac{1.2\times10^{-3}\ \mathrm{mA\ cm^{-2}}}{0.19\ \mathrm{mA\ cm^{-2}}} = 10^{-2.2}, \quad (182)$$

$$w_{\mathrm{c2}} = \frac{w_{\mathrm{c2}}j_{\mathrm{CO_2,L}}}{j_{\mathrm{CO_2,L}}} = \frac{-1.5\times10^{-3}\ \mathrm{mA\ cm^{-2}}}{-6.1\ \mathrm{mA\ cm^{-2}}} = 10^{-3.6}. \quad (183)$$

Small $w_{\mathrm{a2}}\left(=10^{-2.2}\right)$ and $w_{\mathrm{c2}}\left(=10^{-3.6}\right)$ give confirmatory evidence that the active surface is almost lost. Close observation of Figure 5 shows that all $h_{\mathrm{exp}}(j)$ have peculiar humps around (F2). Considering the humps, it is natural to divide the $(\mathrm{F1}) \rightarrow (\mathrm{G})$ into two parts: $(\mathrm{F1}') \rightarrow (\mathrm{F2})$ and $(\mathrm{F2}) \rightarrow (\mathrm{G})$.

(b1) Part Analysis of $(\mathrm{F1}') \rightarrow (\mathrm{G})$

Since $E(j)$ in Figure 20 shows that the stable chemical species of $(\mathrm{F1}') \rightarrow (\mathrm{G})$ are CO and H_2, the following two cathodic reactions can occur competitively:

$$\mathrm{H_2} \leftarrow 2\mathrm{H^+} + 2\mathrm{e^-}\ \left(j_{\mathrm{c1}}, E_{\mathrm{eq1}}\right), \quad (184)$$

$$\mathrm{CO} + \mathrm{H_2O} \leftarrow \mathrm{CO_2} + 2\mathrm{H^+} + 2\mathrm{e^-}\ \left(j_{\mathrm{c2}}, E_{\mathrm{eq2}}\right). \quad (185)$$

(b2) Part analysis of $(\mathrm{F1}') \rightarrow (\mathrm{F2})$

The j in this cathodic region can be expressed as:

$$j = j_{\mathrm{A}} + j_{\mathrm{C}} \approx j_{\mathrm{C}} = w_{\mathrm{c_1}}\,j_{\mathrm{c_1}} + w_{\mathrm{c_2}}\,j_{\mathrm{c_2}}. \quad (186)$$

Considering that CO_2 is consumed and poorly supplied, it will be acceptable that the j_{c2} $(= j_{\mathrm{CO_2,L}})$ is almost constant current. The j_{c1} can be arranged as:

$$j_{\mathrm{c1}} = (j - w_{\mathrm{c2}}\,j_{\mathrm{c2}})/w_{\mathrm{c1}} = \left(j - w_{\mathrm{c2}}\,j_{\mathrm{CO_2,L}}\right)/w_{\mathrm{c1}}. \quad (187)$$

Then, the $h(j)$ is expressed as:

$$h(j) = \frac{\mathrm{d}\,E}{\mathrm{d}\,j} = \frac{\mathrm{d}\,E}{\mathrm{d}\,(w_{\mathrm{c_1}}\,j_{\mathrm{c_1}} + w_{\mathrm{c_2}}\,j_{\mathrm{c_2}})} = \frac{1}{w_{\mathrm{c_1}}\,\mathrm{d}j_{\mathrm{c_1}}/\mathrm{d}E\ + w_{\mathrm{c_2}}\mathrm{d}j_{\mathrm{c_2}}/\mathrm{d}E} = \frac{1}{w_{\mathrm{c_1}}/h_{\mathrm{c_1}}(j_{\mathrm{c_1}}) + w_{\mathrm{c_2}}/h_{\mathrm{c_2}}(j_{\mathrm{c_2}})} = \frac{1}{w_{\mathrm{c1}}}h_{\mathrm{c1}}(j_{\mathrm{c1}}). \quad (188)$$

The above means that the $h(j)$ of $(\mathrm{F1}') \rightarrow (\mathrm{F2})$ is identical to $h_{\mathrm{c1}}(j_{\mathrm{c1}})/w_{\mathrm{c1}}$. Since the $h_{\mathrm{c1}}(j_{\mathrm{c1}})$ is cathodic part of reversible reaction, the $h_{\mathrm{th}}(j)$ is:

$$h_{\mathrm{th}}(j) = \frac{1}{w_{\mathrm{c1}}}h_{\mathrm{c1}}(j_{\mathrm{c1}}) + \left(\frac{l}{\kappa}\right)_{\mathrm{c}} = \frac{1}{w_{\mathrm{c1}}}\left\{\frac{RT}{z\,F}\left(\frac{1}{-\,j_{\mathrm{c1}}} + \frac{2}{j_{\mathrm{c1}} - w_{\mathrm{c1}}\,j_{\mathrm{H^+,L}}}\right)\right\} + \left(\frac{l}{\kappa}\right)_{\mathrm{c}} \quad (189)$$

Substituting Equation (187) into the above:

$$h_{\mathrm{th}}(j) = \frac{RT}{z\,F}\left(\frac{1}{w_{\mathrm{c2}}\,j_{\mathrm{CO_2,L}} - j} + \frac{2}{j - w_{\mathrm{c2}}\,j_{\mathrm{CO_2,L}} - {w_{\mathrm{c1}}}^2\,j_{\mathrm{H^+,L}}}\right) + \left(\frac{l}{\kappa}\right)_{\mathrm{c}}. \quad (190)$$

Employing $w_{c2}\ j_{CO_2,L} = -1.5 \times 10^{-3}$ mA cm^{-2}, $w_{c2}\ j_{CO_2,L} + {w_{c1}}^2\ j_{H^+,L} \approx -1.5 \times 10^{-2}$ mA cm^{-2} (vertical line extrapolated from (F2)), and $(l/\kappa)_c \approx 10^{-3}$ kΩ cm^2, the $h_{th}(j)$ is embodied:

$$h_{th}(j) = \frac{0.026}{2}\left(\frac{1}{-1.5 \times 10^{-3} - j} + \frac{2}{j + 1.5 \times 10^{-2}}\right) + 10^{-3}. \quad (191)$$

The above $h_{th}(j)$ having pink is added to the gray (F1) → (F2) in Figure 21. We can see that the $h_{th}(j)$ is on the $h_{exp}(j)$. The large decrease of $(l/\kappa)_c$ from the previous 80 kΩ cm^2 to 10^{-3} kΩ cm^2 is due to the departure of adsorption CO and CO_2 from the electrode surface. It is originated from the H_2 evolution and the disappearance of CO_2 by the consumption reaction of Equation (185).

(b3) Part analysis of (F2) → (G)

Since a straight line having a slope of −1 was observed on (F2) → (G), we can regard it as an irreversible reaction having rds. Therefore, the total number of reactions occurring on (F2) → (G) are three. They are mutually competitive reactions.

$$H_2 \leftarrow 2H^+ + 2e^- \left(j_{c1}, E_{eq1}\right), \quad (192)$$

$$CO\ +\ H_2O \leftarrow CO_2 + 2H^+ + 2e^-\ \left(j_{c2}, E_{eq2}\right), \quad (193)$$

$$H_{ad}\ \leftarrow H^+ + e^- \left(j_{c3},\ E_{eq3},\ \text{rds, disacussed later}\right). \quad (194)$$

We can calculate the $\alpha_{c3}\ z_3$ using the straight line data of $0.3 \lesssim |j| \lesssim 1$ mA cm^{-2}:

$$\alpha_{c3}\ z_3 = \frac{0.026}{|j|\ \left[h_{exp}(j) - 10^{-3}\right]_{0.3 \lesssim |j| \lesssim 1}} \approx 0.62. \quad (195)$$

Needless to say, the following precondition has been confirmed in advance:

$$\frac{0.026}{\alpha_{c3}\ z_3}\frac{1}{j - \ w_{c3} j_{H^+,L}} = \left[\frac{0.026}{0.7}\frac{1}{j + \ > 100}\right]\ 0.3 \lesssim |j| \lesssim 1\ \ < 10^{-3.4}\ (\approx 0). \quad (196)$$

Although the $\left|w_{c3}\ j_{H^+,L}\right|$ cannot be observed in Figure 5, it is certainly > 100 mA cm^{-2}. The obtained values of α_{c3} and z_3 must simultaneously satisfy the following restrictions:

$$\alpha_{c3}\ z_3 = 0.62 \quad (197)$$

$$z_3 = 1,\ 2,\ \ldots \text{(integer)} \quad (198)$$

$$0 < \alpha_{c3} < 1 \quad (199)$$

The most preferable combination is $\alpha_{c3} = 0.62$ and $z_3 = 1$, because if z_3 = 2, Equation (194) becomes reversible reaction. The result of $z_3 = 1$ means that the rds is one electron transferred reaction. When the conjugate reductant of the H^+ is H_{ad}, it is the well-known reaction having the Tafel–Volmer mechanism:

$$H_{ad} \leftarrow H^+ + e \quad (200)$$

The below reaction (Heyrovsky mechanism) is also possible if the result is z =1, only:

$$H_2 \leftarrow H^+ + H_{ad} + e \quad (201)$$

The net current in this track is shown as:

$$j = \ j_A + j_C \approx \ j_C = w_{c_1}\ j_{c_1} + w_{c_2}\ j_{c_2} + w_{c_3}\ j_{c_3} \quad (202)$$

Taking into account of the limited $w_{c_1}\ j_{c_1}\left(=w_{c_1}\ j_{H^+,L}\right)$ and the constant $w_{c_2}\ j_{c_2}\left(=w_{c_2}\ j_{CO_2,L}\right)$, the $h_{th}(j)$ is shown as:

$$h_{th}(j)=\frac{1}{w_{c_1}/h_{c_1}(j_{c_1})+w_{c_2}/h_{c_2}(j_{c_2})+w_{c_3}/h_{c_3}(j_{c_3})}+\left(\frac{l}{\kappa}\right)_c=\frac{1}{w_{c_3}}h_{c_3}(\ j_{c_3})+\left(\frac{l}{\kappa}\right)_c. \quad (203)$$

Arranging Equation (202), j_{c_3} is shown as:

$$j_{c_3}=(j-w_{c_1}\ j_{c_1}-w_{c_2}\ j_{c_2})/w_{c_3} \quad (204)$$

Similarly, the $h_{th}(j)$ is expressed as:

$$\begin{aligned} h_{th}(j)&=\frac{1}{w_{c_3}}\left\{\frac{RT}{\alpha_{c3}\ z_3\ F}\left(\frac{1}{-j_{c_3}}+\frac{1}{j_{c_3}-w_{c_3}\ j_{H^+,L}}\right)\right\}+\left(\frac{l}{\kappa}\right)_c\\ &=\frac{1}{w_{c_3}}\left\{\frac{RT}{\alpha_{c3}\ z_3\ F}\left(\frac{1}{-\frac{j-w_{c_1}\ j_{c_1}-w_{c_2}\ j_{c_2}}{w_{c_3}}}+\frac{1}{\frac{j-w_{c_1}\ j_{c_1}-w_{c_2}\ j_{c_2}}{w_{c_3}}-w_{c_3}\ j_{H^+,L}}\right)\right\}+\left(\frac{l}{\kappa}\right)_c\\ &=\frac{0.026}{\alpha_{c3}\ z_3}\left(\frac{1}{w_{c1}\ j_{H^+,L}+w_{c2}\ j_{CO_2,L}-j}+\frac{1}{j-w_{c1}\ j_{H^+,L}-w_{c2}\ j_{CO_2,L}-{w_{c3}}^2\ j_{H^+,L}}\right)+\left(\frac{l}{\kappa}\right)_c. \end{aligned} \quad (205)$$

Employing the assumed value of $w_{c1}\ j_{H^+,L}+\ w_{c2}\ j_{CO_2,L}\approx -5\times10^{-3}$ mA cm^{-2} and $\left|{w_{c3}}^2\ j_{H^+,L}\right|>100$ mA cm^{-2}, $h_{th}(j)$ can be embodied as:

$$h_{th}(j)=\frac{0.026}{0.62}\left(\frac{1}{-5\times10^{-3}-j}+\frac{1}{j\ +\ 5\times10^{-3}+\ >100}\right)+10^{-3}\approx0.042\left(\frac{1}{-5\times10^{-3}-j}\right)+10^{-3}. \quad (206)$$

The pink curve above is added to the gray $(\mathrm{F2})\ \rightarrow\ (\mathrm{G})$. We can see that the $h_{th}(j)$ is almost on the $h_{exp}(j)$, except around (G). This exception may be caused by a fact that the $(l/\kappa)_c$ around (G) is not always constant and probably changeable by the vigorous H_2 evolution.

3.9.2. Analysis of $(\mathrm{G})\ \rightarrow\ (\mathrm{H})\ \rightarrow\ (\mathrm{I})$

The representative $h_{exp}(j)$ of upward track of $(\mathrm{G})\ \rightarrow\ (\mathrm{H})\ \rightarrow\ (\mathrm{I})$ is picked up and shown in Figure 22 together with its $E_{exp}(j)$.

Considering the zigzag curve around (G1), it is natural to divide $(\mathrm{G})\ \rightarrow\ (\mathrm{H})\ \rightarrow\ (\mathrm{I})$ into two parts: $(\mathrm{G})\ \rightarrow\ (\mathrm{G1})$ and $(\mathrm{G1})\ \rightarrow\ (\mathrm{H})\ \rightarrow\ (\mathrm{I})$.

(a) Part analysis of $(\mathrm{G})\ \rightarrow\ (\mathrm{G1})$

This part consists of the same cathodic reactions of $(\mathrm{F2})\ \rightarrow\ (\mathrm{G})$, but the electrons pumped into the system are gradually decreased this time. Similarly, as before, the $\alpha_{c3}\ z_3$ can be calculated using the actual current range indicating a line slope of -1. The result is shown as:

$$\alpha_{c3}\ z_3=\frac{0.026}{|j|\ \left[h_{exp}(j)-10^{-3}\right]_{0.1\lesssim|j|\lesssim1}}\approx0.55. \quad (207)$$

The above result of 0.55 is different from the previous result of 0.62. Clear reasons are unknown, but one of them must be due to change of electrode surface after or before being attacked by *her*. In an example case of $\alpha_{c3}\approx0.6$ and $w_{c1}\ j_{H^+,L}+w_{c2}\ j_{CO_2,L}\approx-1.5\times10^{-2}$ mA cm^{-2}, the previous Equation (206) is changed to the following $h_{th}(j)$:

$$h_{th}(j)=\frac{0.026}{0.6}\left(\frac{1}{-1.5\times10^{-2}-j}+\frac{1}{j\ +\ 1.5\times10^{-2}+\ >100}\right)+10^{-3}\approx0.043\left(\frac{1}{-1.5\times10^{-2}-j}\right)+10^{-3}. \quad (208)$$

The above is drawn in pink in Figure 23 in which the gray $h_{\mathrm{exp}}(j)$ is shown for comparison.

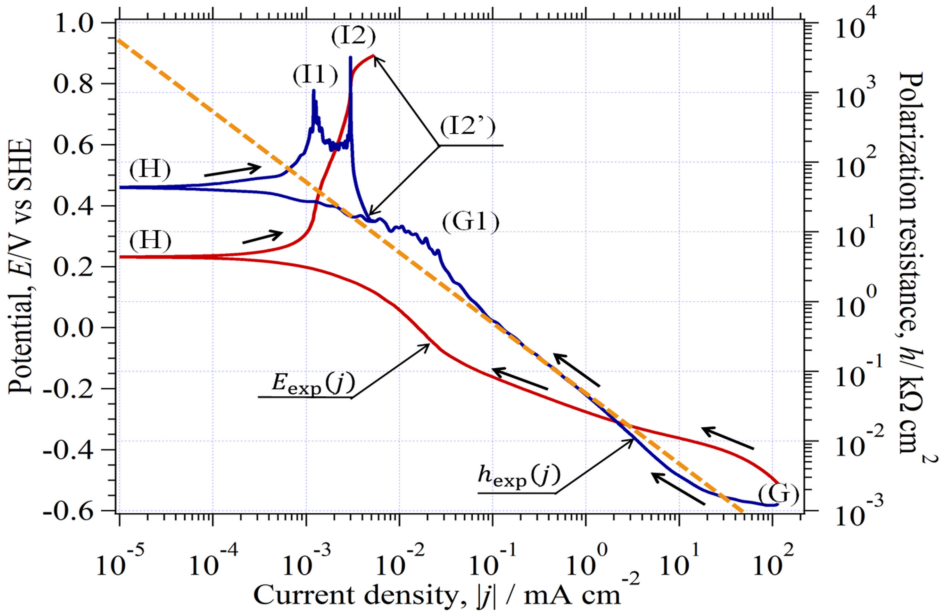

Figure 22. The representative (G) → (H) → (I) of $E_{\mathrm{exp}}(j)$ and $h_{\mathrm{exp}}(j)$ in Figures 4 and 5, respectively, are shown. The orange dashed line with the Tafel slope is shown as a reference.

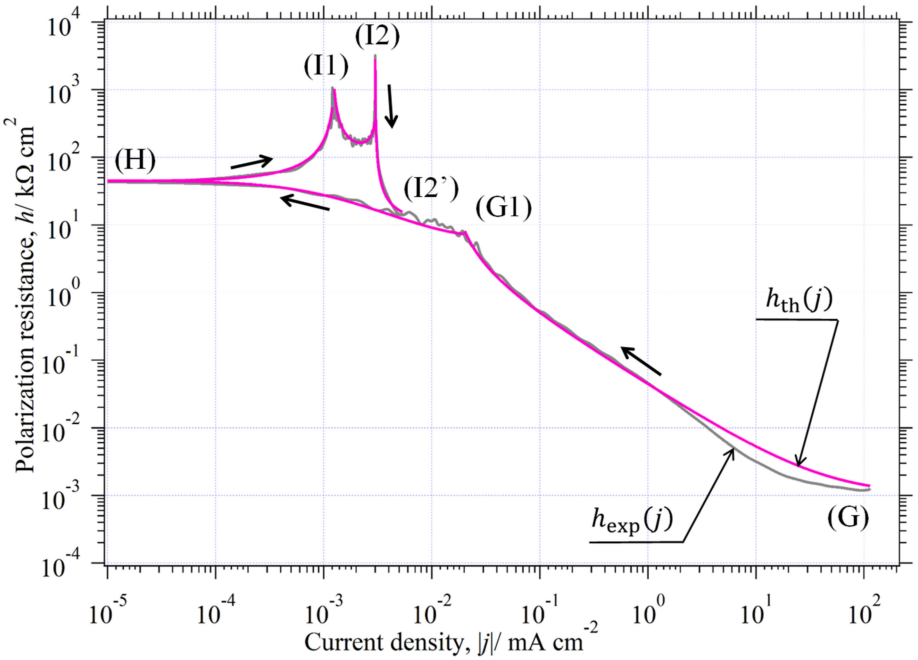

Figure 23. Comparison between pink $h_{\mathrm{th}}(j)$ and gray $h_{\mathrm{exp}}(j)$ is shown. A part of (G) → (G1) is shown. Other parts of (G1) → (H) → (I1), (I1) → (I2), and (I2) → (I2′) are also shown, which will be discussed later.

A similar result that the $h_{\mathrm{th}}(j)$ was almost on the $h_{\mathrm{exp}}(j)$ except around (G) was obtained.

(b) Analysis of (G1) → (H) → (I1)

Considering the zigzag behavior in the cathodic region and the vertical line in the anodic region, the reactions are supposed to be a mixture of Equations (192)–(194). In this paper, the main reactions are assumed as the below, which are irreversible reactions:

$$CO_{ad} + H_2O \rightarrow CO_2 + H^+ + H_{ad} + e\ (j_{a4}, E_{eq4}), \tag{209}$$

$$H_2 \leftarrow H^+ + H_{ad} + e\ (j_{c5}, E_{eq5}). \tag{210}$$

Since the above system is a mixed system having large $h_{exp}(0)$, each branch reaction is categorized to the irreversible. The $j_a(0)$ of irreversible reaction almost equals to j_0, the j_0 can be calculated using the common Equation (57).

$$j_0 = \frac{0.026}{z\ (\ h_{exp}(0) - l/\kappa)} = \frac{0.026}{(1) \times (\ 43 - 10^{-3})} = 6 \times 10^{-4}\ \text{mA cm}^{-2}. \tag{211}$$

Employing Equation (56), $h_{th}(j)$ of the anodic branch of Equation (209) ($\alpha_{a4} \approx 0.28$ by trial and error) and the cathodic branch of Equation (210) ($\alpha_{c5} \approx 0.6$) are embodied as:

$$[h_{th}(j)]_{j>0} = [h_{irrev}(j)]_{j>0} + \left(\frac{l}{\kappa}\right)_a = \frac{0.026}{z_4}\left\{\frac{1}{j_0 + (\alpha_{a4} - \alpha_{c4})\ j}\right\} + \left(\frac{l}{\kappa}\right)_a = \frac{0.026}{1}\left(\frac{1}{6 \times 10^{-4}\ - 0.45\ j}\right) + 10^{-3}, \tag{212}$$

$$[h_{th}(j)]_{j<0} = [h_{irrev}(j)]_{j<0} + \left(\frac{l}{\kappa}\right)_c = \frac{0.026}{z_5}\left\{\frac{1}{j_0 + (\alpha_{a5} - \alpha_{c5})\ j}\right\} + \left(\frac{l}{\kappa}\right)_c = \frac{0.026}{1}\left(\frac{1}{6 \times 10^{-4} - 0.2\ j}\right) + 10^{-3}. \tag{213}$$

The above $h_{th}(j)$ with pink is added to Figure 23. We can see that the pink $h_{th}(j)$ is on the gray $h_{exp}(j)$.

(c) Analysis of (I1) → (I2)

The stable chemical species of (I1) → (I2) are H^+ and CO_2. Since two clear vertical lines were observed at (I1) and (I2), these anodic reactions relate to two limiting diffusion processes. The candidate reactions are:

$$CO_{ad} + H_2O \rightarrow CO_2 + H^+ + H_{ad} + e\ (j_{a4}, E_{eq4}), \tag{214}$$

$$H_2 \rightarrow H^+ + H_{ad} + e\ (j_{a5}, E_{eq5}), \tag{215}$$

$$H_2 \rightarrow 2H^+ + 2e\ (j_{a2}, E_{eq2}). \tag{216}$$

The above j is expressed as:

$$j = j_A + j_C \approx j_A = w_{a2}\ j_{a2} + w_{a4}\ j_{a4} + w_{a5}\ j_{a5}\ . \tag{217}$$

It is impossible to distinguish j_{a5} from j_{a2}, but the observed $j_{H_2,L}$ is a summation of them. Considering the constant values of $w_{a4}\ j_{a4} + w_{a5}\ j_{a5} = w_{a4}\ j_{CO_{ad},L} + w_{a5}\ j_{H_2,L}\left(\approx 1.3 \times 10^{-3}\ \text{mA cm}^{-2}\right)$, the j_{a2} is arranged as:

$$j_{a2} = \left(j - w_{a4}\ j_{CO_{ad},L} - w_{a5}\ j_{H_2,L}\right)/w_{a2} = \left(j - 1.3 \times 10^{-3}\right)/w_{a2}. \tag{218}$$

Similarly, the $h(j)$ is expressed as:

$$h(j) = \frac{h_{a2}(j_{a2})}{w_{a2}} = \frac{h_{a2}\left(\left(j - 1.3 \times 10^{-3}\right)/w_{a2}\right)}{w_{a2}}. \tag{219}$$

Since the above $h_{a2}(j_{a2})$ is the anodic branch of the reversible *HERher*, its $h_{th}(j)$ is:

$$h_{\mathrm{th}}(j) = \frac{h_{\mathrm{a2}}\left(\left(j-1.3\times10^{-3}\right)/w_{\mathrm{a2}}\right)}{w_{\mathrm{a2}}} + \left(\frac{l}{\kappa}\right)_{\mathrm{a}} = \frac{1}{w_{\mathrm{a2}}}\frac{R\ T}{z_2\ F}\left(\frac{1}{\left(j-1.3\times10^{-3}\right)/w_{\mathrm{a2}}} + \frac{2}{w_{\mathrm{a2}}\ j_{\mathrm{H_2,L}} - \left(j-1.3\times10^{-3}\right)/w_{\mathrm{a2}}}\right) + \left(\frac{l}{\kappa}\right)_{\mathrm{a}}$$
$$\approx \frac{0.026}{2}\left(\frac{1}{j-1.3\times10^{-3}} + \frac{2}{{w_{\mathrm{a2}}}^2\ j_{\mathrm{H_2,L}} + 1.3\times10^{-3} - j}\right) + \left(\frac{l}{\kappa}\right)_{\mathrm{a}}. \quad (220)$$

For an example, when ${w_{\mathrm{a2}}}^2\ j_{\mathrm{H_2,L}} \approx 2\times10^{-3}$ mA cm^{-2}, and $(l/\kappa)_{\mathrm{a}} \approx 140$ kΩ cm^2, the above is embodied as:

$$h_{\mathrm{th}}(j) = \frac{0.026}{2}\left(\frac{1}{j-1.3\times10^{-3}} + \frac{2}{3.3\times10^{-3}-j}\right) + 140. \quad (221)$$

The above is drawn with pink in Figure 20. We can see that the pink $h_{\mathrm{th}}(j)$ is on the gray $h_{\mathrm{exp}}(j)$. The large increase of $(l/\kappa)_{\mathrm{a}}$ from 10^{-3} kΩ cm^2 to 140 kΩ cm^2 is probably due to the residue $\mathrm{H_{ad}}$ and the newly produced $\mathrm{H_{ad}}$ by Equations (214) and (215).

(d) Analysis of $(\mathrm{I2}) \rightarrow (\mathrm{I2}')$

The stable chemical species of $(\mathrm{I2}) \rightarrow (\mathrm{I2}')$ are $\mathrm{H^+}$ and $\mathrm{CO_2}$, too. It is characteristic that three-digit drop of $h_{\mathrm{exp}}(j)$ was observed. Considering the significant decrease, it is apparent that the $\mathrm{H_{ad}}$ consuming reaction had occurred. The oxidation reaction of $\mathrm{H_{ad}}$ should be newly added to the previous reactions:

$$\mathrm{H_{ad}} \rightarrow \mathrm{H^+ + e^-}\left(i_{\mathrm{a3}}, E_{\mathrm{eq3}}\right), \quad (222)$$

The j is:

$$j = j_{\mathrm{A}} + j_{\mathrm{C}} \approx j_{\mathrm{A}} = w_{\mathrm{a2}}\ j_{\mathrm{a2}} + w_{\mathrm{a3}}\ j_{\mathrm{a3}} + w_{\mathrm{a4}}\ j_{\mathrm{a4}} + w_{\mathrm{a5}}\ j_{\mathrm{a5}} \quad (223)$$

Similarly, when the vertical value at (I2) is the constant value of $w_{\mathrm{a2}}\ j_{\mathrm{a2}} + w_{\mathrm{a4}}\ j_{\mathrm{a4}} + w_{\mathrm{a5}}\ j_{\mathrm{a5}} = (w_{\mathrm{a2}} + w_{\mathrm{a5}})j_{\mathrm{H_2,L}} + w_{\mathrm{a4}}\ j_{\mathrm{CO_{ad},L}}\left(\approx 3.2\times10^{-3}\ \mathrm{mA\ cm^{-2}}\right)$, the j_{a3} is expressed as:

$$j_{\mathrm{a3}} = \left(j - 3.2\times10^{-3}\right)/w_{\mathrm{a3}}. \quad (224)$$

Since the $h_{\mathrm{a3}}(j_{\mathrm{a3}})$ is the anodic branch resistance of irreversible reaction, the $h_{\mathrm{th}}(j)$ is expressed when $(l/\kappa)_{\mathrm{a}} \approx 10^{-3}$ kΩ cm^2 and $\alpha_{\mathrm{a3}}\ z_3 \approx 0.7$:

$$h_{\mathrm{th}}(j) = \frac{h_{\mathrm{a3}}\left(\left(j-3.2\times10^{-3}\right)/w_{\mathrm{a3}}\right)}{w_{\mathrm{a3}}} + \left(\frac{l}{\kappa}\right)_{\mathrm{a}}.$$
$$= \frac{R\ T}{\alpha_{\mathrm{a3}}\ z_3\ F}\left(\frac{1}{j-3.2\times10^{-3}} + \frac{1}{{w_{\mathrm{a3}}}^2\ j_{\mathrm{H_{ad},L}} + 3.2\times10^{-3} - j}\right) + \left(\frac{l}{\kappa}\right)_{\mathrm{a}} \quad (225)$$

Under assumption of

$$\frac{1}{{w_{\mathrm{a3}}}^2\ j_{\mathrm{H_{ad},L}} - j + 3.2\times10^{-3}} \approx 0, \quad (226)$$

Equation (225) will be approximated to:

$$h_{\mathrm{th}}(j) \approx \frac{0.026}{0.7}\frac{1}{j - 3.2\times10^{-3}} + 10^{-3}. \quad (227)$$

The above $h_{\mathrm{th}}(j)$ of $(\mathrm{I2}) \rightarrow (\mathrm{I2}')$ is drawn with pink in Figure 23. We can see that the pink $h_{\mathrm{th}}(j)$ is on the gray $h_{\mathrm{exp}}(j)$. The large drop of $(l/\kappa)_{\mathrm{a}}$ to 10^{-3} kΩ cm^2 from the previous 140 kΩ cm^2 is due to complete disappearance of $\mathrm{H_{ad}}$.

3.9.3. Analysis of $(I2') \rightarrow (J) \rightarrow (K)$

The representative $h_{exp}(j)$ of downward track of $(I2') \rightarrow (J) \rightarrow (K)$ is picked up and shown in Figure 24 together with its $E_{exp}(j)$.

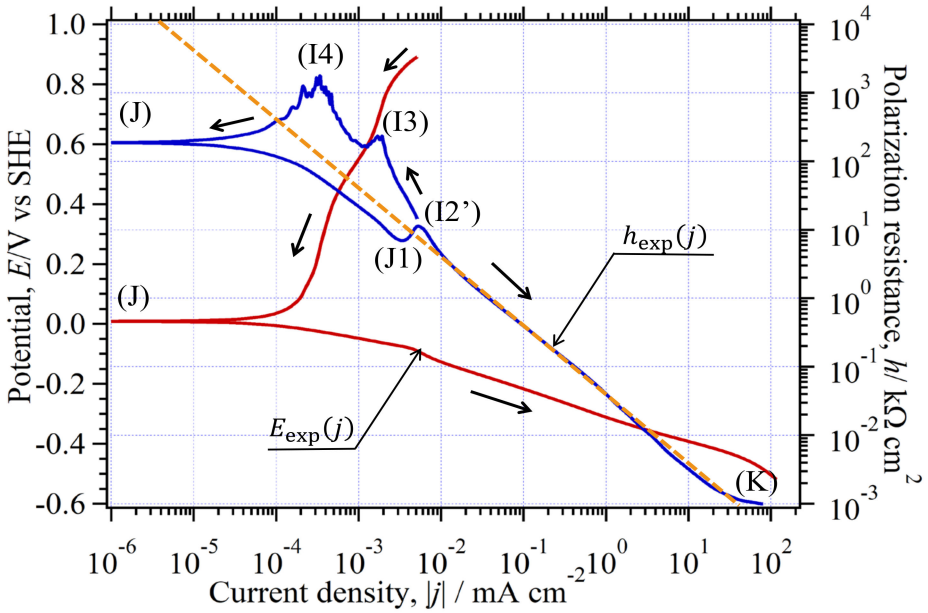

Figure 24. The representative $(I2') \rightarrow (J) \rightarrow (K)$ of $E_{exp}(j)$ and $h_{exp}(j)$ in Figures 4 and 5, respectively, are shown. The orange dashed line with the Tafel slope is shown as a reference.

The reactions in this track should be the same reactions as that of $(G) \rightarrow (I2')$. We can obtain the numerical $h(j)$ using the same equations but different data. Similarly, it is necessary to divide $(I2') \rightarrow (J) \rightarrow (K)$ into five parts: $(I2') \rightarrow (I3)$, $(I3) \rightarrow (I4)$, $(I4) \rightarrow (J) \rightarrow (J1)$, $(J1) \rightarrow (J1')$, and $(J1') \rightarrow (K)$. The $h_{th}(j)$ divided into five parts is shown in Figure 25 with pink together with the gray $h_{exp}(j)$ curve.

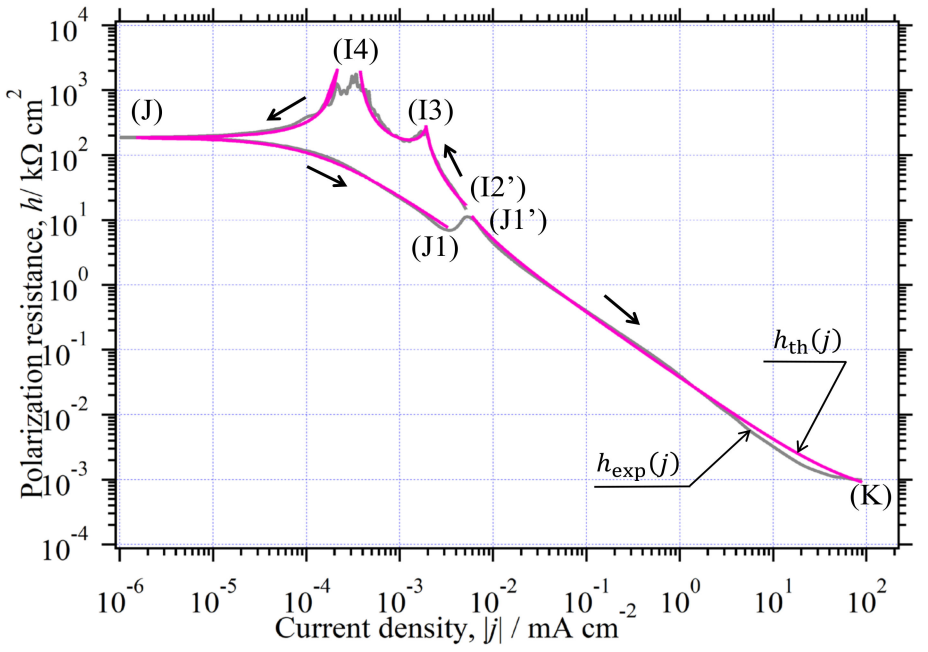

Figure 25. Comparison between pink $h_{th}(j)$ and gray $h_{exp}(j)$ in $(I2') \rightarrow (J) \rightarrow (K)$ is shown. All divided parts of $(I2') \rightarrow (I3)$, $(I3) \rightarrow (I4)$, $(I4) \rightarrow (J) \rightarrow (J1)$, $(J1) \rightarrow (J1')$, and $(J1') \rightarrow (K)$ are also shown together.

(a) Part analysis of $(\mathrm{I2}') \rightarrow (\mathrm{I3})$

Using the same as Equation (227) but different data, the $h_{\mathrm{th}}(j)$ of $(\mathrm{I2}') \rightarrow (\mathrm{I3})$ is embodied as:

$$h_{\mathrm{th}}(j) \approx \frac{0.026}{0.5} \frac{1}{j - 1.8 \times 10^{-3}} + 10^{-3} \tag{228}$$

The overlap between the $h_{\mathrm{th}}(j)$ and the $h_{\mathrm{exp}}(j)$ shows the result of good approximation. The different data used are two: $\alpha_{\mathrm{a3}} = 0.5$ (from the previous value of 0.7) and $(w_{\mathrm{a2}} + w_{\mathrm{a5}}) j_{\mathrm{H_2,L}} + w_{\mathrm{a4}}\ j_{\mathrm{CO_{ad},L}} \approx 1.8 \times 10^{-3}$ mA cm^{-2} (from the previous value of 3.2×10^{-3} mA cm^{-2}). Clear reasons for the differences are unknown, but one of them may be due to the appearance or disappearance of $\mathrm{H_{ad}}$.

(b) Part analysis of $(\mathrm{I3}) \rightarrow (\mathrm{I4})$

The $h_{\mathrm{th}}(j)$ in this region is the same as Equation (221), but different data.

$$h_{\mathrm{th}}(j) = \frac{0.026}{0.5} \left(\frac{1}{j - 0.35 \times 10^{-3}} + \frac{1}{2.2 \times 10^{-3} - j} \right) + 70 \tag{229}$$

The reason for change of $z = 2$ to $z = 0.5$ is by curve fitting result. The actual reaction may be different from Equations (214)–(216). The further experiments are needed. The above is drawn with pink in Figure 25. We can see that the pink $h_{\mathrm{th}}(j)$ is on the gray $h_{\mathrm{exp}}(j)$. The decrease of $(l/\kappa)_{\mathrm{a}}$ to 70 kΩ cm^2 from 140 kΩ cm^2 is probably due to the decrease of the $\mathrm{H_{ad}}$.

(c) Part analysis of $(\mathrm{I4}) \rightarrow (\mathrm{J}) \rightarrow (\mathrm{J1})$

The $h_{\mathrm{th}}(j)$ in this region is the same as Equations (212) and (213), but different data. Similarly, j_0 can be calculated as:

$$j_0 = \frac{0.026}{z\ (\ h_{\mathrm{exp}}(j) - l/\kappa)} = \frac{0.026}{(1) \times\ (\ 190 - 10^{-3})} = 1.4 \times 10^{-4}\ \mathrm{mA\ cm^{-2}}. \tag{230}$$

Employing Equation (56) and the curve fitting, $h_{\mathrm{th}}(j)$ of the anodic branch ($\alpha_{\mathrm{a4}} \approx 0.2$) and the cathodic branch ($\alpha_{\mathrm{c5}} = 0.995$) are expressed as:

$$[h_{\mathrm{th}}(j)]_{j>0} = [h_{\mathrm{irrev}}(j)]_{j>0} + \left(\frac{l}{\kappa}\right)_{\mathrm{a}} = \frac{0.026}{1} \left(\frac{1}{1.4 \times 10^{-4}\ - 0.6\, j} \right) + 10^{-3}, \tag{231}$$

$$[h_{\mathrm{th}}(j)]_{j<0} = [h_{\mathrm{irrev}}(j)]_{j<0} + \left(\frac{l}{\kappa}\right)_{\mathrm{c}} = \frac{0.026}{1} \left(\frac{1}{1.4 \times 10^{-4} - 0.99\, j} \right) + 10^{-3}. \tag{232}$$

The above $h_{\mathrm{th}}(j)$ with pink is added to Figure 25. We can see that the pink $h_{\mathrm{th}}(j)$ is on the gray $h_{\mathrm{exp}}(j)$. Around (J1), there was a gap. This gap is caused by irreversible reactions having values of $\alpha_{\mathrm{a3}} = 0.6$ and $\alpha_{\mathrm{a5}} \approx 0.995$.

(d) Part analysis of $(\mathrm{J1}') \rightarrow (\mathrm{K})$

Using the same Equation (208) and the same data:

$$h_{\mathrm{th}}(j) = \frac{0.026}{0.6} \left(\frac{1}{-1.5 \times 10^{-2} - j} + \frac{1}{j\ +\ 1.5 \times 10^{-2} +\ > 100} \right) + 10^{-3} \approx 0.043 \left(\frac{1}{-1.5 \times 10^{-2} - j} \right) + 10^{-3} \tag{233}$$

The above $h_{\mathrm{th}}(j)$ curves considerably overlapped with the $h_{\mathrm{exp}}(j)$ curves.

3.10. Analysis of Quasireversible HER (Environment (III))

When the CO injection is stopped, the test solution will be gradually occupied by $\mathrm{H_2}$. Complete restoration to the reversible reaction will depend on whether the Pt surface is thoroughly clean or not.

3.10.1. Estimation of w_a at CO Stopped

Figure 6 shows the shape changes of $E_{exp}(j)$ when the CO injection is stopped. We can see that the first $E_{exp}(j)$ followed the irregular track of (M) → (N) → (O)→ (P), but the second and subsequent curve converged to the regular track of (P) → (Q) → (R). Considering the solution saturated with H_2, main reaction is the *HER*:

$$H_2 \rightleftarrows 2\,H^+ + 2e\ (j_1, E_{eq1}). \tag{234}$$

The cathodic branch curve shape in Figure 6 is very similar to that in Figure 2, so we can deduce that the cathodic branch contains reversible *her* process. Focusing on the anodic branch, on the other hand, an apparent tendency of sequential changes of j_{a1} was observed, especially at the potential range of 0.3 V $\leq E \leq$ 0.7 V. Careful reading leads to the fact that the value of j_{a1} at 0.7 V increased with the increase of cycle number (N). The increased w_a can be calculated as:

$$w_a = \frac{[w_a\ j_{a1}]_{\text{at 0.7 V}}}{j_{H_2,L}} = \frac{3\times10^{-2}\ \sim 5\times10^{-2}}{0.74} = 0.04\ \sim 0.07 \tag{235}$$

The increasing w_a as increasing N is another sign that the *hor* gradually recovers from the contaminated state. We can see that there is an interesting fact when calculating $j_A(0)$. Comparing the $h_{exp}(0) \approx 0.02$ kΩ cm^2 in Figure 3 against the $h_{exp}(0) \approx 0.03 \sim 0.06$ kΩ cm^2 in Figure 7, the $j_A(0)$ ratio between them is calculated below:

$$\frac{j_A(0)_{\text{in Figure 3}}}{j_A(0)_{\text{in Figure 7}}} = \frac{\left[\frac{R\ T}{z\ F}\frac{1}{(h_{exp}(0)-l/\kappa)}\right]_{\text{in Figure 3}}}{\left[\frac{R\ T}{z\ F}\frac{1}{(h_{exp}(0)-l/\kappa)}\right]_{\text{in Figure 7}}} = \frac{(h_{exp}(0)-l/\kappa)_{\text{in Figure 7}}}{(h_{exp}(0)-l/\kappa)_{\text{in Figure 3}}} = \frac{(0.03\ \sim 0.06)-10^{-3}}{0.022-10^{-3}} = 1.4\ \sim 2.8 \tag{236}$$

When the above ratio is averaged and assumed to 2, it is the same ratio of $j_A(0)$ between the reversible ($j_A(0) \approx j_d$) and the quasireversible ($j_A(0) \approx j_d/2$). Taking into account the experimental facts, the $j_A(0)$ ratio and the curve shape resembling, the reaction in the environment (III) can be categorized to the quasireversible. This means that the CO-contaminated Pt surface is gradually changed to be clean after several N.

3.10.2. Determination of Kinetic Parameters in the CO-Stopped Solution

In previous sections, we discussed that redox reaction in the H_2SO_4 + H_2 + CO-CO solution is the quasireversible. Some curves are probably on the way of the recovery process from the irreversible to the reversible. Figure 26 shows the enlarged current region at $j \approx 0$. Arrows and numbers of (1)~(12) are the polarization direction and the N, except for the first cycle.

It is clear that the linear relation holds in the range of $|j| \leq 0.02$ mA cm^{-2}. The values of α_c and z are calculated by employing the $h_{exp}(0)$, the calculated slopes, and $j_A(0) = 0.46$ mA cm^{-2} (by graphical determination, detailed in later 3.10.3):

$$z = \frac{R\ T}{F}\frac{1}{j_A(0)(h_{exp}(0)-l/\kappa)} = \frac{0.026}{(0.46)(h_{exp}(0)-0.001)} \tag{237}$$

$$\text{slope} = \left(h_{exp}(0)-\frac{l}{\kappa}\right)\left(\frac{2\ \alpha_a}{w_a\ j_{H_2,L}} + \frac{2\ \alpha_c}{w_c j_{H^+,L}} + \frac{1-2\ \alpha_a}{j_A(0)}\right) \approx (h_{exp}(0)-10^{-3})\left(\frac{2(1-\alpha_c)}{0.7} + \frac{2\ \alpha_c}{-325} + \frac{1-2(1-\alpha_c)}{0.46}\right) \tag{238}$$

The relation between the calculated values (α_c and z) and the N was plotted. The results are shown in Figure 27.

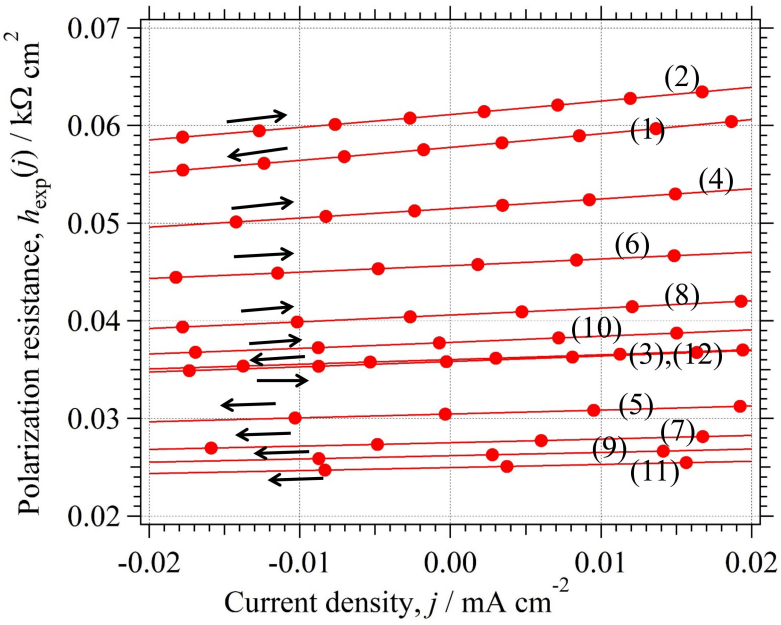

Figure 26. Relationship between $h_{exp}(j)$ and the enlarged j. We can find that there is a linear relation at $|j| \approx 0$ mA cm^{-2} $\left(\leq 0.02 \text{ mA cm}^{-2}\right)$.

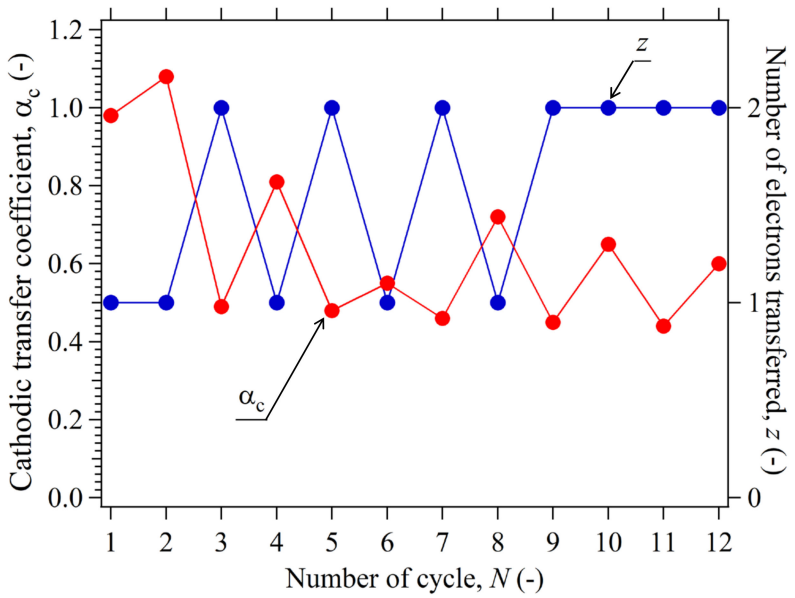

Figure 27. Relationship between the calculated values (α_c and z) and the cycle number (N) is shown. We can see that the α_c and the z converge to 0.6 and 2, respectively, at N = 12.

We can see that the α_c and the z are about 0.5 and 2 at N = 12. In detail, we can find an interesting fact that the α_c of the odd N was smaller than that of the even N. The reason is not so clear, but the α_c is changeable and may be deeply influenced by polarization history. Further confirmations are needed.

3.10.3. Graphical Determination of $j_A(0)$

Employing the determination way of $j_A(0)$ discussed in Section 3.5, we can graphically read its value. One of the tracks (as a representative; (P)–(Q)–(R) of N = 12) was employed. It is the green curve shown in Figure 28.

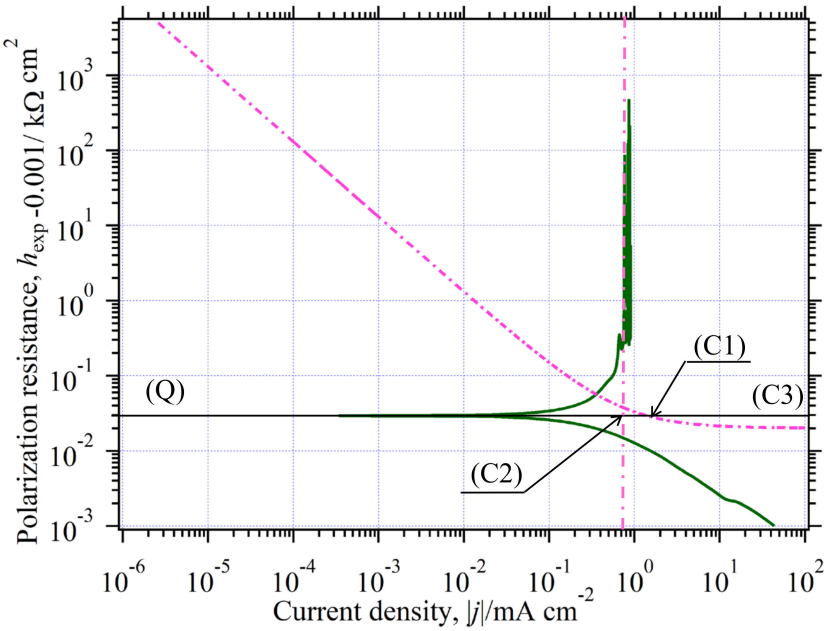

Figure 28. The track of $\log h(j)$ vs. $\log|\ j\ |$ of N=12 in Figure 7 is selected as a representative for the graphical estimation. The $h_{A0}(j_0)$ is drawn in pink with chain curve. The chain line of $w_a\ j_{H_2,L}$ is added for easy reading.

The $h_{A0}(j_0)$ of Equation (75) and the $w_a\ j_{H_2,L}\left(=0.7\ \text{mA cm}^{-2}\right)$ are added to Figure 28 with pink chain curve. The horizontal straight line of $h_{exp}(0)-10^{-3}$ ($\approx 0.03\ \text{k}\Omega\ \text{cm}^2$ at $N=12$) meets the $h_{A0}(j_0)$ at (C1) and the $w_a\ j_{H_2,L}$ at (C2). Three crossed points are shown as:

$$j_0 \approx 1.4\ \text{mA cm}^{-2}: \text{(C1)}, \tag{239}$$

$$w_a\ j_{H_2,L} = 0.7\ \text{mA cm}^{-2}: \text{(C2)}, \tag{240}$$

$$\left|w_c\ j_{H^+,L}\right|: \text{(C3)}\ \left(\text{cannot observed, assumed to} > 10^2\ \text{mA cm}^{-2}\right). \tag{241}$$

Substituting the above readings into Equation (7), we can calculate the $j_A(0)$:

$$j_A(0) = \frac{1}{1/j_0 + 1/\ j_{Red,L} + 1/-\ j_{Ox^{z+},L}} = \frac{1}{1/(\approx 1.4) + 1/0.70 + 1/ > 10^2} \approx 0.46\ \text{mA cm}^{-2}. \tag{242}$$

Employing the $j_A(0)$ and the $h_{exp}(0)$, the z can be roughly calculated to:

$$z = \frac{RT}{F}\frac{1}{j_A(0)\ h(0)} = \frac{0.026}{(0.46)(0.03)} = 1.77 \approx 2. \tag{243}$$

The rough agreement of $j_A(0)\left(\approx 0.46\ \text{mA cm}^{-2}\right)$ with $j_d/2\ \left(=0.70\ \text{mA cm}^{-2}/2 = 0.35\ \text{mA cm}^{-2}\right)$ can also lead to the conclusion that the redox reaction in a H_2SO_4 + H_2 + CO-CO solution is a quasireversible reaction.

3.10.4. Agreement between $E_{exp}(j)$ and $E_{th}(j)$

Employing $\alpha_c = 0.6, l/\kappa = 10^{-3}\ \text{k}\Omega\ \text{cm}^2$, $(l/\kappa)_a = 10^{-3}\ \text{k}\Omega\ \text{cm}^2$, $(l/\kappa)_c = 10^{-3}\ \text{k}\Omega\ \text{cm}^2$, $w_a\ j_{H_2,L} = 0.7\ \text{mA cm}^{-2}$, and $\left|w_c\ j_{H^+,L}\right| > 10^2\ \text{mA cm}^{-2}\left(\approx 325\ \text{mA cm}^{-2}\right)$, the quasireversible $h_{th}(j)$ is calculated using Equations (133)–(137). The calculated result is shown below:

$$h_{th}(j) = h_{quasi}(j) + \frac{l}{\kappa} = \frac{0.0024}{16.5\ -\ j} + \frac{0.018}{0.53\ -\ j} + \frac{0.014}{j+4.60} + \frac{0.0063}{j+338} + 1.5\times 10^{-3}. \tag{244}$$

Taking into account the realistic restrictions, (1) $h_{\mathrm{th}}(j)$ has two terms corresponding to the anodic and cathodic branchs, (2) the numerator is near to 0.013 (=0.026/2), and (3) $h_{\mathrm{th}}(0) = h_{\mathrm{exp}}(0)\left(\approx 0\ \mathrm{k\Omega\ cm^2}\right)$, the above $h_{\mathrm{th}}(j)$ is approximated as below:

$$h_{\mathrm{th}}(j) = 0.013\left(\frac{1}{0.53\ -\ j} + \frac{1}{j + 4.60}\right) + 1.5 \times 10^{-3}. \tag{245}$$

The above $h_{\mathrm{th}}(j)$ above was plotted on the $h_{\mathrm{exp}}(j)$ in Figure 3. The result is shown in Figure 29.

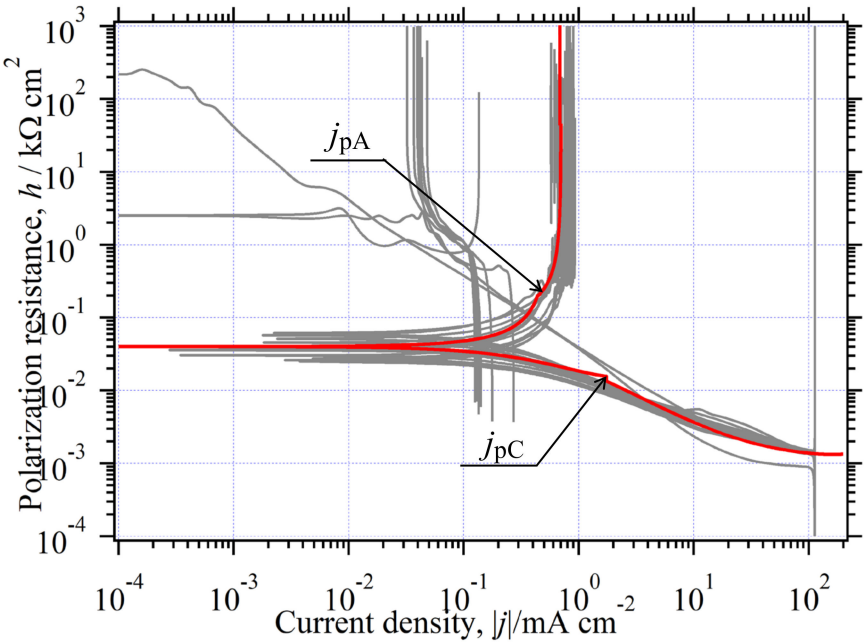

Figure 29. The $h_{\mathrm{th}}(j)$ was plotted on the $h_{\mathrm{exp}}(j)$. We can see that the red $h_{\mathrm{th}}(j)$ is almost overlaid on the gray $h_{\mathrm{exp}}(j)$.

We can see that the red $h_{\mathrm{th}}(j)$ is almost on the gray $h_{\mathrm{exp}}(j)$. In addition to the $h(j)$ curve agreement, it is needed to confirm the agreement between $E_{\mathrm{exp}}(j)$ and $E_{\mathrm{th}}(j)$. In the case of quasireversible reaction, it is necessary for the complete agreement that the $E_{\mathrm{th}}(j)$ is divided into three parts. They are obtained by solving the following differentiated equations under initial conditions:

(1) $w_{\mathrm{c}}\, j_{\mathrm{H^+,L}} \le j \le j_{\mathrm{pC}}\ \left(-325\ \mathrm{mA\ cm^{-2}} \le j \le -1.74\ \mathrm{mA\ cm^{-2}}\right)$

$$\frac{\mathrm{d}\, E_{\mathrm{th}}(j)}{\mathrm{d}\, j} = h_{\mathrm{th}}(j) = 0.027\ \ln\left(\frac{1}{0.437 - j} + \frac{1}{j + 322}\right) + 10^{-3}, \tag{246}$$

$$E_{\mathrm{th}}\left(j_{\mathrm{pC}}\right) = E_{\mathrm{th}}(-1.74) = -0.028\ \mathrm{V\ (an\ initial\ condition)}. \tag{247}$$

The above solution is as below:

$$E_{\mathrm{th}}(j) = -0.16 + 0.027\ \ln\left(\frac{j\ +\ 325}{0.437\ -\ j}\right) + 10^{-3}\, j. \tag{248}$$

(2) $j_{\mathrm{pC}} \le j \le j_{\mathrm{pA}}\ \left(-1.74\ \mathrm{mA\ cm^{-2}} \le j \le 0.437\ \mathrm{mA\ cm^{-2}}\right)$

$$\frac{\mathrm{d}\, E_{\mathrm{th}}(j)}{\mathrm{d}\, j} = h_{\mathrm{th}}(j) = -0.028 + 0.013\ \ln\left(\frac{j + 4.60}{0.53 - j}\right) + 1.5 \times 10^{-3}, \tag{249}$$

$$E_{\mathrm{th}}(j) = 0\ \mathrm{V\ (an\ initial\ condition)}. \tag{250}$$

The solution is:

$$E_{\mathrm{th}}(j) = -0.063 - 0.0024\ \ln(16.5 - j) - 0.018\ \ln(0.53 - j) + 0.014\ \ln(j + 4.60) + 0.063\ \ln(j + 338) + 1.5 \times 10^{-3} j. \quad (251)$$

(3) $j_{\mathrm{pA}} \le j \le w_{\mathrm{a}}\, j_{\mathrm{H_2,L}}$ $\left(0.437\ \mathrm{mA\ cm^{-2}} \le j \le 0.70\ \mathrm{mA\ cm^{-2}}\right)$

$$\frac{\mathrm{d}\, E_{\mathrm{th}}(j)}{\mathrm{d}\, j} = h_{\mathrm{th}}(j) = 0.046\left(\frac{1}{0.70 - j} + \frac{1}{1.74 + j}\right) + 10^{-3}, \quad (252)$$

$$E_{\mathrm{th}}(j_{\mathrm{pA}}) = E_{\mathrm{th}}(0.437) = 0.024\ \mathrm{V\ (an\ initial\ condition)}. \quad (253)$$

The result is shown as:

$$E_{\mathrm{th}}(j) = -0.074 + 0.046\ \ln\left(\frac{1.74 + j}{0.70 - j}\right) + 10^{-3}\, j. \quad (254)$$

The concrete $E_{\mathrm{th}}(j)$ is drawn with red on the gray $E_{\mathrm{exp}}(j)$. The result is shown in Figure 30.

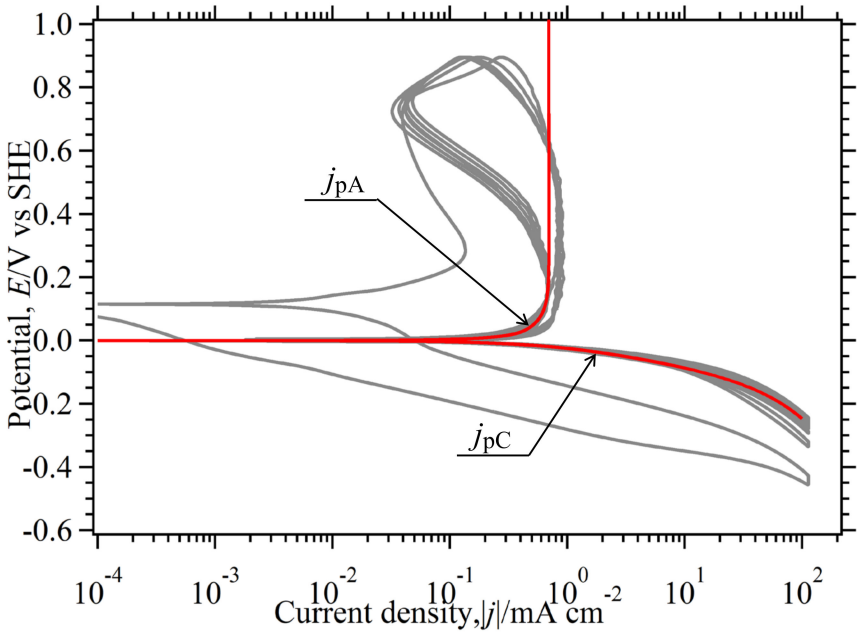

Figure 30. The curve of $E_{\mathrm{th}}(j)$, which is obtained by solving the differentiated equations, is drawn with red. The cathodic part of $E_{\mathrm{th}}(j)$ is on the gray $E_{\mathrm{exp}}(j)$.

The curve technique using $h(j)$ shows that the cathodic part of $E_{\mathrm{th}}(j)$ completely overlaps with $E_{\mathrm{exp}}(j)$. In contrast, the anodic part of $E_{\mathrm{th}}(j)$ shows almost a line compared to the curve of $E_{\mathrm{exp}}(j)$. When considering w_{a} as a function of η or time, the anodic part of $E_{\mathrm{th}}(j)$ will probably show better agreement with $E_{\mathrm{exp}}(j)$. Some mentioned above will be further studied and reported elsewhere.

4. Experimental Section

4.1. Specimens

Two platinum wires (99.98% Pt, NILACO Ltd., Tokyo, Japan) were employed for working and counter electrodes. Each wire was 0.3 mm in diameter and 50 cm in length. The electrodes were formed on a spiral shape. The counter electrode had a geometric area of 4.7 $\mathrm{cm^2}$. The working electrode had an exposure area of 3 $\mathrm{cm^2}$ by masking an insulating area with silicon resin. They were ultrasonically cleaned in warm acetone and immersed in

a HNO_3 solution for 180 s at an ambient temperature. They were rinsed thoroughly with deionized water before every test.

4.2. Test Solution

Chemical grade sulfuric acid (98% H_2SO_4, Wako Pure Chemical Industries, Tokyo, Japan), high purity hydrogen gas (99.99999% H_2, Air-Water Inc., Tokyo, Japan), and carbon monoxide gas (99.95% CO, Air-Water Inc., Tokyo, Japan) were employed. The test solution was saturated with H_2 and injected with CO under atmospheric pressure. The solution was deionized water having 1 dm^3. During experiments, the solution was always maintained in the H_2-saturated condition by continuous H_2 bubbling. The solution pH and electrolyte conductivity of the test solution were about 0.3 and $\geq$20 S m^{-1}, respectively. The dissolved oxygen concentration in the solution was always <0.4 ppm.

4.3. Measurements

Measurements were carried out under the H_2-saturated solution at around 298 K. The CO gas was injected/stopped in a 0.5 mol dm^{-3} H_2SO_4 solution. An automatic electrochemical instrument (Hokuto Denko Inc., HZ7000, Tokyo, Japan) was employed for CV. The Ag/AgCl electrode in the saturated KCl solution (DKK-TOA Co., HS-305D, Tokyo, Japan) was used as a reference electrode. All of the electrode potentials were converted to V vs. SHE and simplified to V in this paper unless otherwise noted. The distance between the working and reference electrodes was <1 cm. The $E(j)$ curve was not corrected for the jR drop because the physical factors such as solution resistance can be compensated using the curve technique, which was detailed in Section 3.6.2. A slow scan rate of 0.3 mV s^{-1} was selected for the steady state measurement because the $E(j)$ unaffected by time is supposed to be the steady state curve [5,34]. Since the resulting data had frequent scattering tendency, smoothing was necessary. Using a commercial software (Igor Pro 6, 6.2.2.0, WaveMetrics, Lake Osawego, OR, USA, 2011), the experimental $E(j)$ was mathematically smoothed. Arranging mathematical formulas, commercially available software (Mathematica ver.10) was used.

5. Conclusions

In order to analyze the CO poisoning effect, a few curve techniques were employed to investigate the hydrogen electrode reaction (*HER* = *hor* + *her*) occurring on the Pt electrode in a 0.5 mol dm^{-3} H_2SO_4 solution saturated with H_2 when CO-injected or not. Using the curve techniques, the followings were confirmed: *HER* before CO injection showed typical reversible reaction, having z = 2. After CO injection, *her* was changed to an irreversible reaction, having z = 1 and $\alpha_c \approx 0.6$. When CO injection was stopped, *HER* gradually changed to quasireversible from an irreversible reaction. The $h(j)$ of *HER* before/after the CO injection were analyzed not only algebraically but also graphically. It was found that *HER* poisoned with CO would change to a reversible, irreversible, or quasireversible reaction depending on CO content in the solution. It was also found that the kinetic parameters transferring among reversible, irreversible, and quasireversible could be determined by employing $h(j)$.

Author Contributions: Conceptualization, O.S. and K.F.; methodology, K.F.; formal analysis, O.S.; investigation, K.F.; data curation, O.S. and K.F.; writing—original draft preparation, O.S.; writing—review and editing, O.S. and K.F.; All authors have read and agreed to the published version of the manuscript.

Funding: This research received no external funding.

Conflicts of Interest: The authors declare no conflict of interest.

Appendix A. List of Symbols

$J(\eta)$ is the net current as a function of overpotential (mA).
$J_a(\eta)$ is the anodic branch current as a function of overpotential (mA).
$J_c(\eta)$ is the cathodic branch current as a function of overpotential (mA).
S is the geometrical surface of electrode (cm^2).
S_a is the effective area where the $J_a(\eta)$ flows (cm^2).
S_c is the effective area where the $J_c(\eta)$ flows (cm^2).
w_a is the weighting factor that has suitably weighted value in proportion to the surface of the anode (-).
w_c is the weighting factor that has suitably weighted value in proportion to the surface of the cathode (-).
$j(\eta)$ is the net current density as a function of overpotential (mA cm^{-2}).
$j_a(\eta)$ is the anodic branch current density as a function of overpotential (mA cm^{-2}).
$j_c(\eta)$ is the cathodic branch current density as a function of overpotential (mA cm^{-2}).
$j_{pa}(\eta)$ is the minimum $j_a(\eta)$ in the state of $j(\eta) = j_a(\eta) + j_c(\eta) \approx j_a(\eta)$ (mA cm^{-2}).
$j_{pc}(\eta)$ is the maximum $j_c(\eta)$ in the state of $j(\eta) = j_a(\eta) + j_c(\eta) \approx j_c(\eta)$ (mA cm^{-2}).
η is the overpotential between an applied potential, E and the E_{eq} (V).
$\eta = E - E_{eq}$ (A1).
E_{eq} is the equilibrium electrode potential (V vs. SHE).
$E_{eq} = E^0 + \frac{R\ T}{z\ F} \ln \frac{\{Ox^{z+}\}_{bulk}}{\{Red\}_{bulk}} = E^{\varnothing} + \frac{R\ T}{z\ F} \ln \frac{[Ox^{z+}]_{bulk}}{[Red]_{bulk}}$ (A2).
E^0 is the standard electrode potential (V vs. SHE).
$E^{\varnothing}$ is the formal electrode potential (V vs. SHE).
z is the number of electrons transferred (-).
F is the Faraday's constant ($F = 96.5 \times 10^3$ A s mol^{-1}).
R is the gas constant $\left(R = 8.31 \text{ J mol}^{-1} \text{ K}^{-1}\right)$.
T is the absolute temperature (K).
$\{Red\}_{bulk}$ is the activity of reductant (Red) in the bulk solution (-).
$\{Ox^{z+}\}_{bulk}$ is the activity of oxidant (Ox^{z+}) in the bulk solution (-).
$[Red]_{bulk}$ is the concentration of the Red in the bulk solution (mol dm^{-3}).
$[Ox^{z+}]_{bulk}$ is the concentration of the Ox^{z+} in the bulk solution (mol dm^{-3}).
f_a is $\alpha_a\ z\ F/RT$ (V^{-1}).
f_c is $\alpha_c\ z\ F/RT$ (V^{-1}).
α_a is the anodic transfer coefficient (-).
α_c is the cathodic transfer coefficient (-) ($= 1 - \alpha_a$).
f is $z\ F/RT$ (V^{-1}).
$f = f_a + f_c = z\ F/RT$ (V^{-1}) (A3).
$j_{Red,L}$ is the limiting diffusion current density of the Red, $\left(\text{mA cm}^{-2}\right)$.
$j_{Red,L} = z\ F\ \frac{D_{Red}}{\delta_{Red}} [Red]_{bulk} = z\ F\ k_{Red} [Red]_{bulk}$ (A4)
$j_{Ox^{z+},L}$ is the limiting diffusion current density of the Ox^{z+}, $\left(\text{mA cm}^{-2}\right)$.
$j_{Ox^{z+},L} = -\ z\ F\ \frac{D_{Ox^{z+}}}{\delta_{Ox^{z+}}} \left[Ox^{+}\right]_{bulk} = -z\ F\ k_{Ox^{z+}} \left[Ox^{z+}\right]_{bulk}$ (A5).
D_{Red} is a diffusion coefficient of the Red ($cm^2\ s^{-1}$).
$D_{Ox^{z+}}$ is a diffusion coefficient of the Ox^{z+} ($cm^2\ s^{-1}$).

δ_{Red} is the Nernst diffusion layer thickness concerning the Red (cm).
$\delta_{Ox^{z+}}$ is the Nernst diffusion layer thickness concerning the Ox^{z+}(cm).
k_{Red} is the rate constant of the Red (cm s^{-1}).
$k_{Ox^{z+}}$ is the rate constant of the Ox^{z+} (cm s^{-1}).
$j_a(0)$ is the total exchange current density $\left(mA\ cm^{-2}\right)$.
j_0 is the exchange current density for charge transfer process $\left(mA\ cm^{-2}\right)$.
$j_0 = z\ F\ k^{\varnothing}\ [Red]_{bulk}^{\alpha_c}\ \left[Ox^{z+}\right]_{bulk}^{\alpha_a}$ (A6).
$k^{\varnothing}$ is the standard heterogeneous rate constant (cm s^{-1}).
$(l/\kappa)_f$ is the polarization resistance relating to oxide film or product layer ($= l_f/\kappa_f$, $k\Omega\ cm^2$).
l_f is the thickness of oxide film or product layer (cm).
κ_f is the conductivity of oxide film or product layer $((k\Omega\ cm)^{-1})$.
$(l/\kappa)_s$ is the polarization resistance relating to solution ($= l_s/\kappa_s$, $k\Omega\ cm^2$).
l_s is the distance between the anodic site and the cathodic site (cm).
κ_s is the conductivity of the solution $((k\Omega\ cm)^{-1})$.

The units used in this paper satisfy the requirements of coherent system [35,36].

References

1. Takahashi, M.; Masuko, N. *Kogyodenkai-No-Kagaku*; AGNE: Tokyo, Japan, 1979; pp. 181–192.
2. Haruyama, S. *Hyomengijyutusha-Notameno-Denkikagaku*, 2nd ed.; Maruzen: Tokyo, Japan, 2005; pp. 65–86; 88–90.
3. Bard, A.J. (Ed.) *Hydrogen Encyclopedia of Electrochemistry of the Elements*; Marcel Dekker: New York, NY, USA, 1969; Volume IXa, pp. 384–592.
4. Adams, R.N. *Electrochemistry at Solid Electrodes*; Marcel Dekker: New York, NY, USA, 1969; pp. 187–212.
5. Charlot, G.; Badoz-Lambling, J.; Tremillon, B. *Les Reactions Electrochimiques*; Droits d'Auteur, Masson: Paris, France, 1959; pp. 13–26; 41–83. (In Japanese)
6. Rieger, P.H. *Electrochemistry*, 2nd ed.; Chapman & Hill: New York, NY, USA, 1994; pp. 151–164; 334–337.
7. Gileadi, E. *Physical Electrochemistry*; Wiley-VCH: Weinheim, Germany, 2011; pp. 99–112; 195–204.
8. Bard, A.J.; Faulkner, L.R. *Electrochemical Methods*, 2nd ed.; John Wiley & Sons: New York, NY, USA, 1980; pp. 1–43.
9. Brteiter, M.W. *Electrochemical Processes in Fuel Cell*; Springer: Berlin, Germany, 1969; pp. 1–184.
10. Bokris, J.O.; Ready, A.K. *Modern Electrochemistry*; Plenum Press: New York, NY, USA, 1983; Volume 1 and 2, pp. 1231–1250.
11. Bortoloti, F.; Garcia, A.C.; Angelo, A.C.D. Electronic effect in intermetallic electrocatalysts with low susceptibility to CO poisoning during hydrogen oxidation. *Int. J. Hydrogen Energy* **2015**, *401*, 10816–10824. [CrossRef]
12. Luque, G.C.; de Chialvo, M.R.G.; Chialvo, A.C. Kinetic Study of the Formic Acid Oxidation on Steady State Using a Flow Cell. *J. Solid State Electrochem.* **2017**, *20*, 1209–1217. [CrossRef]
13. Marozzi, C.A.; de Chialvo, M.R.G.; Chialvo, A.C. Criteria for the selection of the scan rate in the evaluation of the kinetic parameters of the hydrogen oxidation reaction by a potentiodynamic sweep. *J. Electroanal. Chem.* **2015**, *748*, 61–69. [CrossRef]
14. Rau, M.S.; de Chialvo, M.R.G.; Chialvo, A.C. Resolution of the mechanism of CO electrooxidation on steady state and evaluation of the kinetic parameters for Pt and Ru electrodes. *J. Solid State Electrochem.* **2012**, *16*, 1893–1900. [CrossRef]
15. Quaino, P.M.; de Chialvo, M.R.G.; Chialvo, A.C. Hydrogen electrode reaction: A complete kinetic description. *Electrochim. Acta* **2007**, *52*, 7396–7403. [CrossRef]
16. Marozzi, C.A.; Canto, M.R.; Costanza, V.; Chialvo, A.C. Analysis of the use of voltammetric results as a steady state approximation to evaluate kinetic parameters of the hydrogen evolution reaction. *Electrochim. Acta* **2005**, *51*, 731–738. [CrossRef]
17. De Chialvo, M.R.G.; Chialvo, A.C. Hydrogen diffusion effects on the kinetics of the hydrogen electrode reaction. Part I. Theoretical aspects. *Phys. Chem. Chem. Phys.* **2004**, *6*, 4009–4017. [CrossRef]
18. Quaino, P.M.; de Chialvo, M.R.G.; Chialvo, A.C. Hydrogen diffusion effects on the kinetics of the hydrogen electrode reaction Part II. Evaluation of kinetic parameters. *Phys. Chem. Chem. Phys.* **2004**, *6*, 4450–4455. [CrossRef]
19. Fernandez, J.L.; de Chialvo, M.R.G.; Chialvo, A.C. Evaluation of the kinetic parameters of the hydrogen electrode reaction from the analysis of the equilibrium polarisation resistance. *Phys. Chem. Chem. Phys.* **2003**, *5*, 2875–2880. [CrossRef]
20. De Chialvo, M.R.G.; Chialvo, A.C. The Tafel–Heyrovsky route in the kinetic mechanism of the hydrogen evolution reaction. *Electrochem. Commun.* **1999**, *1*, 379–382. [CrossRef]
21. De Chialvo, M.R.G.; Chialvo, A.C. The polarisation resistance, exchange current density and stoichiometric number for the hydrogen evolution reaction: Theoretical aspects. *J. Electroanal. Chem.* **1996**, *415*, 97–106. [CrossRef]
22. De Chialvo, M.R.G.; Chialvo, A.C. Hydrogen evolution reaction: Analysis of the Volmer-Heyrovsky-Tafel mechanism with a generalized adsorption model. *J. Electroanal. Chem.* **1994**, *372*, 209–223. [CrossRef]
23. Seri, O.; Itoh, Y. Differentiating polarization curve technique for determining the exchange current density of hydrogen electrode reaction. *Electrochim. Acta* **2016**, *218*, 345–355. [CrossRef]

24. Seri, O.; Siree, B. The differentiating polarization curve technique for the Tafel parameter estimation. *Catalysts* **2017**, *39*, 1–15. [CrossRef]
25. Seri, O. Differentiating approach to the Tafel slope of hydrogen evolution reaction on nickel electrode. *Electrochem. Commun.* **2017**, *81*, 150–153. [CrossRef]
26. Seri, O. Kinetic parameter determination of ferri/ferrocyanide redox reaction using differentiating polarization curve technique. *Electrochim. Acta* **2019**, *323*, 134776–134784. [CrossRef]
27. Antropov, L.I. *Theoretical Electrochemistry*; MIR: New York, NY, USA, 1972; p. 393.
28. Pearson, J.M. "Null" Methods Applied to Corrosion Measurements. *Trans. Electrochem. Soc.* **1942**, *81*, 484–510. [CrossRef]
29. West, J.M. *Basic Corrosion and Oxidation*, 2nd ed.; Ellis Horwood Ltd.: Chichester, UK, 1980; pp. 103–113.
30. Pourbaix, M. *Atlas of Electrochemical Equilibria*; Pergamon Press: New York, NY, USA, 1966; pp. 449–457.
31. Masuko, N.; Takahashi, M. *Denkikagaku*; AGNE: Tokyo, Japan, 1993; pp. 43–56.
32. Nihon, K. (Ed.) *Kagakubinran, Kisohen II*, 4th ed.; Marzen: Tokyo, Japan, 1993; pp. II156–II160.
33. Kita, H.; Ye, S.; Aramata, A. Reaction route of hydrogen electrode reaction on platinum. *Denki Kagaku Oyobi Kogyo Butsuri Kagaku* **1990**, *58*, 41–44. [CrossRef]
34. Tang, D.; Lu, J.; Zhuang, L.; Lin, P. Calculations of the exchange current density for hydrogen electrode reactions: A short review and a new equation. *J. Electroanal. Chem.* **2010**, *644*, 144–146. [CrossRef]
35. Mills, I.; Homann, K.; Kallay, N.; Kuchitsu, K. *Quantities, Units and Symbols in Physical Chemistry*; Blackwell Scientific Publication: Oxford, UK, 1988; p. 109. (In Japanese)
36. McGlashan, M.L. *Physicochemical Quantities and Units*, 2nd ed.; The Royal Institute of Chemistry: London, UK, 1971; p. 46. (In Japanese)